ROLES OF TNFAIP8 IN

CELL MIGRATION AND PHOSPHOINOSITIDE SIGNALING

Mei Lin

A DISSERTATION

in

Cell and Molecular Biology

Presented to the Faculties of the University of Pennsylvania

in

Partial Fulfillment of the Requirements for the

Degree of Doctor of Philosophy

2020

Supervisor of Dissertation

_____

Youhai H. Chen, M.D., Ph.D., Professor of Pathology and Laboratory Medicine

Graduate Group Chairperson

_____

Daniel S. Kessler, Ph.D., Associate Professor of Cell and Developmental Biology

Dissertation Committee

Erfei Bi, Ph.D., Professor of Cell and Developmental Biology

Paula M. Oliver, Ph.D., Associate Professor of Pathology and Laboratory Medicine

Tatyana Svitkina, Ph.D., Professor of Biology

Wei Guo, Ph.D., Professor of Biology

ACKNOWLEDGMENT

This work has been based on previous findings made from Dr. Youhai Chen's lab. Dr. Honghong Sun first generated TIPE2 knockout mice and characterized the phenotypical outcome. Dr. Svetlana Fayngerts dug into the structures of TIPE family and developed biochemical assays. Without their pioneering work this dissertation would not have been possible. I would like to express my sincere gratitude to my mentor, Dr. Youhai Chen, for his guidance and support throughout my graduate school. I have been impressed by Dr. Chen's enthusiasm and insight for science, which come from critical thinking in the field for years. I believe I have benefited from the training that may not be received elsewhere. I would like also to extend my thanks to the members of Chen lab for the support and assistance over the past few years.

I'm also very grateful to my committee members Dr. Erfei Bi, Dr. Paula Oliver, Dr. Tatyana Svitkina and Dr. Wei Guo for their help and advice. Their suggestions have helped tremendously to steer me in the right direction. The committee have also been very generous with their time to hold my meetings more frequently, and patiently answer additional questions I have.

I would also like to thank the CAMB graduate program, especially Dr. Daniel Kessler, Kathleen O'Connor-Cooley and Christina Strathearn for their diligent work. Special thanks go to Dr. M. Celeste Simon for her generosity and encouragement, which have been invaluable for my graduate study. I would like to express my appreciation and

thanks to Yi Wang, Peiwei Huangyang and Caiyue Xu. Although we come from the same undergraduate institution, we do not know each other before coming to Penn; and I have always felt lucky to be classmates or in the same program with them.

I am sincerely thankful to many people who have helped me during graduate school: Nan Lin, Bihui Xu, Xiaoguai Li, Steven Zhao, Zandra Walton, Jiajun Zhu, Bo Li, Danielle Sanchez, Lili Guo and Tatiana Karakasheva. When I'm writing the thesis, I realize that I have not said thank you in person to many of them and others not listed here. I think I should let them know that they have helped me a lot, more than they have known.

Finally, I would like to thank my family and friends whose love and support get me here today, and make me energized to tackle anything tomorrow.

ABSTRACT

ROLES OF TNFAIP8 IN

CELL MIGRATION AND PHOSPHOINOSITIDE SIGNALING

Mei Lin

Youhai H. Chen, M.D., Ph.D.

Well-coordinated directional cell migration is essential for diverse physiological processes such as embryogenesis and immune responses, while its dysfunction can lead to many pathological conditions including cancer and chronic inflammatory diseases. How shallow gradients of chemoattractants translate into the axes of cellular polarization and direct migration remain not well understood. In this study, we have employed loss- and gain-of-function approaches and found that TNFAIP8-deficient human myeloid HL-60 cells exhibit reduced growth and migratory capacity. TNFAIP8 can serve as a cytosolic inhibitor of Rac/Cdc42 and function through the PAK-LIMK-cofilin pathway, thus controlling trailing edge formation. Biochemical studies and cell-based approaches revealed that TNFAIP8 can interact with PtdIns(4,5)P_2 and PtdIns(3,4,5)P_3 through the conserved TIPE homology (TH) domain. TNFAIP8 can steer cells by enhancing PI3Ks activity and PtdIns(4,5)P_2-dependent actin remodeling through cofilin, reinforcing a positive feedback loop that amplifies phosphoinositide signaling at the leading edge. Consequently, TNFAIP8 is required for chemoattractant-induced polarization by acting as a "dual-role regulator" in cytoskeletal dynamics in response to external stimuli. Additionally, using experimental autoimmune encephalomyelitis (EAE) as a mouse model for multiple sclerosis (MS), we found TNFAIP8 and TIPE2 play redundant roles in

controlling lymphocyte migration and infiltration. Our results support that TNFAIP8 is important in inflammation and tumorigenesis, and represents a potential pharmaceutical drug target to block cell migration for treating human diseases such as cancer.

TABLE OF CONTENTS

LIST OF TABLES

LIST OF FIGURES

CHAPTER 1

INTRODUCTION AND BACKGROUND

1.1 Cell migration

Cell migration plays an essential role in diverse physiological processes such as embryogenesis, immunity and cancer metastasis (Lauffenburger & Horwitz, 1996; Ridley et al., 2003). It is implicated in various fundamental activities including coordinated cell layer movements during gastrulation and embryonic morphogenesis, renewal of adult skin and intestine during tissue repair, and leukocyte infiltration during immune surveillance. Dysregulation of eukaryotic cell migration contributes to many pathological conditions, including chronic inflammatory diseases, cancer metastasis, as well as cardiovascular diseases (Lauffenburger & Horwitz, 1996; Paul, Mistriotis, & Konstantopoulos, 2017; Ridley et al., 2003).

Leukocytes are characterized by the ability to migrate rapidly up against shallow gradients of chemoattractants (referred to as chemotaxis), which is important for immune homeostasis and inflammation (Bloes, Kretschmer, & Peschel, 2015; Gregor, Foeng, Comerford, & McColl, 2017; Jin, Xu, & Hereld, 2008; Kunkel & Butcher, 2002). Leukocytes are normally quiescent as they travel within blood vessels. They migrate into the infected tissue by responding to a variety of chemokines, cytokines or chemicals released by bacteria. The central nervous system (CNS), for example, is an immunologically "privileged" site to which access of leukocytes is tightly controlled by the blood-brain and blood-cerebrospinal fluid barriers (Engelhardt & Ransohoff, 2012; Minagar & Alexander, 2003). The infiltration of the CNS by circulating leukocytes is a common pathogenic mechanism of multiple sclerosis (MS), one of the most common autoimmune disorders (Calabresi et al., 2014; Derfuss, Kuhle, Lindberg, & Kappos, 2013).

It is estimated that around 1,000,000 individuals worldwide are afflicted by multiple sclerosis. Drugs blocking leukocyte chemotaxis such as the FDA-approved fingolimod and natalizumab are highly effective for treating chronic inflammatory diseases like multiple sclerosis (Calabresi et al., 2014; Derfuss et al., 2013).

Cancer cell locomotion is another important form of eukaryotic cell migration. Failure to treat cancer metastases from solid tumors in clinic has been responsible for the majority of patient deaths (Gupta & Massagué, 2006; Steeg, 2016). The importance of tumor cell metastasis has been demonstrated through physiologically relevant confined tracks *in vivo* by time-lapse, deep-tissue imaging of intravital microscopy. (Alexander, Koehl, Hirschberg, Geissler, & Friedl, 2008; Alexander, Weigelin, Winkler, & Friedl, 2013) The cascades for metastasis are complicated and encompass migration of cancerous cells away from the primary site, intravasation into the circulation system, extravasation to secondary tissues and formation of distant metastatic tumors (W. Wang et al., 2005). Cell migration is a pivotal step during these metastatic processes (Talmadge & Fidler, 2010; Wirtz, Konstantopoulos, & Searson, 2011). Polarization is crucial for directional migration, with the formation of a filamentous actin-rich lamellipodium at the front and uropod at the rear (Sánchez-Madrid & Angel del Pozo, 1999). A better understanding of cancer cell motility and relevant mechanisms could be useful in developing therapeutic strategies to abate metastasis-initiating migration in the clinic to combat metastasis.

1.2 Phosphoinositide signaling

Phosphatidylinositol (PtdIns) is a unique membrane phospholipid that can be phosphorylated at the 3, 4 and 5 positions of the inositol ring to generate seven phosphoinositides: PtdIns3*P*, PtdIns4*P*, PtdIns5*P*, PtdIns(3,4)P_2, PtdIns(3,5)P_2, PtdIns(4,5)P_2 (PIP2) and PtdIns(3,4,5)P_3 (PIP3). Among these, PtdIns(4,5)P_2 and PtdIns(3,4,5)P_3 are important lipid second messengers (Swaney, Huang, & Devreotes, 2010; Vivanco & Sawyers, 2002). PtdIns(4,5)P_2 is the most abundant phosphoinositide and binds to proteins important for actin polymerization, focal contacts formation and cell adhesion (Thapa & Anderson, 2012). PtdIns(4,5)P_2 has been proposed to control cell migration through at least three mechanisms: (i) it can maintain cell shape by linking the actin cortex to the membrane via interactions with class I myosins as well as Ezrin/Radixin/Moesin (ERM) proteins; (ii) it can act as a second messenger exerting direct signaling roles through interacting with its effector proteins mediated by defined modules/domains; (iii) it is the precursor of at least three important second messengers: PtdIns(3,4,5)P_3 generated through phosphorylation by Phosphoinositide 3-kinases (PI3Ks), as well as inositol 1,4,5-trisphosphate [I(1,4,5)P3 or IP3] and diacylglycerol (DAG) generated through hydrolysis by phospholipase C (PLC).

Localized accumulation of phosphatidylinositol lipids has been proposed to be the key event directing the recruitment and activation of signaling components required for chemotaxis. PtdIns(3,4,5)P_3 is highly enriched in the leading edge and controls cell migration by promoting actin polymerization through both GTPase-dependent and independent mechanisms (Thapa & Anderson, 2012). Upon the chemoattractant

stimulation, PI3K is locally activated by ligand-bound G-protein coupled receptors (GPCRs) or receptor tyrosine kinases (RTKs). Active PI3K catalyzes phosphorylation at the 3 position of PtdIns(4,5)P_2 to generate PtdIns(3,4,5)P_3, which leads to its enrichment at the leading edge. Also in cancer cells, PI3K generation of PtdIns(3,4,5)P_3 and the subsequent activation of Akt and its downstream cascades (e.g., mTORC1) compose the signaling axis controlling cell survival, proliferation and growth (Merlot & Firtel, 2003; Swaney et al., 2010). The asymmetric distribution of PtdIns(3,4,5)P_3 is also confined spatially by the actions of 3' lipid phosphatases, which convert PtdIns(3,4,5)P_3 back to PtdIns(4,5)P_2. Phosphatase and tensin homolog on chromosome ten (PTEN) is enriched at the back and sides of migratory cells. The Src homology phosphatases (SHIP1 and SHIP2) are also active within cells and can locally dephosphorylate PtdIns(3,4,5)P_3 at the 5' position to produce PtdIns (3,4)P_2, thereby adjusting the local phosphoinositides composition (Thapa et al., 2016; Tsujita & Itoh, 2015).

1.3 Rho family of small GTPases

Rho family of small GTPases are central signaling molecules of cell migration. It belongs to the Ras GTPases superfamily and is conformationally regulated by the binding of GTP and GDP. When bound to GTP, it is active and interacts with downstream effector proteins. These GTPases are activated by guanine nucleotide exchange factors (GEFs) and inactivated by GTPase activating proteins (GAPs). In addition, Rho family can bind to guanine nucleotide dissociation inhibitors (GDIs), which prevent its interaction with the

plasma membrane but not necessarily downstream targets (Hansen & Nelson, 2001; Ridley, 2001). Rho GDP-dissociation inhibitors (RhoGDIs) consist of RhoGDIα, RhoGDIβ and RhoGDIγ. Besides cell migration, Rho proteins have also been found to mediate numerous other relevant processes such as cell adhesion to substrates and cells, vesicle trafficking, protein secretion and transcription (Nobes & Hall, 1999; Schmidt & Hall, 2002). Of the at least 20 Rho family proteins identified so far in human, Rac1/2, Cdc42 and RhoA/B have been the most widely studied for their importance in cell migration. Rac and Cdc42 are mainly active at the leading edge, contributing to spatially confined actin polymerization and protrusion via Arp2/3 and WASP/WAVE dependent mechanisms, while Rho is involved in rear retraction (Nobes & Hall, 1999; Sánchez-Madrid & Angel del Pozo, 1999).

The directed migration of cells requires membrane protrusion, attachment to the substratum, and release of the cell rear followed by retraction of the tail (Sánchez-Madrid & Angel del Pozo, 1999). Phosphoinositides including PtdIns(4,5)P_2 and PtdIns(3,4,5)P_3 are major second messengers relaying these signals from receptors and exert their functions through interacting with PIP effectors such as pleckstrin homology (PH) domain and polybasic motif (PBM) proteins (Rickert, Weiner, Wang, Bourne, & Servant, 2000; Tsujita & Itoh, 2015; Li Zhang, Mao, Janmey, & Yin, 2012). A subset of PH-proteins includes GEFs and GAPs for the Rho family. During chemotaxis cells are polarized, with a filamentous actin-rich lamellipodium at the front and uropod at the rear (Sánchez-Madrid & Angel del Pozo, 1999). This front-to-rear polarity is essential for directional migration, and many polarity complexes, including the Par complex, Crumbs complex and Scribble

complex, are conserved across species and diverse cell types (Crespo et al., 2014; Kamakura et al., 2013). There have been reports on crosstalk between Rho proteins and members of polarity complexes in regulating polarity formation. For example, the Rac activator T-cell-lymphoma invasion and metastasis-1 (TIAM1) binds to partitioning defective-3 (PAR3) polarity protein, connecting Rac activities to polarity signaling (Mertens, Rygiel, Olivo, van der Kammen, & Collard, 2005; Nishimura et al., 2005).

1.4 TIPE protein family

The TIPE (tumor necrosis factor-α-induced protein 8 (TNFAIP8)-like, or TNFAIP8L) family of proteins are newly discovered regulators of inflammation and tumorigenesis. There are four highly homologous mammalian TIPE family members: TNFAIP8, TIPE1 (TNFAIP8L1), TIPE2 (TNFAIP8L2) and TIPE3 (TNFAIP8L3). TIPE proteins have been reported to be risk factors for inflammation and cancer, and their expressions are dysregulated in a number of human diseases (Ahn et al., 2010; Goldsmith, Fayngerts, & Chen, 2017; Hao et al., 2016; Y. Zhang et al., 2012).

TNFAIP8, also known as SCC-S2, is the founding member of TIPE family. TNFAIP8 is expressed in numerous human normal tissues and found to be frequently over-expressed in a wide range of human cancers and promote tumor metastasis (L. Chen et al., 2016; Dong et al., 2010; Duan, Zhu, Guan, & Wang, 2014; Kumar et al., 2004; Li et al., 2015; Z. Sun et al., 2016; Yang et al., 2014; C. Zhang et al., 2013; Y. Zhang et al., 2012). TNFAIP8 is also a risk factor for multiple sclerosis (Hussman et al., 2016) and plantar

fasciitis (S. K. Kim et al., 2018) as revealed from recent genome-wide association studies (GWAS). TNFAIP8 is expressed in various human cancer cell lines, with relatively higher mRNA levels in K562 chronic myelogenous leukemia cells, MOLT4 lymphoblastic leukemia cells and A549 lung carcinoma cells (Kumar et al., 2000).

TIPE2 was initially identified as one of the most highly upregulated genes in the spinal cord of experimental autoimmune encephalomyelitis (EAE) mice, and later found to preferentially express in murine leukocytes (H. Sun et al., 2008). Of the four members of the human TIPE family, TIPE2 is almost exclusively expressed in hematopoietic cells. TIPE2 is reported to be a negative regulator of innate and adaptive immunity and essential for maintaining immune homeostasis (Gus-Brautbar et al., 2012; Lou et al., 2014; H. Sun et al., 2012; Z. Wang et al., 2012). TIPE2 can regulate both carcinogenesis and inflammation (Gus-Brautbar et al., 2012), and is crucial for the polarization of myeloid cells (Fayngerts et al., 2017; H. Sun et al., 2008). TIPE2-deficient leukocytes are hyper-responsive to Toll-like receptors (TLRs) activation and exhibit enhanced phagocytic and bactericidal activities, and TIPE2-deficient mice are more sensitive to intravenously induced septic shock (H. Sun et al., 2008; Z. Wang et al., 2012).

TIPE1 is a less well characterized member of TIPE family. TIPE1 has been found to be expressed in various murine tissues and human cancer cell lines (Cui et al., 2011). Knockdown of TIPE1 inhibited TNFα and zVAD.fmk-induced necroptosis in L929 and NIH3T3 cells (Hitomi et al., 2008), and can induce apoptosis by negatively regulating Rac1 activation in hepatocellular carcinoma cells (Z. Zhang et al., 2015), suggesting TIPE1 may be a potential component of the necroptosis and apoptosis pathways. Additionally, studies

have shown that TIPE1 can function as a prognosis predictor and negative regulator of lung cancer (Wu et al., 2017), and suppress invasion and migration through downregulating Wnt/β-catenin pathway in gastric cancer (Liu et al., 2018).

TIPE3 is reported to exhibit similar expression profiles in mice and human, and is preferentially expressed in secretory epithelial tissues (Cui et al., 2015). TIPE3 expression is also markedly upregulated in cervical, colon, lung and esophageal cancers (Cui et al., 2015; Fayngerts et al., 2014). The recently resolved high-resolution crystal structure of human TIPE3 reveals a large hydrophobic central cavity, which consists of 7 alpha helixes forming a pocket that measures 20 Angstrom in depth and 10 Angstrom in diameter. Although the outer surface is highly charged, the central cavity is predominantly hydrophobic, which is indicated to confer lipid binding capacity (Fayngerts et al., 2014). Additionally, TIPE3 can act as a transfer protein for lipid second messengers that include PtdIns(4,5)P_2 and PtdIns(3,4,5)P_3, and potentiate PI3K signaling (Fayngerts et al., 2014).

1.5 TNFAIP8 and cancer

TNFAIP8 has been implicated in inflammation and tumorigenesis. It is originally identified as one of the most differentially expressed genes in primary and matched metastatic head and neck squamous cell carcinoma (HNSCC) from the same patient (Kumar, Whiteside, & Kasid, 2000; Patel, Wang, Whiteside, & Kasid, 1997). High expression of both TNFAIP8 mRNA and protein has been detected in various clinical specimens compared to healthy tissues. Studies have reported TNFAIP8 as a risk factor for

the progression and poor prognosis of numerous human malignancies, including prostate cancer (C. Zhang et al., 2013), gastric adenocarcinoma (L. Chen et al., 2016; Hu et al., 2016; Li et al., 2015; Yang et al., 2014), esophageal squamous cell carcinoma (ESCC) (Z. Sun et al., 2016), non-small-cell lung cancer (Dong et al., 2010) and non-Hodgkin's lymphoma (Y. Zhang et al., 2012). We have confirmed high TNFAIP8 protein levels in multiple human and mouse cancer cell lines through immunoblot analysis and HL-60 is among the most highly expressing cell lines (Figure 1.1A, B).

Experimental evidence supports the notion that TNFAIP8 plays an important role in oncogenesis. For example, exogenous expression of TNFAIP8 in MDA-MB 435 human breast cancer cells enhances proliferation and invasion *in vitro*, as well as experimental metastasis *in vivo* (C. Zhang et al., 2006), while knocking TNFAIP8 down reduces the tumorigenicity in SGC-7901 and MKN-28 gastric cancer cell lines (Li et al., 2015). The precise functions of TNFAIP8 in carcinogenesis and its mechanisms of actions remain largely unknown.

Human TNFAIP8 has six transcript variants (Variant 1 to Variant 6) with different transcription start sites and exons, and can be translated to four protein isoforms (Isoform a to Isoform d). All transcript variants share the last exon: Variants 1 and 3 share another exon, while Variant 3 has a unique first exon; Variants 2, 5, and 6 share a first exon, and Variants 5 and 6 share a unique second exon (Figure 1.2). Among these recently described expression transcript variants, Variants 3 to 6 are minimally expressed in normal or cancer tissue through the analysis of RNA-seq database (Lowe et al., 2016), whereas Variant 2 is

frequently overexpressed in multiple human malignancies, and Variant 1 is commonly downregulated in cancer.

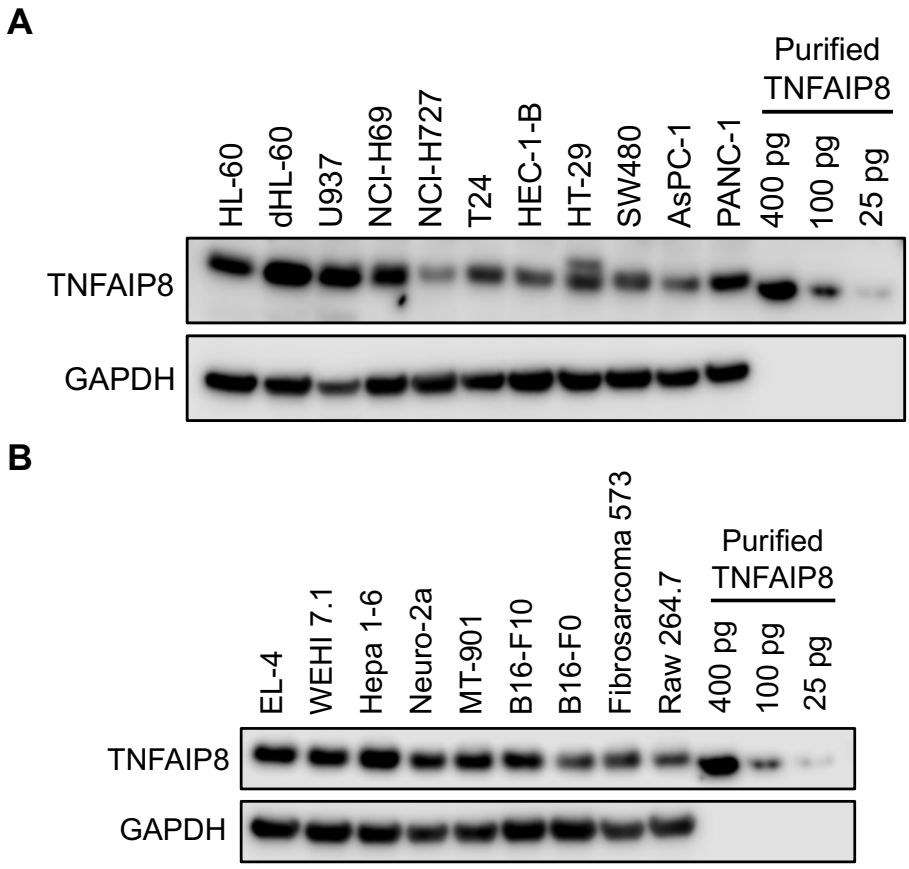

Figure 1.1 TNFAIP8 protein is highly expressed in various cancer cell lines

(A, B) Immunoblot analysis of TNFAIP8 protein levels in various human (A) and mouse (B) cancer cell lines. GAPDH serves as a loading control, and purified human TNFAIP8 isoform b protein is used for quantification. d, differentiated.

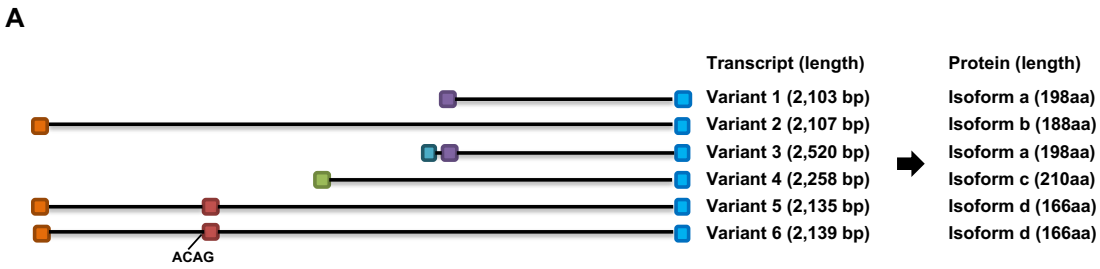

Figure 1.2 The six TNFAIP8 transcript variants (Variant 1 to Variant 6) and four protein isoforms (Isoform a to Isoform d) in humans

(A) At left, the genomic structure is shown for the six transcript variants according to Ensembl genome database. Each rectangle represents an exon. All variants share the last exon (indicated by light blue rectangle). Variant 6 has four additional nucleotides "ACAG" which are immediately upstream of its second exon compared to Variant 5. At right, the length in base pairs (bp) and amino acids (aa) are shown for each transcript. *Adapted from (Lowe et al., 2016)*.

1.6 Hypothesis and specific aims

The ability of cells to migrate up against shallow gradients of chemoattractants requires the temporal and spatial regulation of molecular machineries to sense chemokine gradients by receptors, induce polarized morphology, and rapidly reorganize the cytoskeleton (Jin et al., 2008; Sánchez-Madrid & Angel del Pozo, 1999). Despite intensive studies, how the shallow gradients of chemoattractants translate into axes of cell polarization during chemotaxis remains not well understood. In order for cells to move in one direction, they must first form a defined front (leading edge) and rear (trailing edge). This front-rear polarity is characterized by asymmetrical activation of proteins such as PI3Ks, Rho GTPases and actin regulatory proteins at the leading and trailing edges. While somatic mutations of PI3Ks, PTEN and Ras account for many cases of the aberrant phosphoinositide signaling, other mechanisms for its dysregulation are also being discovered (Thapa et al., 2016; Vivanco & Sawyers, 2002).

The precise cell type-specific functions of TIPEs remain unknown. The high-resolution crystal structures of murine Tnfaip8 C165S mutant, human TIPE2 and human TIPE3 have recently been resolved (Fayngerts et al., 2014; J.-S. Kim et al., 2017; D. Lee et al., 2014; X. Zhang et al., 2008). They reveal a conserved TIPE homology (TH) domain composed of a large hydrophobic central cavity, which implicates lipid binding capacity. In our lab, it has been previously demonstrated that TIPE2 and TIPE3 can function through lipid second messengers that include PtdIns(4,5)P_2 and PtdIns(3,4,5)P_3 (Fayngerts et al., 2017, 2014). In addition, TIPE2 can direct leukocyte polarization (Fayngerts et al., 2017) and directly bind and inhibit Rac (Z. Wang et al., 2012). However, it's not clear if each

TIPE family member shares the same mechanisms of actions in cell migration and tumorigenesis.

Our Specific Aim 1 is to test the hypothesis that TNFAIP8 can promote tumorigenesis through Rho GTPase-dependent signaling pathways. We will use both loss- and gain-of-function approaches to manipulate TNFAIP8 expression in HL-60 cell line, and characterize the phenotypical and functional outcomes. We expect that TNFAIP8 knockout cells would have reduced growth and migratory capacity, and aberrant molecular pathways downstream of Rac/Cdc42 activation. Specific Aim 2 is to test the hypothesis that TNFAIP8 can steer cells by enhancing phosphoinositide signaling and remodeling PtdIns(4,5)P_2-dependent actin dynamics. Both biochemical and cell-based approaches will be used to investigate the functional significances of the hydrophobic central cavity and electrostatic interactions of α0 helix from TIPE homology (TH) domain. We expect that TNFAIP8 mutants deficient in phosphoinositide interactions will be incompetent to rescue the cellular defects of TNFAIP8 knockout HL-60s. Specific Aim 3 is to test the hypothesis that TNFAIP8 and TIPE2 have redundant roles in controlling murine lymphocyte migration, using experimental autoimmune encephalomyelitis (EAE) as a mouse model for neural inflammation. This study will advance a better understanding of TIPE family in inflammation and tumorigenesis, and advise effective pharmaceutical drug design to enhance or block their activities for treating human diseases such as cancer.

CHAPTER 2

TNFAIP8 PROMOTES CANCER CELL MIGRATION

2.1 Introduction

Most of our knowledge about TIPE family proteins has come from animal studies, therefore there is a knowledge gap and necessity to characterize human TIPEs in both health and diseases. To investigate whether the roles of TIPE family are conserved in human, and to facilitate further mechanistic studies, we used CRISPR/cas9 to knock out TNFAIP8 in HL-60, a human promyelocytic leukemia cell line that can be conveniently differentiated into neutrophil-like cells *in vitro* (Collins, 1987; Gallagher et al., 1979; Klinker, Wenzel-Seifert, & Seifert, 1996). We have confirmed that dHL-60 cells express highest level of TNFAIP8 protein among all the cell lines examined (Figure 1.1A, B).

Cell adhesion plays an essential role in leukocyte extravasation to inflamed tissue, and the ability of neutrophils to regulate adhesion derives from their ability to control the affinity states of integrins. Integrin "inside-out" signaling is the process where signals inside the cells cause the external domains of integrins to assume an activated state (Ginsberg, Du, & Plow, 1992; Harburger & Calderwood, 2009; Takagi, Petre, Walz, & Springer, 2002). Lymphocyte function-associated antigen 1 (LFA-1) is an integrin found on neutrophils and other leukocytes. Its affinity is activated by several signaling events including G protein coupled receptor (GPCR) activation, chemokine and cytokine stimulation, and T cell receptors (TCR)-mediated signals, which allows cells to undergo arrest resulting in firm adhesion on endothelia expressing intercellular adhesion molecules (ICAMs) (Springer & Dustin, 2012). In this study, we will use fMLP and TNFα stimulation for HL-60 static adhesion assay on fibronectin or ICAM-1 coated surfaces.

During migration, active Rac-GTP preferentially localizes at the front of the cell, while at the trailing uropod Rac is inactive, which prevents the formation of multiple lamellipodia (Ridley, 2001). Rac-GTP promotes actin polymerization through their effector proteins such as p21-activated kinases (PAKs) and WASP-family verprolin-homologous protein (WAVE) (Nobes & Hall, 1999). Cdc42 can bind and activate the Par polarity complex, which could in turn activate Rac through Tiam1 (Etienne-Manneville, 2004). TIPE2 has been previously reported to be able to inhibit Rac membrane translocation/activation and suppress Rac downstream signaling (Z. Wang et al., 2012). When expressed using an *in vitro* transcription-translation system and mixed together, TIPE2 and Rac can physically associate and directly bind to each other. The hydrophobic C-terminal CAAX motif region of Rac has been found to be responsible for this interaction and targeting/anchoring Rac to the plasma membrane (Z. Wang et al., 2012). The interactions between TNFAIP8 and other Rho family of small GTPases remain to be explored.

2.2 Materials and Methods

2.2.1 Cell lines and culture

The cell lines were obtained from the American Type Culture Collection (ATCC) or Clontech. HEK293T cell line, LentiX-293T cell line, PANC-1 pancreatic carcinoma cell line, EL-4 T cell lymphoma cell line, WEHI 7.1 T cell lymphoma cell line, Hepa 1-6 hepatoma cell line, B16-F0 melanoma cell line, B16-F10 melanoma cell line, Fibrosarcoma 573 cell line and Raw 264.7 macrophage cell line were cultured in Dulbecco's Modified Eagle Medium (DMEM) with 10% FBS, 1% L-glutamine and 1% Penicillin-Streptomycin (D10 medium). U-937 lymphoma cell line, NCI-H69 small cell lung cancer cell line, NCI-H727 lung cancer cell line, AsPC-1 pancreatic adenocarcinoma cell line and MT-901 mammary carcinoma cell line were cultured in RPMI-1640 with 10% FBS, 1% L-glutamine and 1% Penicillin-Streptomycin (R10 medium). T24 urinary bladder cancer cell line and HT-29 colorectal adenocarcinoma cell line were cultured in McCoy's 5A medium containing 10% FBS and 1% Penicillin-Streptomycin. HEC-1-B uterus adenocarcinoma cell line and Neuro-2a neuroblastoma cell line were cultured in Eagle's Minimum Essential Medium (EMEM) composed of Minimum Essential Medium (MEM) containing 1× Non-Essential Amino Acids (NEAA), 1% L-glutamine, 1 mM sodium pyruvate, 10% FBS and 1% Penicillin-Streptomycin. SW480 colorectal adenocarcinoma cell line was cultured in Leibovitz's L-15 medium containing 10% FBS and 1% Penicillin-Streptomycin. HL-60 promyelocytic leukemia cell line was cultured in R10 medium supplied with 25 mM HEPES. As HL-60 cells would acidify their medium quite rapidly, 25 mM HEPES is

essential to counterbalance the pH in culture. HL-60 cell concentration was kept between 1.5 x 10^5 to 10 x 10^5 cells/ml during passage. In order to supply cells of the same quality, frozen cells of the same lot were thawed every two months and used for experiments. HL-60 cells were differentiated by 1.25% (vol/vol) DMSO and 5 ng/ml human G-CSF continuously in culture for 4-6 days before harvest for experiment (cell density was kept at 1.5-2.5 x 10^5 cells/ml). Cell cultures were examined periodically for bacteria contamination and tested for Mycoplasma by LookOut Mycoplasma PCR Detection Kit (Sigma).

2.2.2 Generation of TNFAIP8-deficient HL-60 single clonal cell line by CRISPR/Cas9 system

TNFAIP8-deficient HL-60 cells were generated using CRISPR/Cas9 system and TNFAIP8-specific single guide RNA (sgRNA) or non-targeting control single guide RNA (sgControl) as described (Cho, Kim, Kim, & Kim, 2013; Cong et al., 2013; Garneau et al., 2010; Hsu et al., 2013; Jinek et al., 2012; H. Kim & Kim, 2014; Mali et al., 2013; Ran et al., 2013; T. Wang, Wei, Sabatini, & Lander, 2014). Three sgRNAs were designed to target the earliest sequences of the shared exon of human TNFAIP8 isoforms (Figure 1.2), with optimal on-target and off-target scores (Table 1). The CRISPR target sequences were cloned into LentiCRISPRv2 vector (Ran et al., 2013; Sanjana, Shalem, & Zhang, 2014; Shalem et al., 2014) backbone by adding BsmBI digestion sites using specific primers (Table 2).

Lenti-X 293T cells (Clontech) were pre-cultured in lentivirus packaging medium containing Opti-MEM I reduced serum medium, 1× GlutaMAX, 1 mM sodium pyruvate

and 5% FBS. The constructs were transfected into Lenti-X 293T cells along with 3rd generation lentiviral packaging plasmids. Two batches of lentivirus were harvested, concentrated by Lenti-X Concentrator (Clontech) and titrated by RT-qPCR titration kit (Clontech) as well as antibiotic selection. The functional lentivirus titer was around 1.2 x10^6 Colony Forming Unit (CFU)/ml, and the HL-60 cells were infected at a multiplicity of infection (MOI) of 10. The transduction efficiency measured by EGFP positive control 48 h post transduction was over 80%. The medium was replaced with selection medium (complete culture medium with puromycin at 1 μg/mL final concentration) 48 h post-transduction, and was replaced with fresh medium containing puromycin every 2-3 days until antibiotic-resistant colonies can be identified (around 4-7 days; a typical selection with puromycin takes 7-10 days), while the cells in the untransduced well were dying. The T7EI genomic cleavage detection (GCD) assay (IDT) was performed on the genomic DNA of cells harvested before or three days post puromycin selection. Specific primers amplifying the targeted sequences (Table 3) were used to confirm the efficiency of indel formation following the editing experiments.

The puromycin-resistant cells were passed through a 40 μm cell strainer to break up clumps and generate single cell suspension. The cell suspension was plated at suitable density to TCS semi-solid methylcellulose-based medium (ClonaCell) according to the manufacturer's instructions. After 10-14 days the cultures were inspected for the presence of colonies, and the single clones were picked and expanded in liquid medium for cryopreservation and further analysis.

Table 1

CRISPR sequences targeting the shared exon of all human TNFAIP8 isoforms

		PAM	Direction
TNFAIP8 CRISPR sequence 1	5'- GGATAACACATTCCGGTCAA -3'	AGG	(-)
TNFAIP8 CRISPR sequence 2	5'- TCATCAGCTTGCTATGACCG -3'	TGG	(+)
TNFAIP8 CRISPR sequence 3	5'- AGGTGGATTATACCTTTGAC -3'	CGG	(+)

Table 2

Primers for cloning the target sequences into the LentiCRISPRv2 backbone

	Forward Oligo	Reverse Oligo
LentiCRISPRv2 TNFAIP8 sgRNA1	CACCGGATAACACATTCCGGTCAA	AAACTTGACCGGAATGTGTTATCC
LentiCRISPRv2 TNFAIP8 sgRNA2	CACCGTCATCAGCTTGCTATGACCG	AAACCGGTCATAGCAAGCTGATGAC
LentiCRISPRv2 TNFAIP8 sgRNA3	CACCGAGGTGGATTATACCTTTGAC	AAACGTCAAAGGTATAATCCACCTC

Table 3

Primers of genomic cleavage detection (GCD) assay for CRISPR validation

	Forward Oligo	Reverse Oligo	GCD band size (bp)
sgRNA1 GCD Primer set1	TTTAGTTCGCTTCACTTG	ACCATCACATAGTTTTTG	600 [406 bp,194 bp]
sgRNA1 GCD Primer set2	TTAATTCTTTTCCTCTCTTTTT	GGTTTAAAATTCCCAAAA	540 [371 bp,169 bp]
sgRNA2 GCD Primer set1	CAAATGGTGGGAAAATGAGG	GGATTATACAAGGCAGCCAA	603 [416 bp,187 bp]
sgRNA2 GCD Primer set2	TTAGTTCGCTTCACTTGCTG	GGATTATACAAGGCAGCCAA	556 [369 bp,187 bp]
sgRNA3 GCD Primer set1	ATACCTGTTTTTAGTTCGCTTC	TAGTTTTTGTAAGTGGGG	600 [414 bp,186 bp]
sgRNA3 GCD Primer set2	TTAATTCTTTTCCTCTCTTTTT	GGTTTAAAATTCCCAAAA	540 [371 bp,169 bp]

2.2.3 Transwell migration/invasion assay of dHL-60 and inhibitors study

The migration of differentiated HL-60 towards chemoattractants was performed using the 3 μm pore Transwell filters (Corning) as described (JoVE, Cambridge, 2016; Justus, Leffler, Ruiz-Echevarria, & Yang, 2014). dHL-60 cells were centrifuged gently at 400g for 5 min, washed two times with DPBS, and rested in migration assay buffer for 30 min at 37°C. Migration assay buffer contains Hanks' Balanced Salt solution (HBSS) with Ca^{2+}/Mg^{2+}, 25 mM HEPES and 0.2% Human Serum Albumin (HSA, Sigma, fatty acid and endotoxin free, freshly made). For the invasion assay, the filters were coated with 100 ul of 50 μg/mL Matrigel (Corning), and the plate was placed at room temperature for 1 h to solidify and form a thin gel layer. Just prior to cell seeding, the remaining Matrigel was carefully aspirated from the inserts, washed once with DPBS, and 2 x 10^5 dHL-60 cells were added using reverse pipetting method to avoid bubbles. When studying the effects of inhibitors on transmigration, cell seeding volume was reduced to half (125 μl per well) to allow for the addition of equal volume of test reagents in 2× concentration, and the cells were pre-incubated with the antagonists for 45 min at 37°C before the start of the experiment. The pharmacological inhibitors were used at the following final concentrations: LY-294,002 (100 μM, Sigma), NSC 23766 (300 μM, Sigma), Torin1 (250 nM, Calbiochem), InSolution Z62954982 (100 μM, Calbiochem), Y-27632 (10 μM, Cell Signaling Technology) and FRAX486 (10 μM, Sigma). fMLP and CXCL8 were added to the bottom wells at the concentrations of 10 nM and 3 nM, respectively. dHL-60 cells were allowed to migrate for 1.5 h at 37°C. Prewarmed cell detachment solution (0.05% Trypsin-EDTA, no phenol red) was added to the lower chamber to dissolve any cells attached to

the bottom of the insert. The numbers of cells migrated into the lower chamber and detached by Trypsin-EDTA were quantified by CellTiter-Glo (CTG) assay (Promega). % Migration = the number of cells that migrated in response to chemoattractant / the total number of cells seeded on the chamber. The experiments were performed in duplicates or triplicates.

2.2.4 Static adhesion assay

The 96-well TC-treated cell culture plates were coated with 40 µl of 50 µg/mL fibronectin or 40 µl of 5 µg/mL ICAM-1 (diluted in DPBS) for 2 h at 37°C. Differentiated wild-type and TNFAIP8 knockout dHL-60 cells were serum starved for 2 h in assay buffer containing HBSS with Ca^{2+}/Mg^{2+}, 25 mM HEPES and 0.2% HSA. The cells were subsequently stimulated with fMLP (100-200 nM) or TNFα (30 ng/mL) and plated on fibronectin or ICAM-1 coated surfaces (washed cells were resuspended at the concentration of 3.0 x 10^6 cells/mL; 50 µl was added in order to seed 1.5 x 10^5 cells per well). The plates were incubated for 30 min at 37°C in a CO_2 incubator. The plates were then gently washed three times with HBSS buffer (with Ca^{2+}/Mg^{2+}) to remove cells that were not able to form tight contacts with the ligands. Check under microscope to see if many cells remain in HSA coated wells (cells in HSA negative control wells should be rare; if not, repeat wash). The cells left in the wells were quantified by CellTiter-Glo (CTG) assay (Promega). The average percentage of adherent cells is calculated relative to unwashed wells that represent 100%.

2.2.5 Lipid extraction from cells

Total lipids were isolated from cells as described (BLIGH & DYER, 1959; Clark et al., 2011; Corey et al., 1993; FOLCH, LEES, & SLOANE STANLEY, 1957). Briefly, the cells were pelleted by centrifugation at 400g for 5 min at 4°C, and washed one time with ice-cold PBS. The cells were then resuspended in HBSS buffer with Ca^{2+} and Mg^{2+} at 3 x 10^7 cells/ml. Save 20 µl (around 0.6 x 10^6 cells) to lyse for harvesting actin protein as loading control. Divide the left cells equally (340 µl, around 10.2 x 10^6 cells) into two groups (unstimulated v.s. stimulated) in 15 ml conical tubes. Stimulate 340 µl (around 10.2 x 10^6 cells) aliquot of cells with 10 nM fMLP or vehicle for 60 sec at 37°C. Terminate reactions by addition of 1500 µl quench mix (75 ml stock comprised of 48.4 ml methanol, 24.2 ml chloroform and 2.355 ml 1 M HCl; stock solution prepared using standard glassware). The above steps created primary lipid extracts from cells, which resulted in a thoroughly mixed, single-phase sample (from 340 µl of aqueous sample and 1500 µl of quench mix) in a 15 ml conical tube. 1450 µl $CHCl_3$ was then added, followed by 30 sec vortex and adding 340 µl 2 M HCl. The sample was then thoroughly mixed again and centrifuged in a bench-top microcentrifuge at 1,500g for 5 min at room temperature. This created a two-phase system with an upper aqueous layer and a lower organic phase, with a protein band at the interface. The upper phase was siphoned, and the lower organic phase (~1700 µl) was collected into a fresh 2 ml safe-lock polypropylene tube. The extracted lipids were dried down with light nitrogen stream, and then speed-vacuumed at 35°C for 1 h. The dried lipids can be stored at -20°C or -80°C before experiments.

2.2.6 Protein-lipid overlay assay

Cellular levels of PtdIns(3,4,5)P_3, PtdIns(4,5)P_2 and PtdIns(4)P were measured using protein-lipid overlay assay with GST-GRP1-PH, GST-PLCδ-PH and GST-SidC-3C domains, respectively (Dowler, Kular, & Alessi, 2002; Guillou et al., 2007; Rusten & Stenmark, 2006). The extracted dried lipids were dissolved in a 1:1 mixture of chloroform and methanol containing 0.1% HCl. 1-2 µl aliquots of the lipids were spotted onto nitrocellulose membrane in a consistent pattern. The membranes were allowed to dry in dark at room temperature for 1 h or at 4°C overnight. The membranes were then blocked with TBS-T (10 mM Tris-HCl, pH 8.0, 150 mM NaCl, 0.05% (v/v) Tween 20 detergent) containing 3% fatty acid-free BSA (Sigma), and gently agitated for 1 h at room temperature. The membranes were then incubated with GST-PLCδ-PH, GST-GRP1-PH or GST-SidC-3C (0.5-1.0 µg/ml, Echelon) in TBS-T with 3% fatty acid-free BSA for 1 h at room temperature. Proteins were detected with anti-GST-HRP antibody (Cell Signaling Technology) and chemiluminescence (Pierce). For dot blot studies control membranes were stained with anti-GST-HRP only. For normalization, a small aliquot of cells was lysed in RIPA lysis buffer with protease and phosphatase inhibitors. The lysates were spotted on membranes and immunoblotted with anti-actin (Sigma, 1:4000 dilution) and HRP-conjugated secondary anti-mouse IgG (1:3000 dilution).

For protein-lipid overlay assay of 6His-SUMO tagged TNFAIP8 mutants, the synthetic lyophilized lipids were reconstituted to 1 mM stocks in a 1:1 solution of methanol and chloroform and stored at -80°C before use. DOPC (Avanti Polar Lipids), DOPS (Avanti Polar Lipids), PtdIns(4)P (CellSignals), PtdIns(4,5)P_2 (CellSignals) and

PtdIns(3,4,5)P_3 (CellSignals) were spotted onto nitrocellulose membranes and processed as described above. The membranes were then incubated with 10 nM purified TNFAIP8 or mutant proteins in TBS-T with 3% fatty acid-free BSA, and the binding was detected with anti-6His-HRP antibody (Cell Signaling Technology). Signals were then revealed by chemiluminescence (Pierce) and quantified by desitometry using ImageStudioLite (LI-COR Biosciences) software.

For the estimation of PtdIns(3,4,5)P_3 levels in splenocytes and $CD4^+$ T cells, PtdIns(3,4,5)P_3 Mass ELISA Kit (Echelon) was used for detection and quantification following the manufacturer's instructions.

2.2.7 Western blotting and subcellular fractionation assay

Western blotting and subcellular fractionation assay were performed as previously described (Fayngerts et al., 2017, 2014). For Western blot estimation of protein levels, cells were lysed for 15 min at 4°C in RIPA lysis buffer (Sigma) containing 50 mM Tris-HCl (pH 8.0), 150 mM sodium chloride, 1.0% Igepal CA-630 (NP-40), 0.5% sodium deoxycholate and 0.1% sodium dodecyl sulfate (SDS), protease inhibitor cocktail (Roche cOmplete) and phosphatase inhibitors (Roche PhosSTOP). Cell debris was removed by centrifugation at 14,000g for 15 min at 4°C. In subcellular fractionation experiment, Qproteome Cell Compartment Kit (Qiagen) was used to separate the membrane and cytoplasmic proteins according to the manufacturer's instructions. The protein concentration of the lysates was measured by BCA Protein Assay Kit (Pierce). Equal amount of total protein was separated by SDS-PAGE, transferred to PVDF membranes,

immunoblotted with specific primary and secondary antibodies, and the signals were revealed by chemiluminescence (Pierce). The following antibodies were used for Western blotting: anti-GST, Myc, AKT, GSK-3β, p-GSK-3β (S9), cofilin, p-cofilin (S3), p-LIMK1(T508)/LIMK2(T505), p-p38 (T180/Y182), ATPase, GAPDH, integrin-β1, Histone H3 (Cell Signaling Technology), anti-TIPE2 (Proteintech), anti-TNFAIP8 (Proteintech), anti-Flag (Sigma-Aldrich, monoclonal, M2), anti-actin (Sigma-Aldrich, monoclonal, AC-15), control IgG (Santa Cruz biotechnology), anti-rabbit IgG-HRP (GE Healthcare Life Sciences NA934) and anti-mouse IgG-HRP (GE Healthcare Life Sciences NA931). The densitometric quantification of Western blot signals was performed using ImageStudioLite (LI-COR Biosciences) and ImageJ softwares.

2.2.8 Plasmids and DNA transfection

Full-length murine TIPE2 and human TNFAIP8 isoform b cDNA were generated by PCR and cloned in frame with a N-terminal GST tag into pRK5 expression vector. Wild-type Cdc42 cDNA was obtained from Addgene and subcloned into pRK5 with Myc tag at the N-terminus. Cdc42-17N and Cdc42-61L were generated by mutagenesis from wild-type Cdc42 using Stratagene QuikChange II Mutagenesis Kit (Agilent). HEK293T cells were transfected with plasmid DNA using Fugene 6 reagent (Promega) according to the manufacturer's instructions.

2.2.9 Co-Immunoprecipitation (Co-IP) assay

Immunoprecipitation was performed using Dynabeads protein G (Invitrogen). In brief, 1.5 mg protein G Dynabeads were coated with 5 μg specific antibodies or IgG control for 1 h at room temperature with rotation. After removing unbound antibody, the bead-antibody complex was incubated with 500 μL cell lysates for 4 h at 4°C with gentle rotation. The captured Dynabead-Ab-Ag complex was washed four times with PBS and boiled in 2× Laemmli sample buffer. The eluted proteins were fractionated by SDS-PAGE and detected by Western blot.

2.2.10 GST pull-down assay

Briefly, the cells were transfected with GST-tagged "bait" protein and "prey" protein expressing plasmids, lysed and quantified by BCA assay to adjust to 1-5 mg/ml. The cell lysates with equal total protein amount were incubated with 50 μl prewashed Glutathione Sepharose 4B (GE Healthcare Life Sciences) in 100 μl GST pull-down buffer (20 mM Tris, 150 mM NaCl, 2 mM $MgCl_2$, 0.1% NP-40 and 20 μg/ml BSA) for 2 h at 4°C with gentle rotation. Protein-bound Sepharose was washed 3 times, eluted with glutathione and boiled in 2× Laemmli sample buffer. Supernatants were subjected to SDS-PAGE and Western blot analysis.

2.2.11 Mice

Tnfaip8$^{-/-}$ and *Tipe2*$^{-/-}$ C57BL/6 mice were produced as previously described (H. Sun et al., 2008, 2015). The *Tnfaip8*$^{-/-}$*Tipe2*$^{-/-}$ double-knockout (DKO) mice were generated by crossing *Tnfaip8*$^{-/-}$ with *Tipe2*$^{-/-}$ mice. WT C57BL/6 mice were purchased from Jackson Laboratories. Mice were housed in the Animal Care Facilities of University of Pennsylvania under pathogen-free conditions. Animal procedures were all pre-approved by the Institutional Animal Care and Use Committee of the University of Pennsylvania. All mice experiments conform to the relevant regulatory standards.

2.2.12 Isolation of splenic CD4$^+$ T cells

CD4$^+$ T cells were purified from spleens using EasySep Mouse CD4$^+$ T Cell Isolation Kit (STEMCELL) or Invitrogen Negative Selection CD4 Purification Kit (Waltham, MA) according to manufacturer's instructions. The purity of CD4$^+$ T cells was greater than 90%, and the viability was greater than 90% as judged by flow cytometry. The cells were stimulated with 1 μg/ml anti-CD3 (Clone 2C11, eBioscience) and 1 μg/ml anti-CD28 (Clone 37.15, Biolegend) for 2 days, and rested for 2-3 days in complete RPMI culture medium containing 10% FBS, 1% L-glutamine, 1% Penicillin-Streptomycin and 10 ng/ml IL-2 (Invitrogen).

2.2.13 Flow cytometric analysis of F-actin cellular levels

WT and T2KO dHL-60s, or T2KO cells re-expressing empty vector or TIPE2 were rested in assay buffer containing HBSS with Ca^{2+}/Mg^{2+}, 25 mM HEPES and 0.2% HSA. Cells were treated with or without fMLP (10 nM) for 30, 60, 120 and 300 sec. Cells were then fixed in PBS containing 4% paraformaldehyde overnight at 4C°, and permeabilized in PBS containing 0.1% Triton X-100 for 5 min at room temperature. Cells were stained with control IgG (Santa Cruz Biotechnology) or Phalloidin-AlexaFluor 555 (Thermo Fisher Scientific) for 1 h at room temperature, and analyzed by flow cytometry. The experiments were performed in triplicates.

2.3 Results

2.3.1 Reduced cell proliferation and survival of TNFAIP8-deficient human HL-60 cells generated by CRISPR/cas9

In order to knock out all TNFAIP8 protein isoforms in HL-60 cell line, three sgRNAs were designed to target the earliest sequences of the shared exon (Figure 1.2). After cloning into LentiCRISPRv2 vector (Sanjana et al., 2014; Shalem et al., 2014), the constructs were transfected into Lenti-X 293T cells along with 3rd generation lentiviral packaging plasmids. Since Mycoplasma would interfere with cell attachment, Lenti-X 293T and HL-60 cells were tested periodically to confirm free of Mycoplasma contamination (Figure 2.1A). 1.0 μg/mL puromycin was determined to be the lowest concentration that can result in massive HL-60 cell death in ~3 days, and was used to select the stable cell line (Figure 2.1B).

To validate the cleavage efficiency of sgRNAs, T7EI genomic cleavage detection (GCD) assay was performed on the genomic DNA of cells harvested before (Figure 2.1C, D) and three days after puromycin selection (Figure 2.1E). The single clones were selected from polyclonal population targeted by sgRNA1 and sgRNA2 (at least eight clones respectively for each sgRNA) through semi-solid methylcellulose-based medium. After cell culture expansion, Sanger sequencing was performed in selected single clones to validate that nucleotide insertion or deletions (indels) in the targeted exon generated premature stop codons (Figure 2.2A). In addition, Western blot was performed to validate the complete knockout of TNFAIP8 proteins (Figure 2.2B). These data validated the

efficiency of TNFAIP8 sgRNAs in the infected cells and the establishment of HL-60 cell line by CRISPR/cas9.

We observed that TNFAIP8 knockout (TKO) HL-60 cells showed reduced proliferation in RPMI-1640 medium containing either 10% FBS (Figure 2.3A) or 1% FBS (Figure 2.3B) relative to WT cells. In addition, counting of cells in 1% FBS medium was performed with trypan blue exclusion method, and TKO HL-60s showed lower viability after two days in culture compared to WT cells (Figure 2.3C). These results suggest that TNFAIP8 knockout can lead to defective HL-60 cell proliferation and survival *in vitro*.

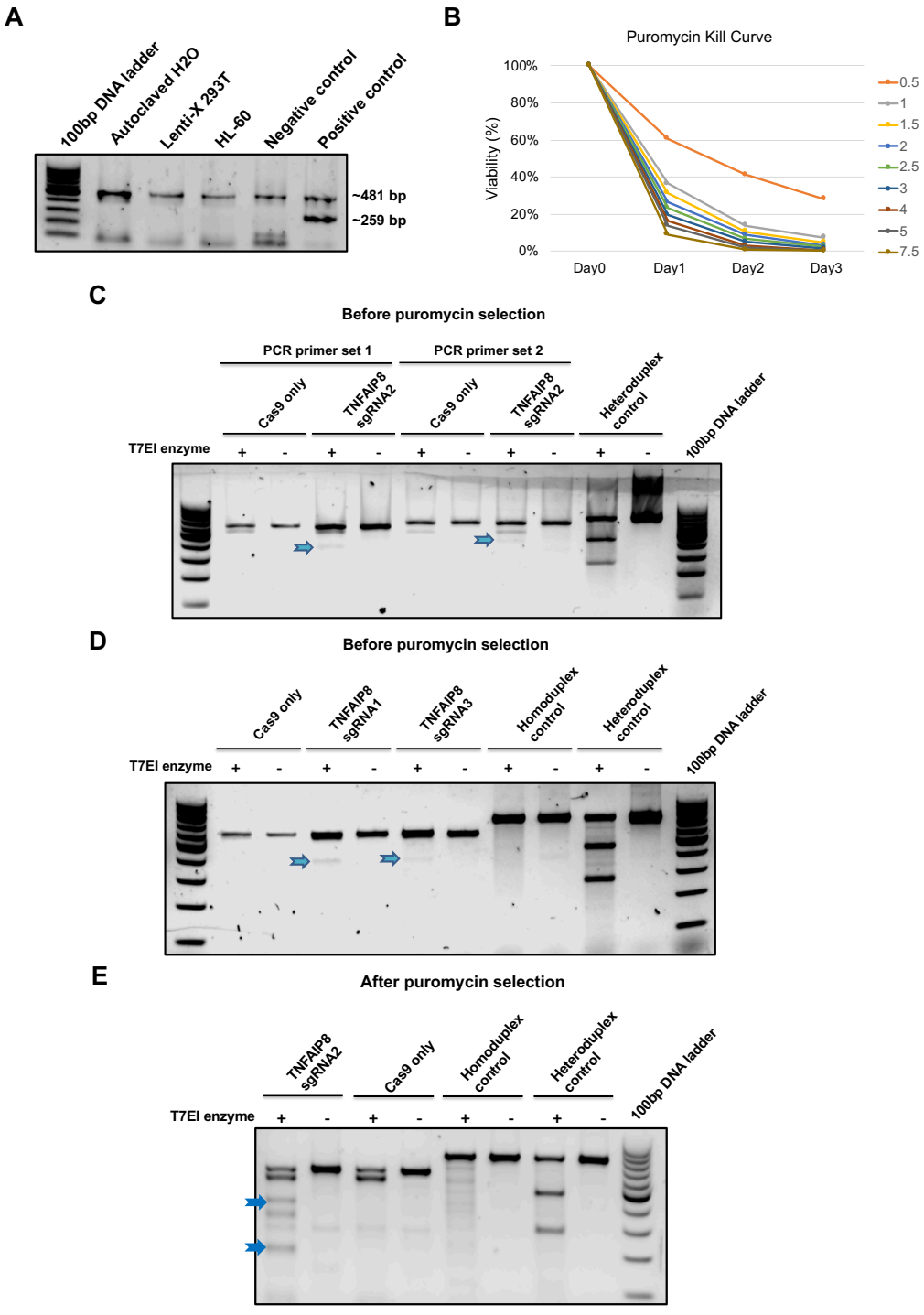

Figure 2.1 Transduction of LentiCRISPRv2-sgTNFAIP8 into HL-60 cells, genomic cleavage validation and puromycin selection

(A) Lenti-X 293T and HL-60 cells were tested to be Mycoplasma-free. Internal controls showed a distinct 481 bp band and appeared in each lane, indicating a successfully performed PCR. The positive control showed a 259 bp band. (B) Puromycin kill curve of HL-60 using the indicated final concentrations (μg/mL). (C-E) The transduction efficiency measured by GFP positive cells 48 h post-infection was over 80%. The T7EI genomic cleavage detection assay was performed on the genomic DNA of cells harvested before (C, D) and three days after puromycin selection (E). Arrows indicate digested reannealed PCR products by T7EI (which cleaved mismatched DNA heteroduplexes).

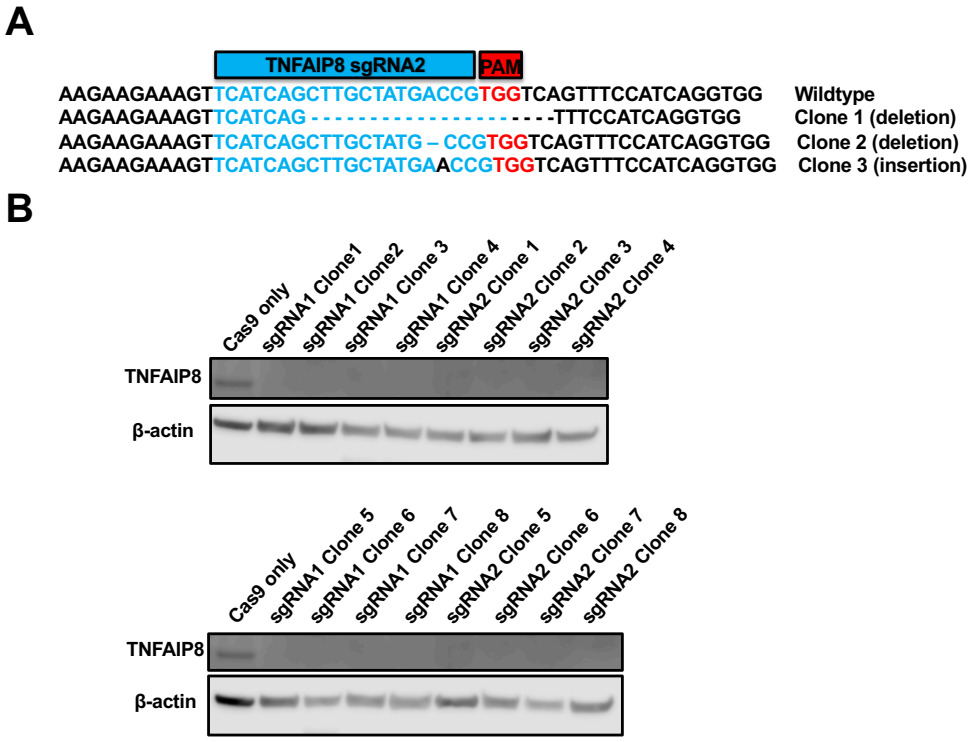

Figure 2.2 Validation of CRISPR/cas9-mediated TNFAIP8 gene knockout in HL-60 cells

(A, B) Three sgRNAs targeting the earliest sequences of the shared exon of human TNFAIP8 isoforms were cloned into LentiCRISPRv2 vector. After puromycin selection, the single clones were derived from semi-solid methylcellulose-based medium for each sgTNFAIP8 and expanded in culture. Sanger sequencing (A) and Western blot (B) were performed to validate the indels that generated premature stop codons and truncated TNFAIP8 proteins.

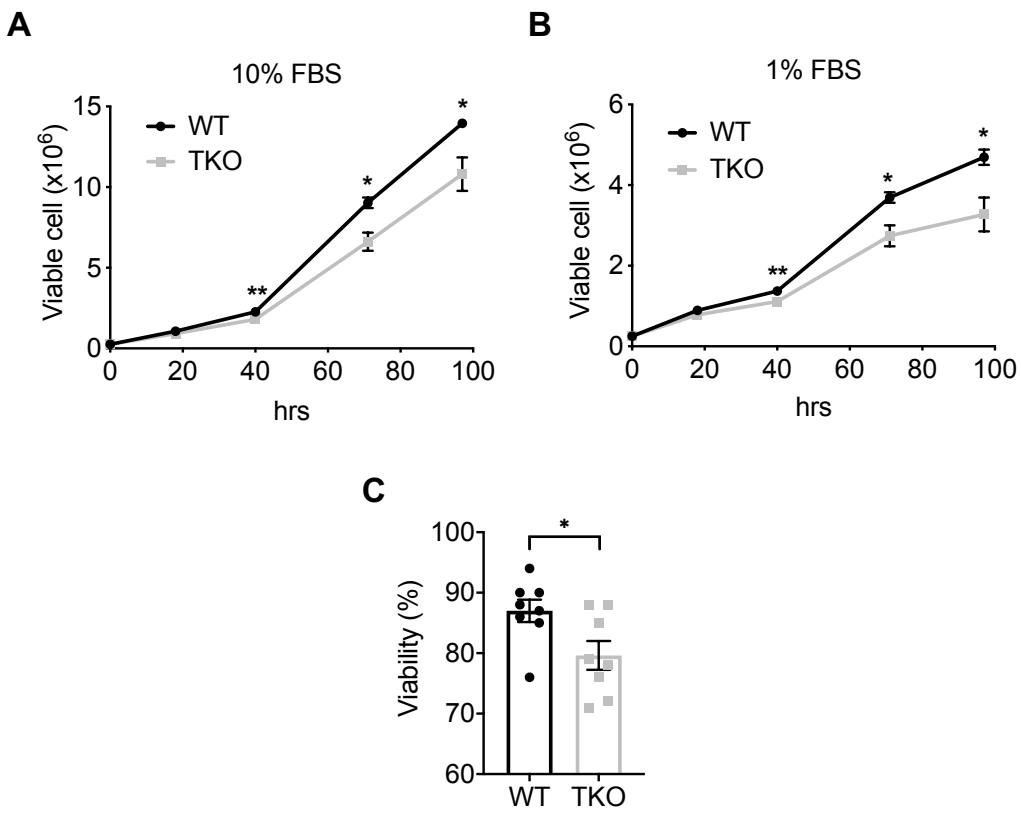

Figure 2.3 TNFAIP8 deficiency decreases the proliferation and cell survival of HL-60 cells *in vitro*

(A, B) Proliferation of wild-type and TNFAIP8 knockout (TKO) HL-60 cells was measured by CellTiter-Glo (CTG) assay in RPMI-1640 medium containing 10% FBS (A) or 1% FBS (B) over the indicated time. (C) Relative viability was measured after two days culture in 1% FBS containing medium by cell counting with trypan blue. $n = 4$ (A, B) or $n = 8$ (C) individual HL-60 WT or TKO clonal cell lines established from CRISPR/cas9. $*P < 0.05$; $**P < 0.01$ (unpaired Student's *t*-test). The experiments were performed three times independently with similar results (mean ± s.e.m.).

2.3.2 TNFAIP8 deficiency decreases chemotaxis and adhesion of dHL-60 neutrophils *in vitro*

To investigate whether the deficiency of TNFAIP8 affects chemotaxis in differentiated HL-60 (dHL-60) neutrophil-like cells, we first tested the chemoattractant EC50 concentrations as well as concentrations 1-2 logs above and below the expected EC50 for neutrophils (Carrigan, Weppler, Issekutz, & Stadnyk, 2005; Henkels, Frondorf, Gonzalez-Mejia, Doseff, & Gomez-Cambronero, 2011; Krause et al., 1985; Millius & Weiner, 2009; Sai, Walker, Wikswo, & Richmond, 2006; Zahn, Zwirner, Spengler, & Götze, 1997). The Boyden chambers with 3 μm pore size filters were incubated at 37°C for 1.5 h, during which chemoattractant gradients were maintained between the compartments. Among the conditions tested (fMLP 10 nM-100 μM, CXCL8 1-486 nM), 10 nM fMLP was found to be optimal for dHL-60 migration, with around five to eight-fold cell number increases through the Transwell filters (Figure 2.4A). CXCL8 induced around two-fold more chemotaxis within a wide range of concentrations (Figure 2.4B).

To demonstrate if TNFAIP8 is necessary and sufficient in regulating dHL-60 chemotaxis, TNFAIP8 expression was rescued by lentiviral titration and infection into knockout cell line to equal the endogenous level (Figure 2.5A). We found that TNFAIP8-deficient dHL-60 cells display significant defect in transmigration towards both fMLP and CXCL8, but do not have obvious defect in random migration (without chemoattractant), relative to that of WT counterparts. These effects were true on either bare Transwell membranes (Figure 2.5B) or Matrigel coated filters (Figure 2.5C). Furthermore, the chemotaxis defect can be completely “rescued” by re-expressing a wild-type TNFAIP8

transgene (Figure 2.5). These results indicate that TNFAIP8 is essential for the chemotaxis of human dHL-60 cells *in vitro*.

To explore if TNFAIP8 knockout affects dHL-60 adhesion, wild-type and TKO cells were serum starved and subsequently stimulated with fMLP or TNFα before being placed on surfaces coated with fibronectin or ICAM-1. We found TNFAIP8-deficient dHL-60 cells exhibit reduced adhesion to fibronectin (Figure 2.6A, B) or ICAM-1 (Figure 2.6C, D) coated surfaces compared to their WT counterparts when treated with fMLP (Figure 2.6A, C) or TNFα (Figure 2.6B, D). They didn't significantly differ when no chemokine was added. These results indicate that TNFAIP8 knockout confers deficiency in ECM adhesiveness.

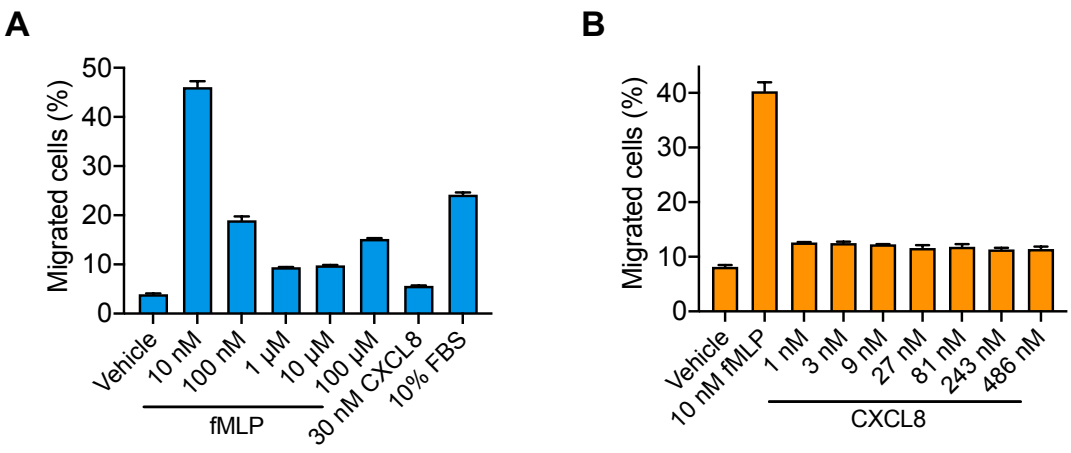

Figure 2.4 Condition optimization for Transwell migration assay

(A, B) Migration of wild-type dHL-60 cells through 3 μm pore size non-coated Transwell filters towards various concentrations of fMLP (A) or CXCL8 (B). Data shown are percentages of cells migrated across the membrane. Data are representative of two independent experiments with similar results.

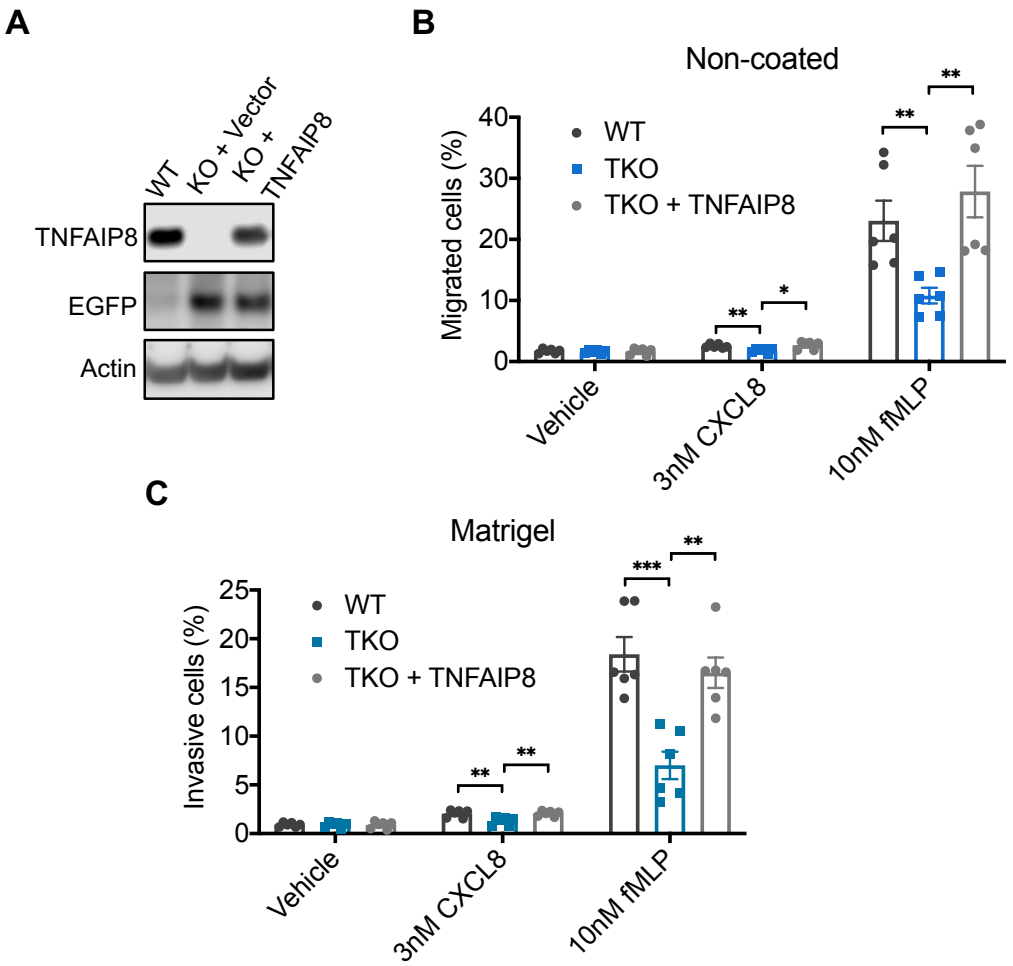

Figure 2.5 TNFAIP8 is required for the chemotaxis of neutrophil-like dHL-60 cells *in vitro*

(A) The protein levels of TNFAIP8 and EGFP in wild-type, knockout and lentiviral rescued TNFAIP8-expressing dHL-60 cells were examined by Western blot. (B, C) Migration of wild-type and TKO dHL-60 cells on non-coated (A) or Matrigel coated (B) Transwell filters towards 10 nM fMLP or 3 nM CXCL8. $n = 6$ clones (B, C). $^{*}P < 0.05$; $^{**}P < 0.01$; $^{***}P < 0.001$ (unpaired Student's *t*-test). Data are representative of three independent experiments with similar results (mean ± s.e.m.).

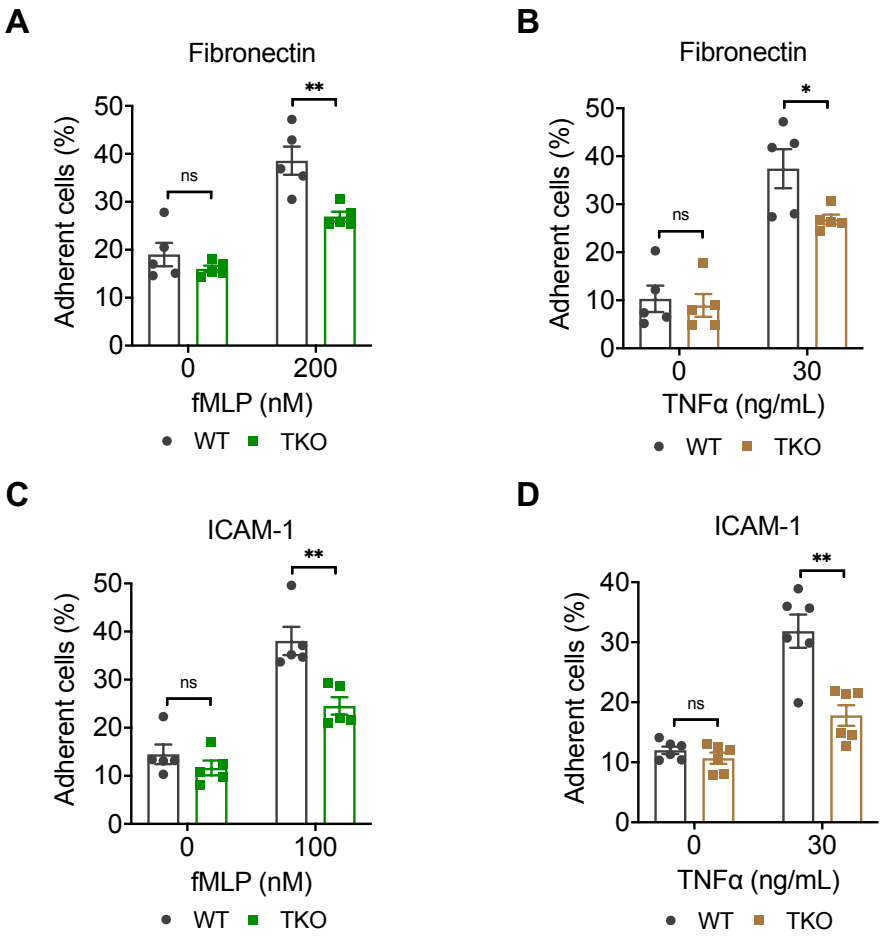

Figure 2.6 TNFAIP8 promotes dHL-60 adhesion *in vitro*

(A-D) Wild-type and TKO dHL-60 cells were serum starved for 2 h and subsequently stimulated with fMLP (100 or 200 nM) (A, C) or TNFα (30 ng/mL) (B, D), and plated on Fibronectin (A, B) or ICAM-1 (C, D) coated surfaces. The average percentage of adherent cells is calculated relative to unwashed cells that represent 100%. $n = 5$ clones (A-C) or $n = 6$ clones (D). ns, not significant; $*P < 0.05$; $**P < 0.01$ (unpaired Student's *t*-test). Data are representative of three independent experiments with similar results (mean ± s.e.m.).

2.3.3 TNFAIP8 and TIPE2 subcellular localization in quiescent and CXCL8-treated cells

To gain more mechanistic insights on human TIPE proteins, we studied the subcellular fractionation of proteomic samples from several cancer cell lines by Qproteome Cell Compartment assay. The cellular components from cytosol, membrane, nuclear and cytoskeleton were validated by Western blot using antibodies against GAPDH, integrin-β1/ATPase, Histone H3 and β-actin, respectively (Figure 2.7A-D). We found TNFAIP8 protein localizes in the cytoplasm under resting conditions in HL-60 leukemia cell line, U-937 lymphoma cell line and NCI-H69 small cell lung carcinoma cell line (Figure 2.7A-C). Moreover, in dHL-60 neutrophils, increased TIPE2 membrane localization was observed after CXCL8 treatment and subcellular fractionation (Figure 2.7D).

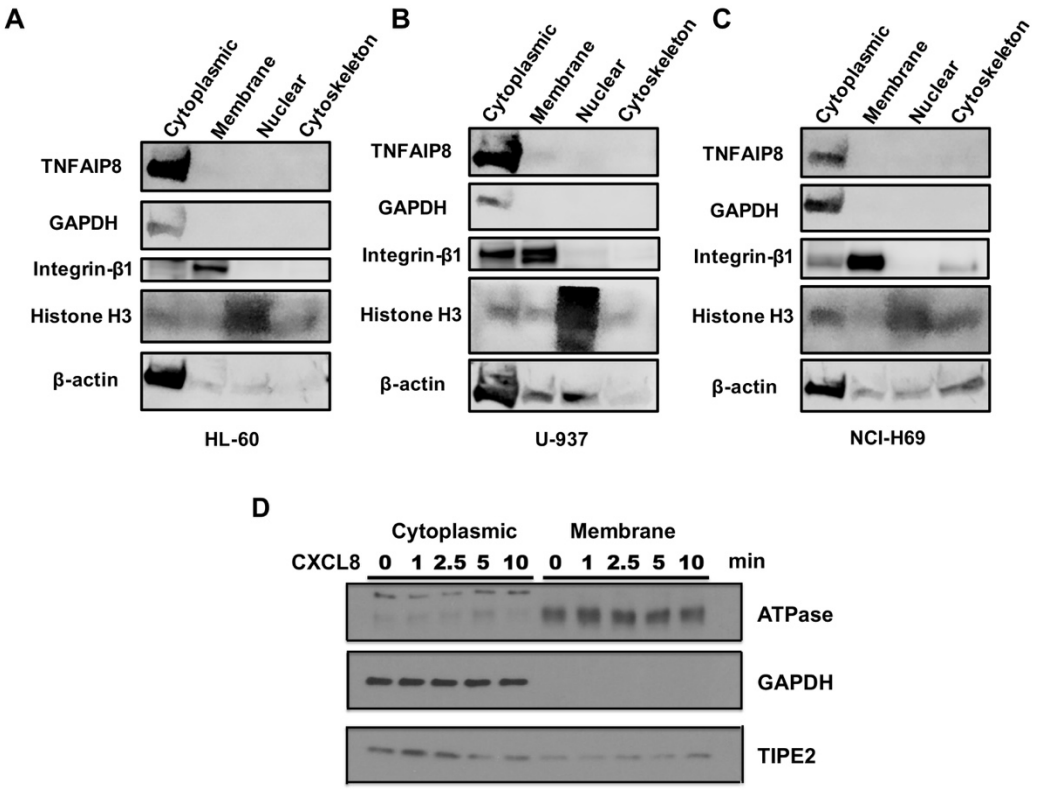

Figure 2.7 TNFAIP8 and TIPE2 subcellular localization in quiescent and CXCL8-treated cells

(A-C) TNFAIP8 localizes in the cytosol under resting condition in various human cancer cell lines. The subcellular fractionations of proteomic samples from HL-60 promyelocytic leukemia cell line (A), U-937 lymphoma cell line (B) and NCI-H69 small cell lung carcinoma cell line (C) were derived by Qproteome Cell Compartment assay (Qiagen). The cellular components from membrane, cytosol, nuclear and cytoskeleton were analyzed by Western blot using antibodies to the indicated proteins. (D) Increased TIPE2 membrane localization in dHL-60 cells after CXCL8 treatment for the indicated time.

2.3.4 TNFAIP8 regulates cellular phosphoinositide levels

To test if there are changes in the total phosphoinositide levels in resting and stimulated dHL-60 cells, protein-lipid overlay assay was performed with GST-GRP1-PH (specifically binds to PtdIns(3,4,5)P_3), GST-PLCδ-PH (specifically binds to PtdIns(4,5)P_2), and GST-SidC-3C protein (specifically binds to PtdIns(4)P). We observed significantly increased total levels of PtdIns(3,4,5)P_3 and PtdIns(4)P, but reduced PtdIns(4,5)P_2 in TNFAIP8 knockout dHL-60 cells under resting condition (Figure 2.8A, B). By contrast, the differences diminished after 60 sec fMLP treatment and the cellular levels of these phosphoinositides became comparable in WT and TKO cells (Figure 2.8A, B).

Moreover, we observed significant increase in total PtdIns(3,4,5)P_3 level in TNFAIP8 and TIPE2-deficient (DKO) murine splenocytes (Figure 2.9A) and thymocytes (Figure 2.9B) through protein-lipid overlay assay. Consistently, by a Mass ELISA Assay (Echelon Biosciences), cellular levels of PtdIns(3,4,5)P_3 in DKO splenocytes (Figure 2.9C) and $CD4^+$ T cells (Figure 2.9D) were found to be 4 to 8-fold higher than wild-type under resting condition.

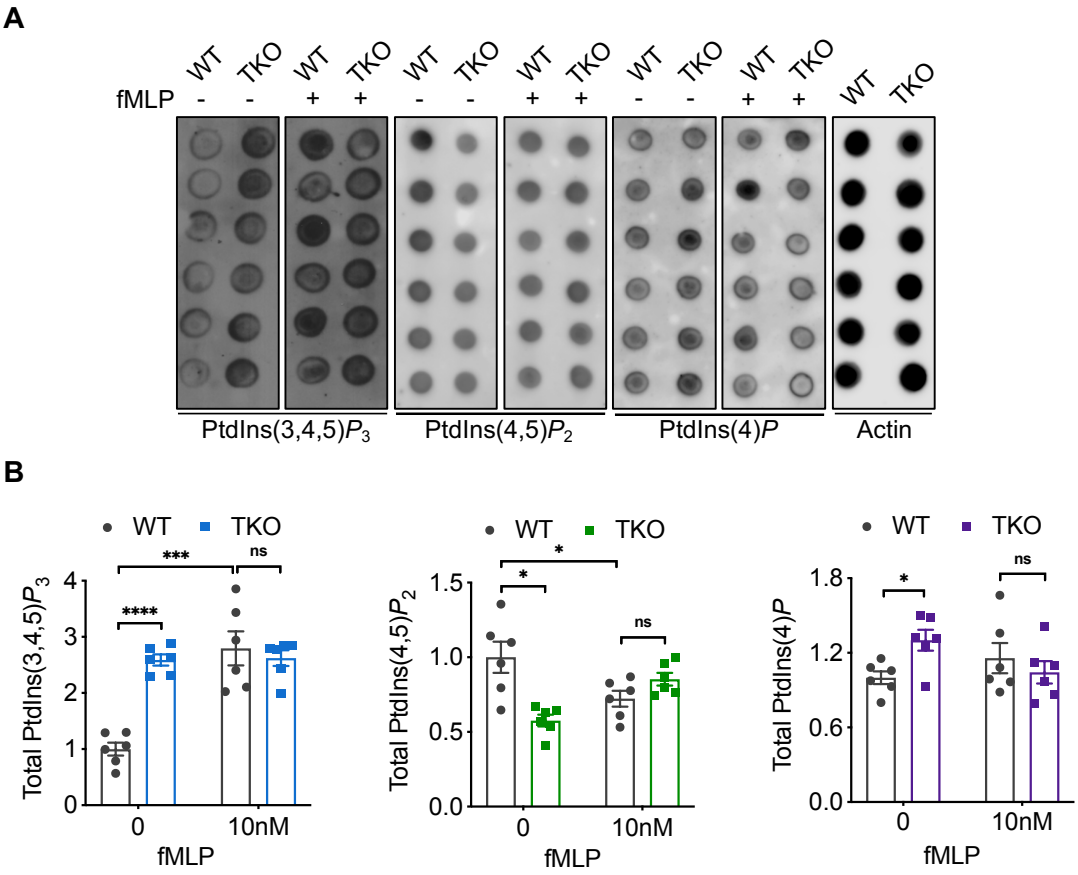

Figure 2.8 Increased total PtdIns(3,4,5)P_3 and PtdIns(4)P but reduced PtdIns(4,5)P_2 levels in TNFAIP8-deficient dHL-60 cells under resting condition

(A, B) Cellular levels of PtdIns(3,4,5)P_3, PtdIns(4,5)P_2 and PtdIns(4)P in wild-type and TNFAIP8 knockout dHL-60 cells were measured by protein-lipid overlay assay with GST-GRP1-PH, GST-PLCδ-PH or GST-SidC-3C protein. dHL-60 cells were stimulated with DMSO vehicle or 10 nM fMLP at 37°C for 60 sec. n = 6 clones (A, B) individual HL-60 wild-type or TKO clonal cell lines established from CRISPR/cas9. Signal from unstimulated wild-type dHL-60 cells was set as 1. ns, not significant; *P < 0.05; ***P < 0.001; ****P < 0.0001 (unpaired Student's t-test). The experiments were performed at least three times independently with similar results (mean ± s.e.m.).

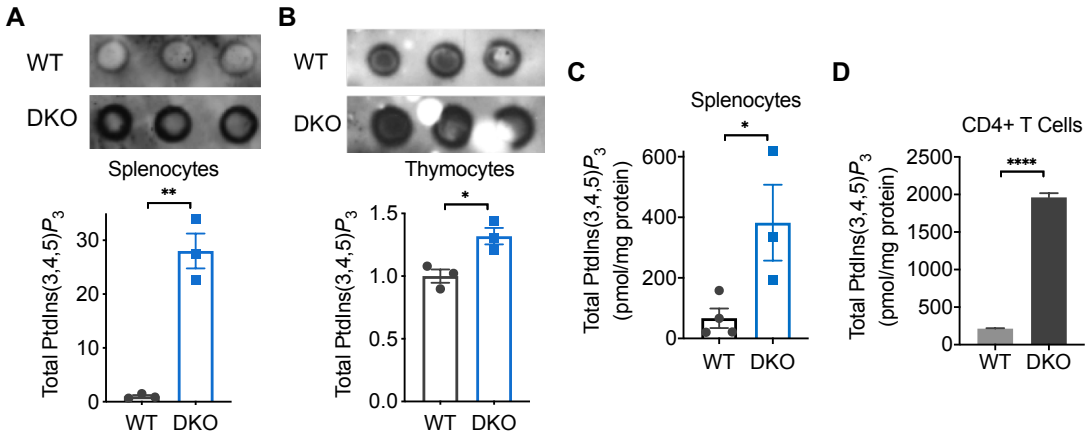

Figure 2.9 Increased total PtdIns(3,4,5)P_3 level in TNFAIP8 and TIPE2-deficient murine splenocytes, thymocytes and CD4$^+$ T cells under resting condition

(A, B) Cellular levels of PtdIns(3,4,5)P_3 in wild-type and *Tnfaip8*$^{-/-}$*Tipe2*$^{-/-}$ (DKO) splenocytes (A) or thymocytes (B) were measured by protein-lipid overlay assay with GST-GRP1-PH protein (3 mice per group). Signal from wild-type cells was set as 1. (C, D) Cellular levels of PtdIns(3,4,5)P_3 in wild-type and DKO splenocytes (C) or CD4$^+$ T cells (D) were measured by PtdIns(3,4,5)P_3 Mass ELISA Kit (Echelon Biosciences) (3-4 mice per group). *$P < 0.05$; **$P < 0.01$; ****$P < 0.0001$ (unpaired Student's *t*-test). Data represent two independent experiments with similar results (mean ± s.e.m.).

2.3.5 Regulation of signaling pathways by TIPE family

The severing activity of cofilin is inactivated by LIMK phosphorylation at the Ser3 position. TNFAIP8-deficient HL-60 cells exhibited upregulated phosphorylated cofilin (S3) and LIMK (LIMK1 T508/LIMK2 T505) signals as determined by Western blot (Figure 2.10A). By contrast, no differences were observed in the p-GSK-3β (S9) and p-p38 (T180/Y182) MAP kinase pathways between WT and TKO cells (Figure 2.10A). To further explore the mechanisms by which TNFAIP8 regulates cell migration, we manipulated the molecular activities using several pharmacological blockers. The transmigration of both WT and TKO cells could be attenuated markedly by the antagonists LY-294,002 (PI3K inhibitor), NSC 23766 (selective inhibitor of Rac1-GEF interaction), Torin1 (mTOR inhibitor XI), InSolution Z62954982 (Rac1 inhibitor II), Y-27632 (ROCK inhibitor) and FRAX486 (PAK inhibitor). In addition, NSC 23766, InSolution Z62954982, Y-27632, FRAX486 and Torin1 effectively reduced the difference between WT and TKO group (Figure 2.10B), suggesting the importance of these molecular pathways in TNFAIP8 regulation of dHL-60 cell migration. Consistently, we observed decreased F-actin polymerization in TIPE2-deficient dHL-60 neutrophils upon fMLP stimulation (Figure 2.11A). Furthermore, over-expression of wild-type TIPE2 protein in TIPE2 knockout HL-60 cells increased F-actin formation compared to the cells infected with empty retroviral construct (Figure 2.11B), confirming that this F-actin change was caused by TIPE2.

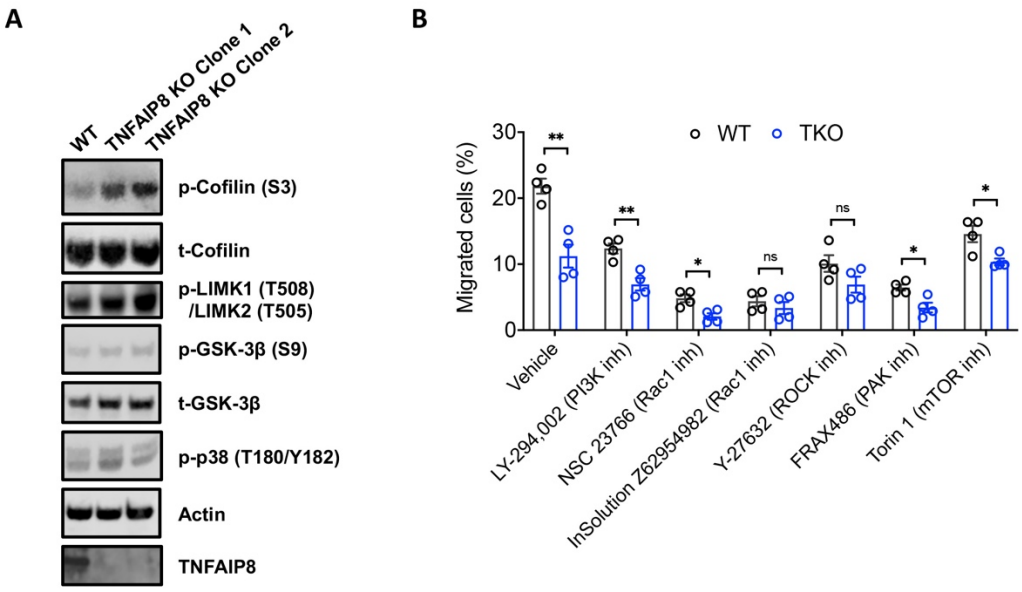

Figure 2.10 Regulation of signaling pathways by TNFAIP8

(A) Wild-type and TNFAIP8 knockout HL-60 cells were analyzed by Western blot using antibodies against the indicated proteins. (B) Migration of WT and TKO dHL-60 cells across 3 μm pore size non-coated Transwell filters towards 10 nM fMLP, with or without pretreatment with the indicated inhibitors (n = 4 clones). ns, not significant; *P < 0.05; **P < 0.01 (unpaired Student's t-test). Data are representative of two independent experiments with similar results (mean ± s.e.m.).

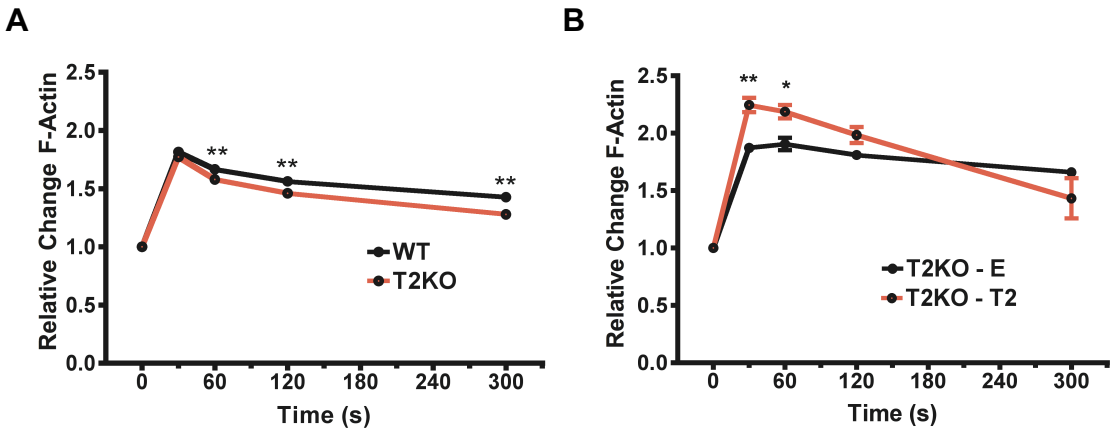

Figure 2.11 Quantitative measurements of the responses of WT and T2KO dHL-60 cells to fMLP stimulation

(A-B) Flow cytometric analyses of actin polymerization (F-actin) in WT and T2KO dHL-60 cells (A), and dHL-60 cells expressing empty retroviral vector (E) or TIPE2 (T2) (B). Cells were stimulated with fMLP at the indicated time, stained with fluorescent dye-conjugated phalloidin and examined by flow cytometer. $*P < 0.05$; $**P < 0.01$ (unpaired Student's *t*-test). The experiments were performed in triplicates and repeated two times with similar results (mean ± s.d.).

2.3.6 TIPE family proteins can associate with Cdc42, Cdc42-17N, Par3 and AKT

TIPE2 has been reported to co-immunoprecipitate with Rac in 293T cells or dHL-60 cells stimulated with fMLP (Fayngerts et al., 2017). We assessed immunoblot of TNFAIP8, TIPE2, Cdc42 in 293T cells expressing recombinant GST-tagged TNFAIP8/TIPE2 and Myc-tagged Cdc42, following immunoprecipitation (IP) with anti-GST or the control antibody immunoglobulin (IgG). We found Myc-Cdc42 was able to immunoprecipitate with GST-TNFAIP8 (Figure 2.12A) or GST-TIPE2 (Figure 2.12B) when expressed in 293T cells. Additionally, TIPE2 associated with Par3 (Figure 2.12C) but not Par6 (data not shown) when GST-tagged TIPE2 was expressed and immunoprecipitated in 293T cells. Furthermore, TIPE2 was found to preferentially associate with the Cdc42-17N mutant, which is a GDP-bound form of Cdc42, rather than the Cdc42-61L mutant, which is a GTP-bound form (Figure 2.12D). In addition, IP with TIPE2 antibody and Western blot for AKT revealed endogenous association of these two molecules in Raw 264.7 macrophages (Figure 2.12E). These results indicate TIPEs may function through Rho family of small GTPases such as Rac and Cdc42, as well as PI3K-AKT pathway to contribute to actin remodeling in directional migration.

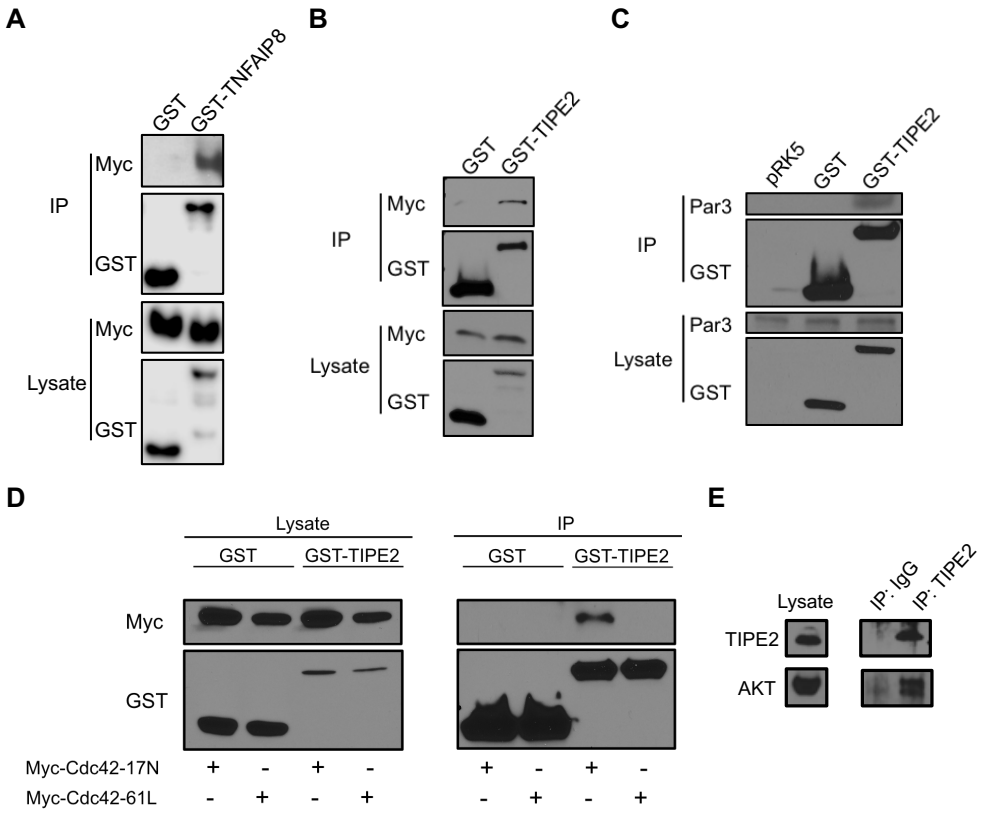

Figure 2.12 Co-Immunoprecipitation (Co-IP) analysis of TNFAIP8 and TIPE2 with Cdc42, Cdc42-17N, Par3 and AKT

(A-D) Immunoblot analysis of the indicated proteins in 293T cells expressing recombinant GST-tagged TNFAIP8 (A) or TIPE2 (B-D), and Myc-tagged Cdc42 (A, B) or Cdc42-17N (D), assessed before (below) or after (above) immunoprecipitation with anti-GST or the control antibody immunoglobulin (IgG). (E) Lysates of Raw 264.7 cells were subjected to IP with anti-TIPE2 or control IgG. The precipitates were analyzed by Western blot using TIPE2- or AKT-specific antibodies. Data represent at least two independent experiments with similar results.

2.4 Discussion

In this part of study, we conducted CRISPR/cas9-mediated TNFAIP8 gene knockout in HL-60 cells. In addition to decreased proliferation and cell survival, we have observed defective migration and adhesion upon fMLP and cytokine stimulation on various ECM substrates including fibronectin, Matrigel and ICAM-1 in these differentiated neutrophil-like cells. As transmigration defect can be caused by either velocity or directionality, two-dimensional chemotaxis could be further studied in μ-slide chemotaxis chambers with migratory tracks recorded by time-lapse microscopy. As we have seen some pharmacological inhibitors affect the migratory difference between WT and TKO dHL-60s, it would be interesting to examine if membrane translocation and polarization of endogenous TNFAIP8 and TIPE2 proteins change after treating with these inhibitors.

We have seen the reductions in the total PtdIns(3,4,5)P_3 and PtdIns(4)P levels but not PtdIns(4,5)P_2 in TKO as compared to WT cells, suggesting TNFAIP8 can regulate phosphoinositide metabolism and signaling. Similar approaches could be employed to test if TNFAIP8 overexpression could reduce cellular level of PtdIns(3,4,5)P_3. Besides protein-lipid overlay assay with PH domains, cellular levels of phosphoinositides could be examined by immunoblotting (dot blot) with anti-PtdIns(3,4,5)P_3/PtdIns(4,5)P_2 antibodies, or through immunofluorescence confocal microscopy. It would be interesting to further visualize the subcellular changes of PtdIns(3,4,5)P_3 and PtdIns(4,5)P_2 levels regulated by TNFAIP8 expression. Wild-type or knockout cells can be infected with PLCδ-PH-GFP or AKT-PH-GFP/GRP1-PH-GFP as biosensors, treated with or without stimulation, fixed and

visualized by confocal microscopy. The ratios of signals on plasma membrane over those in the cytoplasm in the same cell can be quantified based on fluorescence intensity.

NSC 23766, InSolution Z62954982, Y-27632, FRAX486 and Torin1 inhibitors attenuated dHL-60 migration markedly, and effectively reduced the difference between WT and TKO cells, indicating that TNFAIP8 may function through Rac and Cdc42 to contribute to actin remodeling. The degree of overall Rac/Cdc42 activation can be determined by Pak1 protein-binding domain (PBD) pull-down assay. The localized activation can be tested by immunofluorescence confocal microscopy using specific antibodies against p-AKT, Rac-GTP and Cdc42-GTP, as well as the polarization of F-actin. It would also be interesting to check if TNFAIP8 deficiency reduces the ratio of membrane-bound versus the cytosolic endogenous Rac, or if TNFAIP8 knockout impairs the binding of Cdc42 to the Par complex.

The results in this chapter suggest that TIPEs can bind to Rho GTPases to prevent their activation and maintain the quiescent cellular state. Exposure to chemoattractants upregulates TIPEs membrane translocation, which can set free the Rho GTPases. The free activated Rac/Cdc42 can then initiate downstream effector signaling, leading to directional migration. In the TKO cells, the quiescent state can not be maintained in the absence of TNFAIP8, which results in constitutively elevated level of PtdIns(3,4,5)P_3. Thus, TIPE family may represent a novel negative regulator of Rho GTPases, similar to the unique class of Rho GDP-dissociation inhibitors (RhoGDIs).

CHAPTER 3

TNFAIP8 INTERACTS WITH PHOSPHOINOSITIDES AND MEDIATES SIGNALING OF PHOSPHOINOSITIDE-BINDING PROTEINS

3.1 Introduction

Through protein-lipid overlay assay, we have previously screened the binding of TIPEs to all eight phosphoinositides and seven other biologically important eukaryotic lipids including lysophosphatidic acid (LPA), lysophosphocholine (LPC), phosphatidyl-ethanolamine (PE), phosphatidylcholine (PC), sphingosine-1-phosphate (S(1)P), phosphatidic acid (PA) and phosphatidylserine (PS) (Fayngerts et al., 2014). TIPEs were found to predominantly interact with PtdIns(4,5)P_2, PtdIns(3,5)P_2, PtdIns(3,4)P_2 and PtdIns(3,4,5)P_3, out of the 15 lipids screened. One caveat of lipid strip was that more water-soluble or electronically charged phosphoinositides like PtdIns(3,4,5)P_3 could be easier to wash away. To determine if the screened lipid-protein interactions were also true in the model lipid bilayer, sedimentation-based binding assays (Kavran et al., 1998; A. Lee & Lemmon, 2001; Tortorella & London, 1994) have been employed. Additionally, we also used Surface Plasmon Resonance (SPR) for real-time, label-free detection of these biomolecular interactions. In principle, the plasmons are generated when polarized light strikes the gold film at the interface between two media, and the decreased intensity of reflected light at the resonance angle will be in proportion to the mass on sensor surfaces (Beseničar, Maček, Lakey, & Anderluh, 2006; Homola, Yee, & Gauglitz, 1999).

Cofilin is a member of the actin depolymerizing factor (ADF)/cofilin family and functions as an actin-severing protein (Prunier, Prudent, Kapur, Sadoul, & Lafanechère, 2017). By severing and depolymerizing older filaments, cofilin can increase the availability of filament ends and the actin monomers, thereby promoting newer filamentous actin (F-actin) formation. Therefore, cofilin can regulate actin dynamics by enhancing membrane

protrusion and promoting cell motility *in vivo*, and is reported to be a key regulator in the chemotaxis of metastatic cancer cells (Song et al., 2006; van Rheenen, Condeelis, & Glogauer, 2009; W. Wang, Eddy, & Condeelis, 2007). The activities of cofilin are tightly controlled through several mechanisms in cells, of which the most well-studied include phosphorylation and binding to phosphoinositides. Firstly, cofilin can be inactivated by phosphorylation at serine 3 (Ser3) by LIM kinases (LIMKs) and testis-specific kinases (TES kinases or TESKs), which are regulated by Rho GTPases (Prunier et al., 2017). Ser3 phosphorylation site locates in the actin-binding domain, which renders cofilin inactive towards F-actin binding. The dephosphorylation of Ser3 by slingshot homolog (SSH) or chronophin (CIN) phosphatases circumvents this inhibition. Secondly, the dephosphorylated cofilin can still be inhibited by its binding to PtdIns(4,5)P_2 (Bravo-Cordero, Magalhaes, Eddy, Hodgson, & Condeelis, 2013; Ghosh et al., 2004). The local excitation global inhibition (LEGI) mechanism has been proposed for cofilin activation in polarized cells (Mouneimne et al., 2006; van Rheenen et al., 2009). This mechanism involves global phosphorylation of cytosolic cofilin resulted from external stimulation activated LIMK, and the local release and translocation of plasma membrane (PM) cofilin to the F-actin compartments (active cofilin), resulted from PLC mediated PtdIns(4,5)P_2 reduction. In this chapter, we'll examine the interaction of TNFAIP8 with phosphoinositides and whether it can mediate signaling of phosphoinositide-binding proteins.

3.2 Materials and Methods

3.2.1 DNA constructs

Expression plasmids of human TNFAIP8 isoform b, murine TNFAIP8 isoform 1 and the PH domains from phospholipase C-δ1 (PLCδ-PH) and general receptor for phosphoinositides (GRP1-PH) were constructed by cloning PCR-amplified cDNA into pET-SUMO vector (LifeSensors, Malvern, PA), in frame with the N-terminal 6His-SUMO tag. The mutagenesis was performed using Stratagene QuikChange II Mutagenesis Kit (Agilent) according to the manufacturer's instructions. The TIPE2 Entrance mutant was generated by replacing amino acid residues 28H, 75R, 91R and 183K with glutamine (Q). The murine TNFAIP8 isoform 1 Entrance mutant was generated by replacing the three positively charged amino acids H86, R87, K103 positioned at the opening of the hydrophobic cavity with Q. TNFAIP8 2Q mutant was generated by replacing K41 and K42 in the α0 helix with Q (the corresponding positions in TIPE2 K15,16Q mutant). Two additional lysines 46 and 50 in the α0 helix were mutated to construct the 4Q mutant. The lentiviral expression plasmids of TNFAIP8, TIPE2 and mutants were constructed by cloning the open reading frame of each cDNA into the multiple cloning site of pGL-LU-EGFP vector.

3.2.2 Protein purification

Protein purification has taken advantage of the pET-SUMO fusion tag system. In principle, recombinant 6His-SUMO tagged proteins were expressed from *Escherichia coli*

(*E. coli*) BL21(DE3) and purified using Ni-NTA resin. 6His-SUMO tagged proteins were eluted from beads, followed by cleavage with SUMO Protease 1. The 6His-SUMO fusion proteins and 6His tagged SUMO Protease 1 after cleavage were removed by affinity chromatography on a second Ni-chelating resin. Untagged native proteins were eluted, separated by SDS-PAGE and stained with Coomassie Blue G-250.

A fresh bacteria colony was inoculated to 10 ml of LB broth containing 200 μg/ml Ampicillin and 50 μg/ml Chloramphenicol, and grown at 37°C overnight. Use the overnight seed culture (1:50 dilution) to inoculate 500 ml 2 x YT or Terrific Broth medium, containing antibiotics and 0.2% glucose. The cells were grown with vigorous shaking at 37°C until an OD600 of around 0.6 (0.5-0.7) was reached. Bacteria double every ~20 min so it's important to check the OD600 timely to avoid overgrowing. Optionally take a pre-induction sample by spinning down 1 ml of culture and decant the medium. Boil the pellet in 50 μl 4 x SDS sample buffer and freeze until use. Induce protein expression by adding 250 μl of 1 M Isopropyl β-d-1-thiogalactopyranoside (IPTG) stock to a final concentration of 0.5 mM, and shake vigorous at 16°C overnight.

The cells were harvested by centrifugation at 4°C, 4,000g for 20 min. All purification steps afterwards were carried out at 4°C to prevent protein degradation. The lysis buffer was composed of 50 mM sodium phosphate (NaH_2PO_4), 300 mM NaCl, 10% glycerol, 10 mM Imidazole and 0.1% (w/v) CHAPS, and adjusted to pH 7.6. The lysis buffer was pre-cold, and was added 20 mM 2-Mercaptoethanol (β-ME) and protease inhibitors (cOmplete mini tablet, EDTA-free, Roche) right before use. The bacteria pellet was resuspended in 20 ml lysis buffer per 500 ml culture, transferred to 50 ml falcon tubes,

and added 400 µl 50 mg/ml lysozyme stock to 1 mg/ml final concentration. Incubate on ice for 30 min during which pipet up and down 4-5 times. Sonicate to disrupt the cells by using 6 x 10 sec bursts at 200-300W with a 10 sec cooling period between each burst. If the lysate was very viscous, optionally add Benzonase nuclease (Sigma) at the amount of 3 units (U) per ml of original cell culture volume processed. Alternatively, draw the lysates through narrow-gauge syringe needles several times. Centrifuge lysates at 10,000 g, 4°C for 20-30 min to pellet the cellular debris. During centrifugation equilibrate the Ni-NTA matrix (Qiagen) with lysis buffer; 1ml of Ni-NTA slurry (0.5ml bed volume capable of binding 2.5-5 mg protein) was needed per 4 ml cleared lysates. Collect the supernatant and save 20 µl for SDS-PAGE analysis. Add cleared lysates to equilibrated Ni-NTA matrix and mix gently by shaking (200 rpm on a rotary shaker) at 4°C for 60 min. It's important to never vigorously agitate a protein sample: the preferred method of mixing protein solutions was to gently mix using a micro-pipettor with polypropylene tips, but not larger pipettor with polystyrene tips; alternatively, for larger solutions gently invert in a 15 to 50 ml capped polypropylene tube. Also avoid introducing foam or air bubbles as these would denature proteins. Spin down at 1000g for 1 min to collect the beads. Wash with 12 ml wash buffer 4 times by spinning down at 1000g for 1 min and discard the supernatant. The wash buffer was composed of 50 mM NaH_2PO_4, 500 mM NaCl, 10% glycerol and 30 mM Imidazole, and adjusted to pH 7.6. Elute the protein 4-5 times with 1 ml elution buffer by mixing the tube well and gently rotating for 2 min at 4°C. The elution buffer was composed of 50 mM NaH_2PO_4, 500 mM NaCl, 10% glycerol, 250 mM Imidazole and 0.1% (w/v) CHAPS, and adjusted to pH 7.6. Take 20 µl of each eluate and the beads for SDS-PAGE analysis. The eluates were exchanged to SUMO protease buffer using Slide-A-Lyzer cassettes (Thermo

Fisher Scientific) at 4°C overnight, which was coupled with the cleavage step with SUMO Protease 1 added. The SUMO protease buffer was composed of 50 mM NaH_2PO_4, 300 mM NaCl, 10% glycerol, 0.01% (w/v) CHAPS and 1 mM DTT, and adjusted to pH 7.2. Save 20 µl post-cleavage protein samples for SDS-PAGE analysis. The cut 6His-SUMO tag, uncut 6His-SUMO fusion proteins and 6His tagged SUMO Protease 1 in the post-cleavage protein solution were removed by a second round of Ni-NTA affinity chromatography. The required amount of Ni-NTA agarose needed to capture the 6His-tagged contaminants was calculated. Ni-NTA resin was equilibrated with SUMO protease buffer, and mixed gently with dialyzed protein solution. The mixture was incubated for 10 min at 4°C with gentle rotation, and centrifuged at 1000g for 1 min to pellet the resin. The supernatant and beads were collected and subjected to SDS-PAGE analysis (Figure 3.1A).

If the protein was to be used the following day, a part of the protein was dialyzed overnight against 4 L of HBS (25 mM HEPES, 150 mM NaCl, pH 7.4) buffer using Slide-A-Lyzer cassettes (Thermo Fisher Scientific). If the protein concentration became too diluted, Amicon Ultra centrifugal filters (MilliporeSigma) were used to concentrate the proteins. Final eluates with untagged native proteins were at least 95% pure as judged from overloaded Coomassie Blue G-250 stained SDS gels (Figure 3.1A, B). Protein concentrations were determined based on absorbance at 280 nm using calculated extinction coefficients. For long-term storage, the proteins were dialyzed overnight against 1 L of Tris-HCl storage buffer. The storage buffer was composed of 50 mM Tris-HCl, 50 mM NaCl and 25% glycerol (or ethylene glycol), supplemented with 0.02% (w/v) sodium azide (NaN_3, anti-microbial agent), 5 mM TCEP (reducing agent) and 1 mM EDTA (metal

chelator to avoid metal-induced oxidation of -SH groups and help to maintain the protein in a reduced state). Based on protein concentration, aliquot single use amount to sterile Eppendorf (EP) tubes. Snap freeze in liquid nitrogen and store in -80°C freezer. The thawing process should be rapid and placed on ice as a quick freeze and a quick thaw were usually the best practices for retaining protein activities (preventing phase partitioning of the salts/protein). Once thawed, the sample was gently mixed using a micro-pipettor to make sure the solution was homogeneous. Check the protein solution for cloudiness (if the protein solution was found to be cloudy upon thawing, the protein bioactivity was likely to have been adversely affected). Prior to experiments, purified proteins were dialyzed exhaustively in 4 L HBS buffer at 4°C overnight.

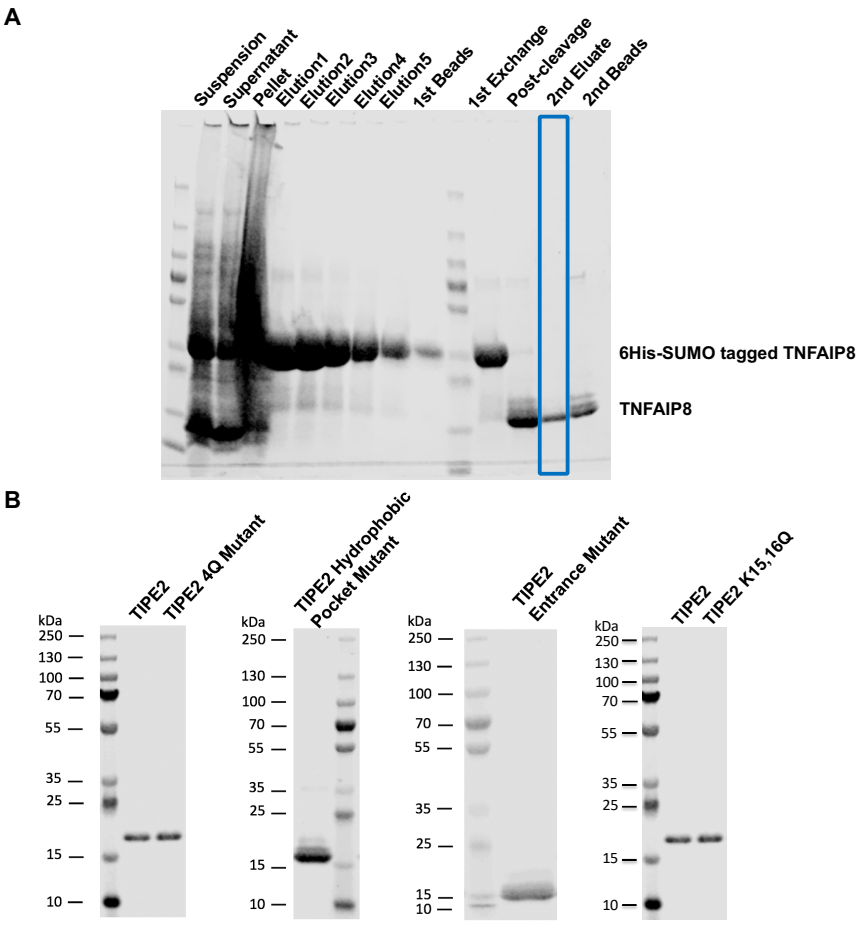

Figure 3.1 Protein purification of TNFAIP8 using pET-SUMO fusion tag system

(A-B) Recombinant 6His-SUMO tagged TNFAIP8 (A), TIPE2 and mutants (B) were expressed from *Escherichia coli* (*E. coli*) BL21(DE3) and purified using Ni-NTA resin. 6His-SUMO tagged proteins were eluted with 250 mM Imidazole from beads, followed by cleavage with SUMO Protease 1. The 6His-SUMO fusion proteins and 6His tagged SUMO Protease 1 after cleavage were removed by affinity chromatography on a second Ni-chelating resin. Untagged native proteins were eluted, separated by SDS-PAGE and stained with Coomassie Blue G-250. Purified proteins (A, B) were at least 95% pure judging from overloaded Coomassie Blue stained SDS gels.

3.2.3 Phosphoinositide binding assay

Sedimentation-based phosphoinositide binding assays were performed as previously described (Fayngerts et al., 2017, 2014). Dioleoylphosphatidylcholine (DOPC) and brominated distearoyl PC (brominated PC) were purchased from Avanti Polar Lipids. PtdIns(4,5)P_2 and PtdIns(3,4,5)P_3 were purchased from CellSignals. Purified trypsin inhibitor of *Glycine max* (soybean) (Sigma-Aldrich) was used as a control protein. The following small unilamellar vesicles (SUVs) were used at a concentration of 2 mM (1 mM available lipids for binding): (i) 10% PtdIns(4,5)P_2 + 10% DOPC + 80% brominated PC, (ii) 10% PtdIns(3,4,5)P_3 + 10% DOPC + 80% brominated PC, or (iii) 20% DOPC + 80% brominated PC. Proteins were used at a concentration of 5 μM. Samples were incubated 1 h at room temperature (RT), and subjected to ultracentrifugation as described (Kavran et al., 1998; A. Lee & Lemmon, 2001; Tortorella & London, 1994). The relative amount of proteins in supernatant and pellet was determined by Coomassie Blue G-250 staining of SDS-PAGE gels containing the resolved proteins.

3.2.4 Phosphoinositide extraction and transfer assays

The small unilamellar vesicles (SUVs) were produced and sedimentation-based phosphoinositide extraction and transfer assays were performed as previously described (Fayngerts et al., 2017). Recombinant TNFAIP8, Entrance mutant and PLCδ-PH were expressed from *Escherichia coli* BL21(DE3) cells (Agilent) and purified using Ni-NTA

Agarose (Qiagen). For the sedimentation-based PtdIns(4,5)P_2 extraction assay, 100 μM SUVs composed of 10% BODIPY FL PtdIns(4,5)P_2 in DOPC background with or without 10% unlabeled PtdIns(4,5)P_2 or PtdIns(3,4,5)P_3 were mixed with 10 μM purified trypsin inhibitor, PLCδ-PH or TNFAIP8, incubated for 1 h at room temperature, and centrifuged as described (Kavran et al., 1998; A. Lee & Lemmon, 2001). In sedimentation-based PC extraction assay, 100 μM SUVs composed of 10% BODIPY FL PC with 10% unlabeled PtdIns(3,4,5)P_3 were mixed with 10 μM purified TNFAIP8 or Entrance mutant, incubated 1 h at room temperature, and centrifuged as described above. The fluorescence intensity of supernatant (corresponding to BODIPY FL PtdIns(4,5)P_2 or BODIPY FL PC extraction) was detected using Infinite 200 Pro fluorescence plate reader (Tecan). In sedimentation-based PtdIns(4,5)P_2 transfer assay, supernatant generated in TNFAIP8 sedimentation-based PtdIns(4,5)P_2 extraction assay was mixed with 500 μM 100% PC SUVs or HBS buffer alone, incubated for 1 h at room temperature, and centrifuged as described. The fluorescence intensity of supernatant (corresponding to soluble TNFAIP8-BODIPY FL PtdIns(4,5)P_2) was detected as above.

3.2.5 Surface Plasmon Resonance (SPR) assay

SPR assays were carried out using a BIAcore T200 instrument (GE Healthcare). Briefly, the surface of L1 sensor chip was cleaned by a 5 min injection of 40 mM octyl D-glucoside at a flow rate of 5 μl/min. Vesicles containing DOPC alone, 3% or 10% (mole/mole) of PtdIns(4,5)P_2 or PtdIns(3,4,5)P_3 were generated through 50 nm NanoSizer Liposome Extruders (T&T Scientific). Vesicles were immobilized on L1 sensor chip

surface, resulting in a signal of around 6500 to 8500 resonance units (RUs). Purified test proteins were injected over the surface at five or more sequentially diluted concentrations, at a flow rate of 3 μl/min. All experiments were performed at 25˚C in HBS buffer (pH 7.4). The sensorgrams were recorded during the association and disassociation, and were analyzed using BIAevaluation software (GE Healthcare). SPR signals were corrected for background (DOPC) binding, and a binding isotherm was generated from equilibrium response (R_{eq}) versus the concentration (C) of proteins. The equilibrium dissociation constant (K_D) was derived from steady-state affinity analysis by nonlinear least-squares fitting of the binding isotherm using the equation $R_{eq}=R_{max}/(1+K_D/C)$. The percentage of maximal binding was determined at each protein concentration as equilibrium response divided by the maximum response measured at saturation.

3.2.6 PI3K enzymatic assay

PI3K-mediated phosphorylation of PtdIns(4,5)P_2 was measured by determining ATP consumption using the ADP-Glo Lipid Kinase Assay Kit (Promega) according to the manufacturer's instructions. Reaction buffer consisted of 0.4 nM PI3K (p110α/p85α), 50 μM phosphatidylserine + PtdIns(4,5)P_2 (at 3:1 ratio), 25 μM ATP, and different concentrations of TNFAIP8 protein. 2 μM BSA was used as a negative control protein. Control experiment without phospholipid substrates showed only background level of ATP consumption. PI3K-catalyzed generation of PtdIns(3,4,5)P_3 was determined at 60 min after reaction initiation, and the value in the absence of TNFAIP8 protein was set to 1.

3.2.7 F-actin depolymerization assay

Small unilamellar vesicles (SUVs) were produced as described (Fayngerts et al., 2017; Kavran et al., 1998; A. Lee & Lemmon, 2001). Actin Polymerization Biochem Kit (Cytoskeleton) was used to investigate F-actin depolymerization by cofilin in the absence or presence of control protein BSA, TNFAIP8, TIPE2, and SUVs containing 10% PtdIns(4,5)P_2, 10% PtdIns(3,4,5)P_3 or 10% PtdIns(4,5)P_2 plus 10% PtdIns(3,4,5)P_3, according to the manufacturer's protocol with minor modifications. 2 mM SUVs (1 mM total available lipids) were pretreated with 11 μM control protein BSA or TNFAIP8/TIPE2 protein for 1 h; then 11 μM cofilin was added to each reaction and incubated for 20 min. In addition, 11 μM cofilin was also incubated with 11 μM TIPE2 or BSA for 20 min (control reactions). Pyrene-labeled F-actin stock was diluted with General Actin Buffer containing 25 mM Tris-HCl (pH 8.0) and 0.2 mM $CaCl_2$ to the concentration of 0.1 mg/ml. For each sample, 100 μl of diluted pyrene-labeled F-actin stock was used. The fluorescence signals were detected by Infinite 200 Pro fluorescence plate reader (Tecan). The fluorescence were measured immediately before and after adding 10 μl of one of the following reagents: (a) BSA (22 μM), (b) cofilin (11 μM) + BSA (11 μM), (c) cofilin (11 μM) + TNFAIP8/TIPE2 (11 μM), (d) cofilin (11 μM) + BSA (11 μM) + SUVs, (e) cofilin (11 μM) + TNFAIP8/TIPE2 (11 μM) + SUVs, or (f) vehicle (i.e., 25 mM HEPES, 150 mM NaCl, pH 7.5). The experiments were performed in duplicates or triplicates. The fluorescence measurements of each sample before adding the above reagents were set as 100%. The curves were fitted to one-phase exponential decay equations (GraphPad Prism) to assess the degree/span of F-actin depolymerization, which was calculated as differences

in fluorescence before and after adding the above reagents for each sample. Additionally, results were also presented as the differences in the remaining F-actin over a period of time. TNFAIP8 or TIPE2 alone did not affect F-actin depolymerization, which was not shown.

3.2.8 Re-expression of proteins in knockout cells by lentivirus infection

Expression constructs were transfected into Lenti-X 293T cells (Clontech) using Lipofectamine 3000 reagent (Thermo Fisher Scientific) following the manufacturer's protocol. Lentivirus was produced by co-transfecting pGL-LU-TNFAIP8/TIPE2-EGFP, pGL-LU-mutants-EGFP or FUGW expression vectors with 3rd generation lentiviral packaging plasmids (pRSV-Rev, pCMV-VSV-G, and pMDLg/pRRE). Two batches of lentivirus-containing medium were harvested 24 h and 52 h after transfection, followed by filtering through a 0.45 μm Steriflip PVDF membrane (MilliporeSigma). Lentivirus was concentrated 100-fold using Lenti-X Concentrator (Clontech), and titrated by RT-qPCR Titration Kit (Clontech) as well as EGFP-positive cell counts. Transduction was performed by incubating cells with medium containing the lentivirus at a multiplicity of infection (MOI) of 10-100 in the presence of 4 μg/ml Polybrene (Sigma) for 12-24 h. The amount of lentivirus used was titrated and adjusted to ensure the levels of overexpressed proteins were similar to the endogenous levels in HL-60 cells or murine $CD4^+$ T cells. Cells were allowed to recover in complete medium for 24 h and then isolated by fluorescence activated cell sorting (FACS) before being used for experiments.

3.2.9 Transmigration assay of $CD4^+$ T cells

$CD4^+$ T cells were purified from mouse spleens using Invitrogen negative selection beads, and stimulated with 1 μg/ml anti-CD3 (Clone 2C11, eBioscience) and 1 μg/ml anti-CD28 (Clone 37.15, Biolegend) for 2 days. The cells were rested for 2-3 days in complete RPMI culture medium containing 10% FBS, 1% L-glutamine, 1% Penicillin-Streptomycin, and 10 ng/ml IL-2 (Invitrogen). The chemotaxis assay was performed using 96-well Neuro Probe ChemoTx Transwell with 3 μm pore size (Neuro Probe) according to manufacturer's protocol. Briefly, the bottom wells were filled with 30 μl of assay buffer with or without 100 ng/ml CCL21, and $CD4^+$ T cells were added to the upper wells pre-coated with 15 μg/ml Fibronectin (Sigma). After incubation at 37°C for 1 h, migrated cells collected from the bottom wells were quantified using a cell counter. For migration assay with $CD4^+$ T cells expressing TIPE2 or TIPE2 Entrance mutant, DKO $CD4^+$ T cells were electroporated using the cell-type specific Nucleofector Kit (Lonza), with TIPE2- or Entrance mutant-expressing plasmid 24 h before the migration assay.

3.3 Results

3.3.1 TNFAIP8 interacts with phosphoinositides and can act as a transfer protein of lipid second messengers

For more quantitative biochemistry assays, the purification of TNFAIP8 and other proteins was optimized using Ni-chelating affinity chromatography (Figure 3.2A). The protein quality and frozen storage procedure were assessed by dynamic light scattering (DLS). Purified proteins were dialyzed in Tris buffer containing 25% glycerol and were flash frozen. After thawing and dialysis in HBS buffer, the size distribution of the hydrodynamics radius of molecules in solution was measured by DynaPro NanoStar instrument (Figure 3.2B). A single, narrow peak at a size corresponding to the TNFAIP8 protein suggests it stable as monomer (Figure 3.2B).

TIPE family has been shown to predominantly interact with PtdIns(3,4)P_2, PtdIns(3,5)P_2, PtdIns(4,5)P_2 and PtdIns(3,4,5)P_3 through protein-lipid overlay assay (Fayngerts et al., 2014). To determine if this lipid-protein interaction is also true in the model lipid bilayer, a sedimentation-based binding assay (Kavran et al., 1998; A. Lee & Lemmon, 2001; Tortorella & London, 1994) was done by mixing purified TNFAIP8 protein with small unilamellar vesicles (SUVs). If the protein binds to these liposomes, which can be precipitated by ultracentrifuge, it would be detected in the pellet fraction rather than in the supernatant. These SUVs were made to contain 10% PtdIns(4,5)P_2 or 10% PtdIns(3,4,5)P_3 in a phosphatidylcholine (PC) background. We found TNFAIP8 protein sediment efficiently with SUVs containing 10% phosphoinositides. By contrast,

only background level sedimented with 100% PC, and a negative control protein trypsin inhibitor exhibited no binding to either type of vesicles (Figure 3.3A).

Next, we used Surface Plasmon Resonance (SPR) for real-time, label-free detection of biomolecular interactions (Beseničar et al., 2006; Homola et al., 1999). Supported lipid bilayer was immobilized on a L1 chip by flowing 50 nm extruded SUVs containing DOPC and 3 or 10 mol% of PtdIns(4,5)P_2 (Figure 3.3B) or PtdIns(4,5)P_3 (Figure 3.3C). The steady-state equilibrium dissociation constants (K_D) of human TNFAIP8 isoform b protein to PtdIns(4,5)P_2 and PtdIns(3,4,5)P_3 were 3.16 and 4.06 μM, respectively (Figure 3.3B, C), suggesting that TNFAIP8 bound to these lipids with medium affinities.

TIPE2 has been reported to be a carrier protein of both PtdIns(4,5)P_2 and PtdIns(3,4,5)P_3 (Fayngerts et al., 2017), but whether TNFAIP8 can act on these lipid second messengers is unknown. Phosphoinositide-extraction assay showed that when TNFAIP8 was incubated for 1 h with 100 μM vesicles containing 10% BODIPY FL PtdIns(4,5)P_2 and 10% PtdIns(3,4,5)P_3, increased amount of BODIPY FL PtdIns(4,5)P_2 fluorescence was detected in the supernatant after ultracentrifugation, whereas equivalent experiments with trypsin inhibitor or PLCδ-PH domain showed no significant fluorescence in the supernatant (Figure 3.4A). This result suggests that TNFAIP8 can effectively remove fluorescence labeled PtdIns(4,5)P_2 from the SUVs and solubilize it in the supernatant. In addition, the ability of extraction was compromised by the TNFAIP8 Entrance mutant (with H86, R87, K103 laying in the opening of the hydrophobic cavity mutated to Qs) (Figure 3.4B). It is important to note that this was specific to BODIPY FL PtdIns(4,5)P_2

vesicles, as neither TNFAIP8 nor Entrance mutant was able to extract BODIPY FL PC from 100 μM vesicles containing 20% BODIPY FL PC as control (Figure 3.4B).

To explore if TNFAIP8 was capable of inserting extracted PtdIns(4,5)P_2 into a lipid bilayer, we analyzed the transfer of BODIPY FL PtdIns(4,5)P_2 from the soluble TNFAIP8/ BODIPY FL PtdIns(4,5)P_2 complexes detected in the supernatant in Figure 3.4A to 100% PC vesicles. We collected supernatant from the mixture of TNFAIP8 with 100 μM BODIPY FL PtdIns(4,5)P_2-containing vesicles that had been subjected to ultracentrifugation, and incubated them with vesicles containing 500 μM 100% PC for 1 h. The mixture was then recentrifuged, and the level of BODIPY FL PtdIns(4,5)P_2 fluorescence remaining in the supernatant was measured. Addition of 100% PC vesicles led to a substantial decrease in fluorescence (corresponding to the presumed TNFAIP8/BODIPY FL PtdIns(4,5)P_2 complexes in the supernatant) (Figure 3.4C). The concomitant loss of BODIPY FL PtdIns(4,5)P_2-derived fluorescence from the supernatant was not accompanied by changes in TNFAIP8 protein concentrations in the supernatant (Figure 3.4D), suggesting that TNFAIP8 had transferred the BODIPY FL PtdIns(4,5)P_2 to the PC vesicles.

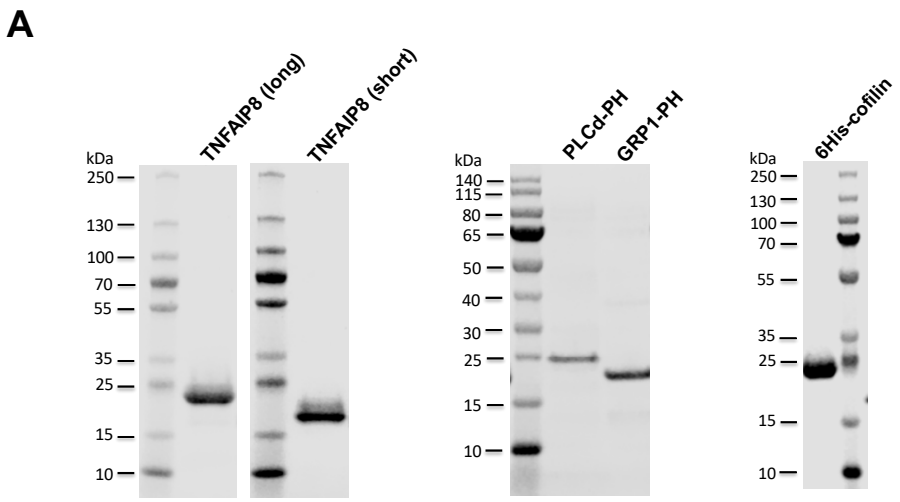

B

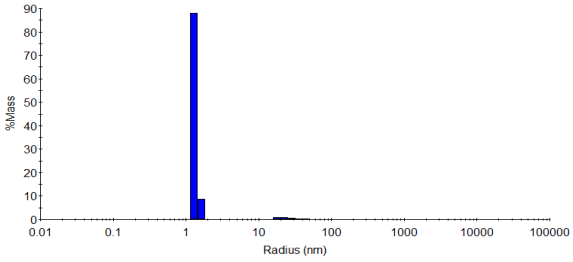

Cumulant fit			
Radius (nm)	%PD	Baseline	SOS
32.3	18.5	1	7.971
Regularization fit			
Peak	Radius (nm)	%PD	%Mass
Peak 1	1.3	7.5	96.8
Peak 2	27.1	41.52	3.2

Figure 3.2 Protein purification and frozen storage assessed by dynamic light scattering (DLS)

(A) Recombinant 6His-SUMO tagged TNFAIP8, PH domains and 6His-cofilin were purified from BL21(DE3) *E. coli* using Ni-NTA resin and were at least 95% pure judging from overloaded Coomassie Blue stained SDS gels. (B) Purified TNFAIP8 protein was dialyzed in Tris buffer containing 25% glycerol and was flash frozen. After thawing and dialysis in HBS buffer, the size distribution of the hydrodynamics radius of molecules in solution was measured by DynaPro NanoStar (Wyatt Technology). Data represent at least three independent experiments with similar results.

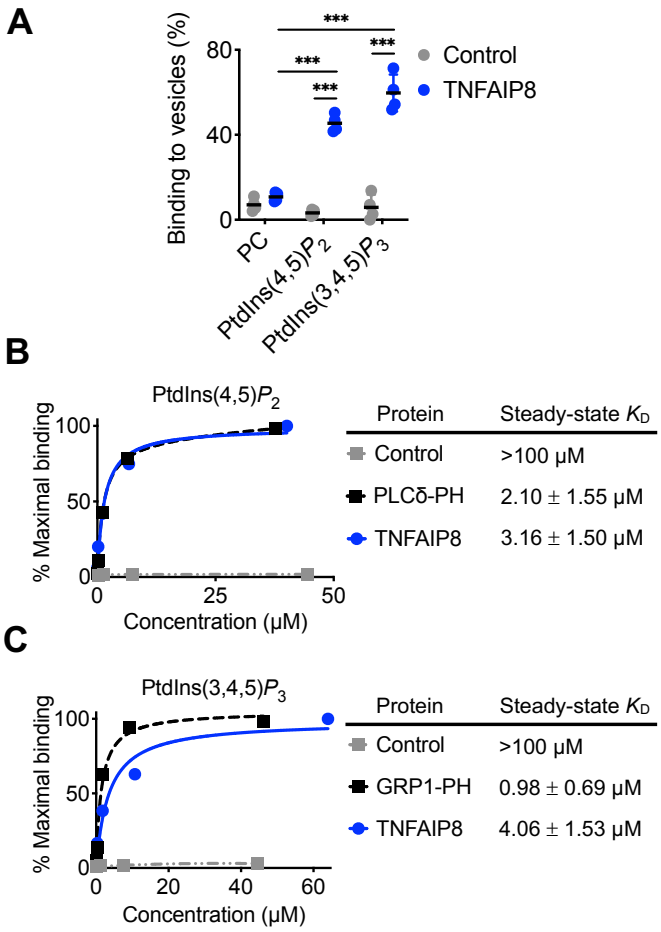

Figure 3.3 TNFAIP8 can bind to PtdIns(4,5)P_2 and PtdIns(3,4,5)P_3 present in small unilamellar vesicles (SUVs)

(A) Sedimentation-based phosphoinositide binding assay showing the proportion of TNFAIP8 and control protein trypsin inhibitor bound to SUVs containing 100% PC, 10% PtdIns(4,5)P_2 or 10% PtdIns(3,4,5)P_3. (B, C) SPR analysis of TNFAIP8 binding to DOPC membranes containing 10% (mole/mole) PtdIns(4,5)P_2 (B) or PtdIns(3,4,5)P_3 (C) on L1 sensor chip. Purified PLCδ-PH and GRP1-PH domains were used as positive controls, and trypsin inhibitor as a negative control. The percentage of maximal binding (left panel) and equilibrium K_D (right panel) are shown. ***$P < 0.001$ (Student's *t*-test (A)). The values are mean ± s.d. (A-C). Data are pooled from four (A) independent experiments, or represent three (B, C) independent experiments.

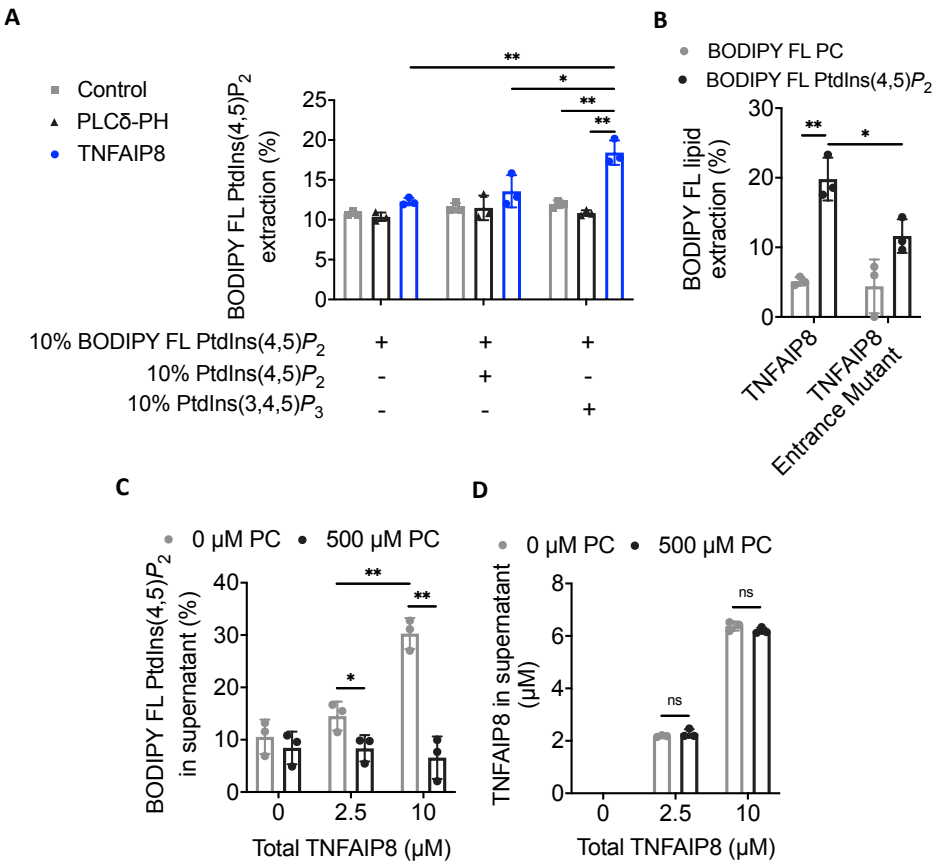

Figure 3.4 TNFAIP8 can function as a phosphoinositide transfer protein

(A) Phosphoinositide-extraction assay showing the proportion of PtdIns(4,5)P_2 (labeled with the fluorescent dye BODIPY) extracted from SUVs containing 10% BODIPY FL PtdIns(4,5)P_2 with (+) or without (-) 10% unlabeled PtdIns(4,5)P_2 or PtdIns(3,4,5)P_3 (grid beneath plot), in the presence of trypsin inhibitor (Control), PLCδ-PH or TNFAIP8 (key). FIU, fluorescence intensity units. (B) Phosphoinositide-extraction assay was used to determine the percentages of BODIPY FL PtdIns(4,5)P_2 extracted from 100 μM 20% BODIPY FL PtdIns(4,5)P_2 vesicles and the percentages of BODIPY FL PC extracted from 100 μM 20% BODIPY FL PC vesicles in the presence of 10% unlabeled PtdIns(3,4,5)P_3, and transferred to supernatant by TNFAIP8 or Entrance mutant. (C, D)

The sedimentation-based transfer assay showing the depletion of BODIPY FL PtdIns(4,5)P_2 from soluble TNFAIP8-BODIPY FL PtdIns(4,5)P_2 in supernatant (C) and fractions of TNFAIP8 remaining in supernatant (D) after incubation with buffer alone or 100% PC vesicles. Proteins were used at a concentration of 10 μM. ns, not significant; *$P < 0.05$; **$P < 0.01$ (unpaired Student's *t*-test). The experiments were repeated at least two times with similar results (mean ± s.d.).

3.3.2 TIPE family can regulate PtdIns(4,5)P_2-dependent signaling and actin remodeling through phosphoinositide-binding proteins

To further investigate the actions of TNFAIP8 at the leading edge, we studied the functional significance of TNFAIP8 interactions to phosphoinositides. TIPE2 has been reported to be able to act as an "enhancer" for PI3Ks (Fayngerts et al., 2017). To determine if TNFAIP8 could also promote the activity of PI3Ks, an ADP-Glo PI3K assay was performed with increasing concentrations of TNFAIP8 protein or 2 μM BSA as control. Addition of TNFAIP8 to the PI3K (p110α/p85α) significantly potentiated PtdIns(3,4,5)P_3 generation in a dose-dependent manner (Figure 3.5). The protein concentration needed to increase PI3K activity by 2-fold was estimated to be in the range of 500-600 nM (Figure 3.5).

To understand the impact of TNFAIP8 binding to phosphoinositides on cofilin activity, we tested cofilin-mediated F-actin depolymerization in the presence or absence of purified TNFAIP8 and phosphoinositides. SUVs containing either PtdIns(4,5)P_2 or PtdIns(4,5)P_2 plus PtdIns(3,4,5)P_3 significantly decreased cofilin-induced F-actin depolymerization (Figure 3.6). TNFAIP8 could best rescue the reduction in F-actin depolymerization caused by SUVs containing both PtdIns(4,5)P_2 and PtdIns(3,4,5)P_3, while TNFAIP8 or control protein alone had no effect on F-actin depolymerization (Figure 3.6). These results indicate that the ability of TNFAIP8 to interact with phosphoinositides impacts cofilin-induced F-actin remodeling. Consistently, TIPE2 showed similar effects by this actin depolymerization biochemistry assay (Figure 3.7), suggesting that TIPE

family could regulate phosphoinositide-dependent signaling at the leading edge of migratory cells.

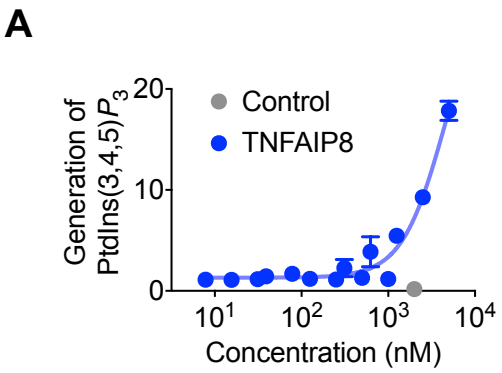

Figure 3.5 The effects of TNFAIP8 on PtdIns(3,4,5)P_3 generation by PI3Ks

(A) Phosphorylation of PtdIns(4,5)P_2 by PI3Ks as measured in the ADP-Glo kinase assay, in the presence of increasing concentrations of TNFAIP8 protein or 2 μM BSA (Control). Data represent mean ± s.e.m. of two independent experiments done in duplicates.

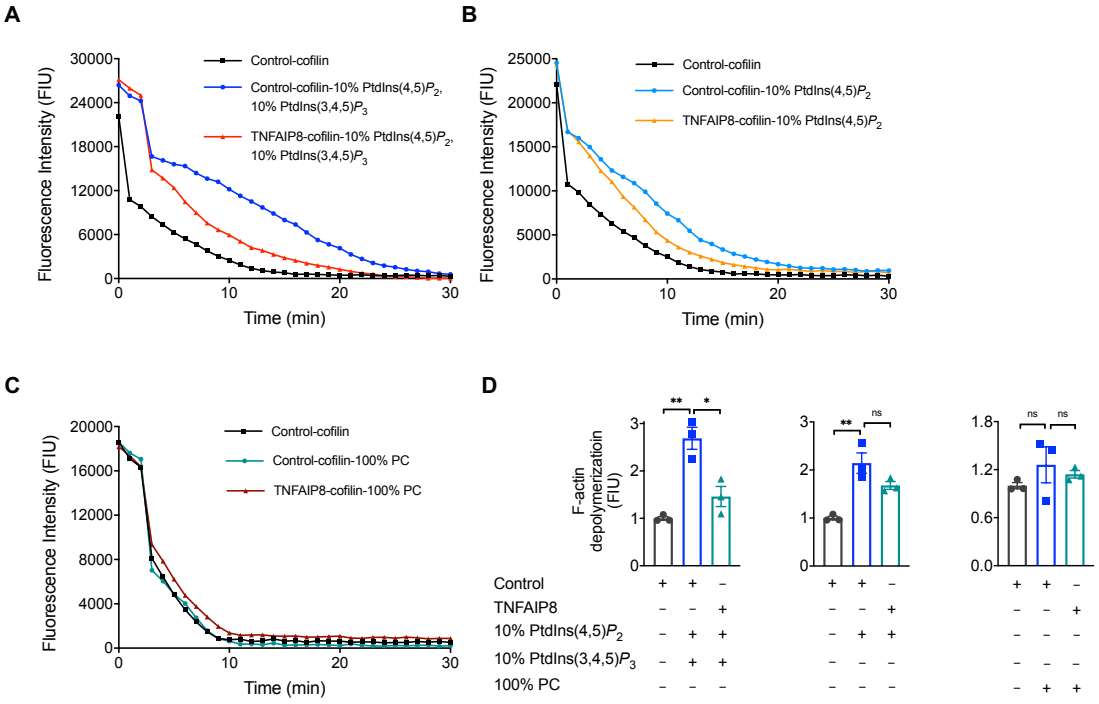

Figure 3.6 The effect of the interaction of TNFAIP8 with phosphoinositides on cofilin-dependent depolymerization of F-actin

(A-C) Representative time course of cofilin-dependent F-actin depolymerization performed in the presence or absence of control protein (A-C), TNFAIP8 (A-C), small unilamellar vesicles (SUVs) containing 10% PtdIns(4,5)P_2/10% PtdIns(3,4,5)P_3 (A), 10% PtdIns(4,5)P_2 (B) or 100% PC (C). Data is shown as the difference in pyrene labeled F-actin fluorescence intensity units (FIU) over the indicated time. (D) Quantification of cofilin-dependent F-actin depolymerization in the presence of various combinations of control protein or TNFAIP8 plus SUVs containing 10% PtdIns(4,5)P_2 with or without PtdIns(3,4,5)P_3 or 100% PC (grid beneath plot). ns, not significant; *$P < 0.05$; **$P < 0.01$ (unpaired Student's *t*-test). Data represent mean ± s.d. of three independent experiments (A-D).

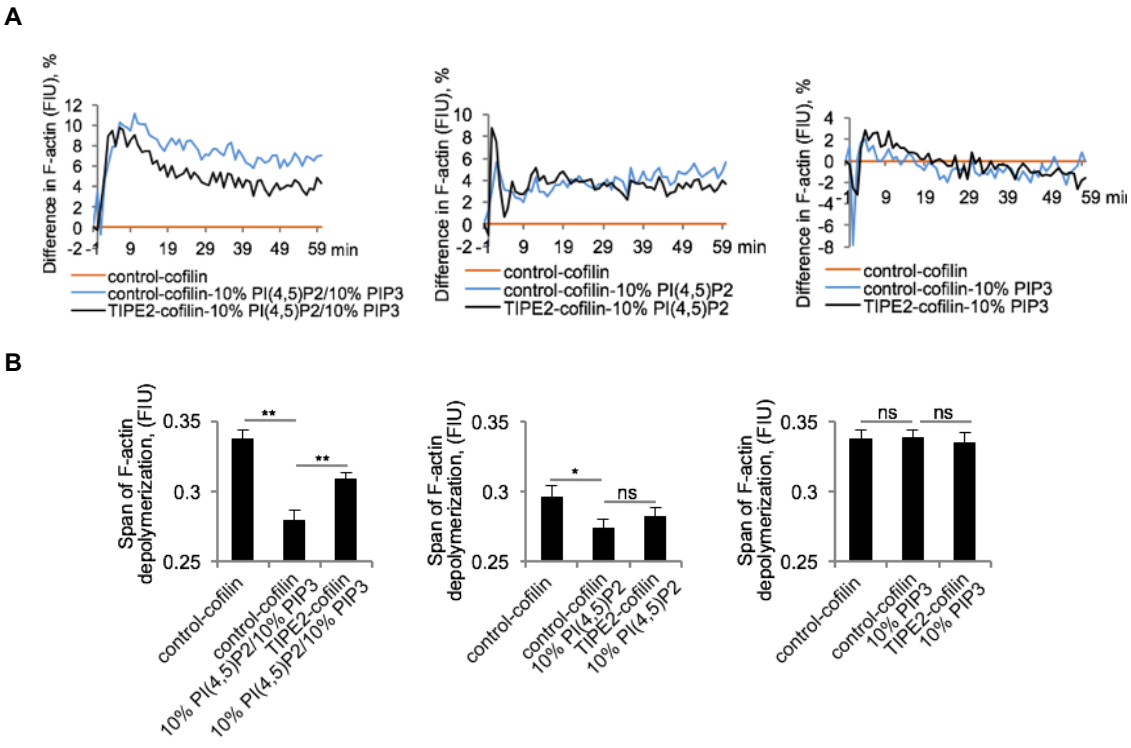

Figure 3.7 The effect of TIPE2 binding to phosphoinositides on cofilin-dependent F-actin depolymerization

(A) Time course of cofilin-dependent F-actin depolymerization performed in the presence or absence of control protein, TIPE2, SUV containing 10% PtdIns(4,5)P_2/10% PtdIns(3,4,5)P_3 (left panel), SUV containing 10% PtdIns(4,5)P_2 (middle panel) or SUV containing 10% PtdIns(3,4,5)P_3 (right panel). Results are shown as the difference in the remaining F-actin over the indicated time between samples containing control protein and samples containing control protein + SUV or TIPE2 + SUV. (B) The degree of cofilin-dependent F-actin depolymerization in the presence of control protein, control protein + SUV, or TIPE2 + SUV was analyzed as described above. FIU, fluorescence intensity units. ns, not significant; *$P < 0.05$; **$P < 0.01$ (unpaired Student's *t*-test). The experiments were repeated three times (mean ± s.e.m.).

3.3.3 TH domain and α0 helix of TNFAIP8 are important for its phosphoinositides interactions

The high-resolution crystal structures of murine Tnfaip8 C165S mutant, human TIPE2 and human TIPE3 have recently been resolved (Fayngerts et al., 2014; J.-S. Kim et al., 2017; D. Lee et al., 2014; X. Zhang et al., 2008), and they reveal a conserved TIPE homology (TH) domain composed of a large hydrophobic central cavity. To test the importance of the hydrophobic pocket in lipid binding capacity, we compared the protein topographies of these crystal structures. CASTp 3.0 program analytically identifies and measures the surface accessible pockets as well as interior inaccessible cavities for proteins and other molecules (A. Binkowski et al., 2006; T. A. Binkowski, Naghibzadeh, & Liang, 2003; C. Chen, Tian, Lei, Liang, & Zhao, 2018). The area and volume of the cavity of murine Tnfaip8 C165S mutant is 580 and 406 SA (solvent accessible surface, or Richards' surface), respectively (Figure 3.8A). The 41 wall residues comprising the cavity were shown in the stick model and highlighted in blue in the sequence annotation panel (Figure 3.8A). Among them, three positively charged amino acids H86, R87, K103 (highlighted in purple rectangles, Figure 3.8A) lay in the opening of the cavity and were mutated to Qs for TNFAIP8 Entrance mutation. The 31 hydrophobic amino acids comprising the pocket of murine Tnfaip8 C165S mutant were compared to all wall residues of human TIPE2 and human TIPE3 cavities, and identical or similar amino acids in the corresponding positions were identified and indicated (Figure 3.8B). Four representative conserved amino acids

L44 (α1 helix), L65(α2 helix), L99(α3 helix), L158 (α5 helix) were selected to mutate to the much bulkier Ws for Hydrophobic Pocket mutation.

It has been shown previously that the positively charged residues of α0 helix of TIPE2 protein contributed to its interaction with phosphoinositides, and may function as a flexible lid of the cavity (Fayngerts et al., 2017). We generated murine TNFAIP8 isoform 1 2Q (K41,42Q) mutant, in which lysines 41 and 42 in the α0 helix were replaced with glutamines (the corresponding positions in TIPE2 K15,16Q mutant). We also mutated two additional lysines 46 and 50 in the α0 helix to construct the 4Q mutant (Figure 3.9A). We constructed all the mutants to pET-SUMO and expressed in BL21(DE3) *E. coli*, and found TNFAIP8 L44W, L65W and L99W mutant were expressed at much lower levels judging from crude lysates (data not shown) and 1st elution, compared to TNFAIP8 2Q, 4Q, Entrance and L158W mutant, which led to impure protein after 2nd elution using SUMO fusion tag system (Figure 3.9A). These results indicate that the hydrophobic cavity formed by TH domain is important for the structural integrity/stability of TNFAIP8 protein. TNFAIP8 4Q, Entrance and L158W mutant were successfully purified, and were used for subsequent experiments (Figure 3.9B).

Through protein-lipid overlay assay, binding of purified 6His-SUMO tagged TNFAIP8, 4Q, Entrance, and L158W mutant proteins to lipids spotted on strips was determined by immunoblot using antibody against 6His-tag (Figure 3.10A). Consistently, we found TNFAIP8 predominantly interact with PtdIns(4,5)P_2 and PtdIns(3,4,5)P_3 out of the five lipids spotted (Figure 3.10A). TNFAIP8 4Q and Entrance mutant exhibited marked reductions in phosphoinositides binding, while L158W mutation almost abolished the

ability to bind phosphoinositides (Figure 3.10A, B). On a L1 SPR sensor chip, we found murine TNFAIP8 isoform 1 protein exhibit a steady-state K_D of 4.06 μM and 3.80 μM to PtdIns(4,5)P_2 and PtdIns(3,4,5)P_3, respectively (Figure 3.11 and Table 4). The TNFAIP8 4Q, Entrance and L158W mutant compromised the binding affinity by 3 to 7-fold (Figure 3.11 and Table 4). These results indicate that α0 helix and TH domain are important for the ability of TNFAIP8 protein to recognize and interact with PtdIns(4,5)P_2 and PtdIns(3,4,5)P_3 present in lipid bilayers.

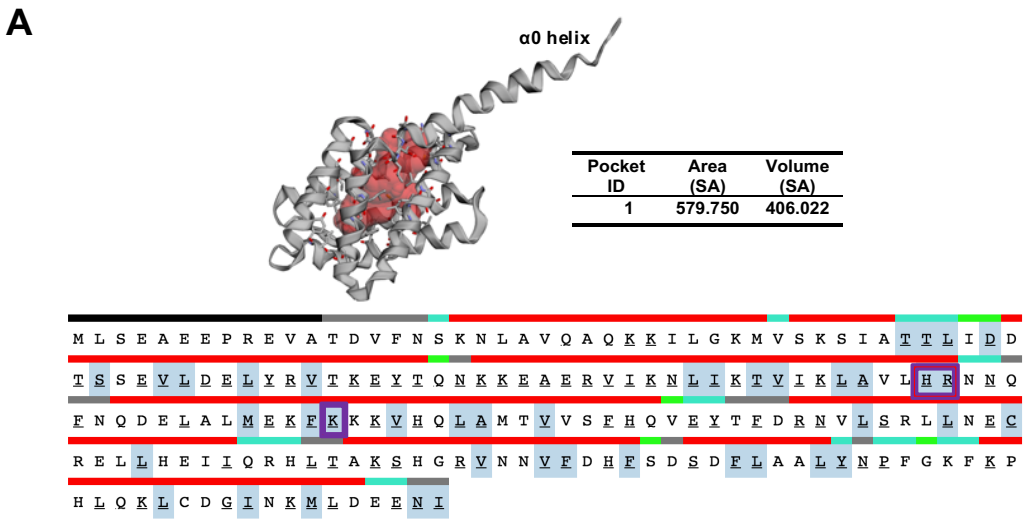

B

	mTNFAIP8 (isoform b)	Human TIPE2	Human TIPE3
	L32		○
α1	V40	○	○, I
	L41	○	○, F
	L44	○	○
	V47	○	
α2	L65	○	○
	I66	○	
	V69	○, A	○, A
	L72	○, V	○, I
	A73	○	○, G
α3	M89	○, A	○, V
	F92	○	○
	V96	○, L	○, L
	L99	○, G	
	A100	○	○
	V103	○, A	○, I

	mTNFAIP8 (isoform b)	Human TIPE2	Human TIPE3
α4	L118	○	○
	L122	○	○
	L129	○	○, V
α5	V145	○, I	○, I
	V148	○	○
	F149	○	○
	F152	○	○
	F157	○, L	○
	L158	○	○
	L161	○	○
	Y162	○	○
α6	L175	○, I	○, I
	I179	○, L	○
	M182	○, L	○, L
	I188	○, L	○, L

Figure 3.8 Structural analysis and mutagenesis of TNFAIP8 protein

(A) Protein topography of the crystal structure of murine Tnfaip8 C165S mutant was analyzed by CASTp 3.0. The wall residues comprising the pocket (red) were shown in the stick model (in the graph) and highlighted in blue (in the sequence annotation panel). Red bars in the sequence annotation panel represent alpha-helixes. Three positively charged amino acids H86, R87, K103 (highlighted in purple rectangles) were positioned at the opening of the cavity. (B) Protein topography of the crystal structures of murine Tnfaip8 C165S, human TIPE2, human TIPE3 were compared by CASTp 3.0. The 31

hydrophobic amino acids out of all the wall residues comprising the pocket of murine Tnfaip8 C165S mutant were listed. Identical (represented by circles) or similar amino acids in the corresponding positions of human TIPE2 and TIPE3 were indicated. Four representative conserved amino acids L44 (α1), L65(α2), L99(α3), L158 (α5) were selected to mutate to Ws for Hydrophobic Pocket mutation.

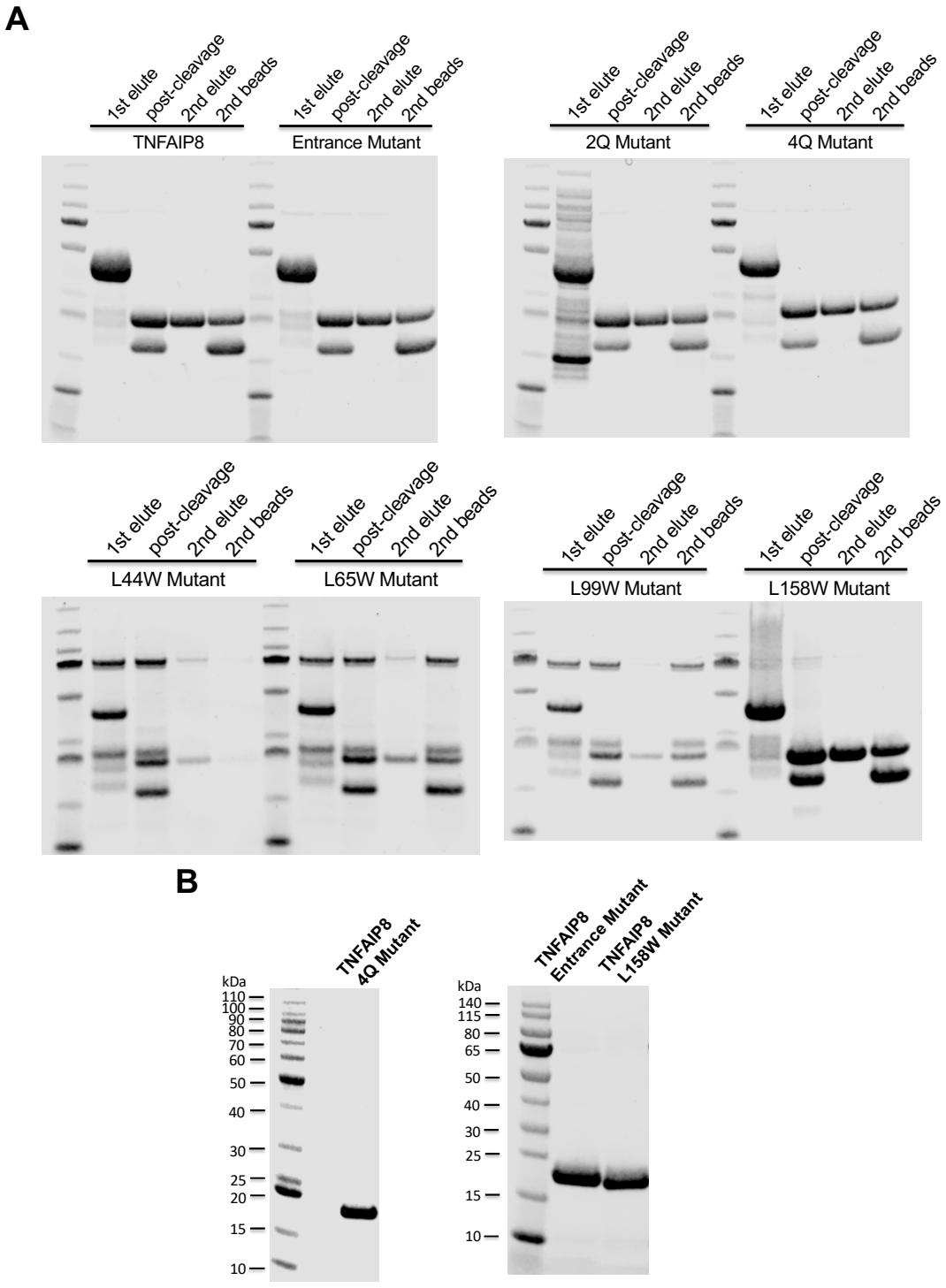

Figure 3.9 Expression and purification of TNFAIP8 mutant proteins

(A) TNFAIP8 L44W, L65W and L99W mutant were expressed at much lower levels compared to TNFAIP8 2Q, 4Q, Entrance and L158W mutant, which led to impure protein after 2nd elution using pET-SUMO fusion tag system. (B) TNFAIP8 4Q, Entrance and L158W mutant were purified from BL21(DE3) *E. coli* using Ni-NTA resin and were at least 95% pure judging from overloaded Coomassie Blue stained SDS gels.

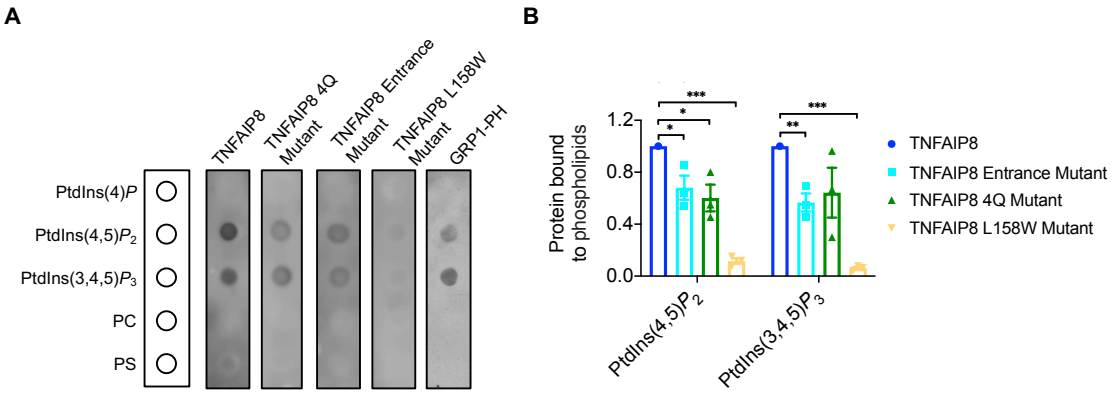

Figure 3.10 TNFAIP8 interacts with phosphoinositides through its TH domain

(A, B) Binding of purified 6His-SUMO tagged TNFAIP8, TNFAIP8 4Q, TNFAIP8 Entrance, and TNFAIP8 L158W mutant proteins to lipids spotted on strips by protein-lipid overlay assay. Immunoblot was performed using antibody against 6His-tag. Signal from wild-type TNFAIP8 was set as 1. **P* < 0.05; ***P* < 0.01; ****P* < 0.001 (unpaired Student's *t*-test). Data represent mean ± s.e.m. of three independent experiments.

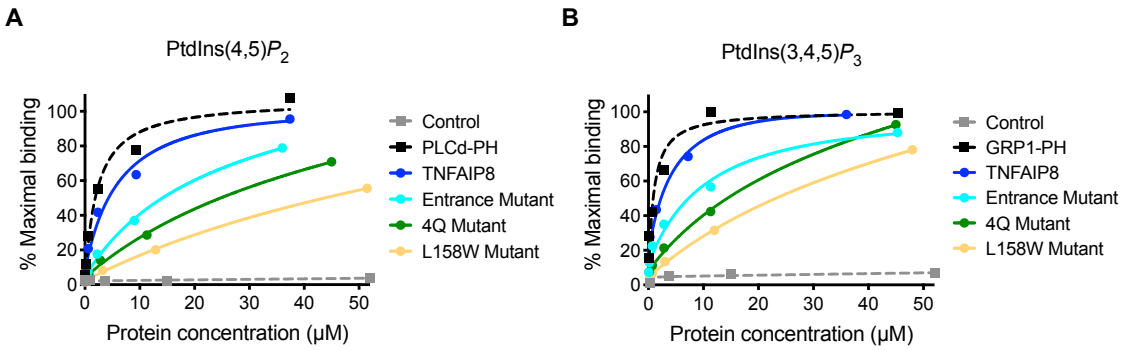

Figure 3.11 SPR analysis of TNFAIP8 mutants

(A, B) SPR analysis of the binding of murine TNFAIP8 isoform 1 and the indicated mutants to DOPC membranes containing 3% (mole/mole) PtdIns(4,5)P_2 (A) or PtdIns(3,4,5)P_3 (B) on L1 sensor chip. Purified PLCδ-PH and GRP1-PH domains were used as positive controls, and trypsin inhibitor as a negative control (Control). Data are representative of three independent experiments with similar results.

Table 4

Kinetics and affinity parameters for binding of TNFAIP8 and mutants to supported lipid bilayers containing PtdIns(4,5)P_2 and PtdIns(3,4,5)P_3 measured by Surface Plasmon Resonance (SPR)

A supported lipid bilayer was generated on L1 sensor chip by flowing extruded SUVs containing DOPC and 3% (mole/mole) of PtdIns(4,5)P_2 or PtdIns(3,4,5)P_3. Sequential dilutions of the indicated proteins were injected over the surfaces, and the association and disassociation were monitored and measured as described in Materials and Methods section. k_a, association rate constant; k_d, dissociation rate constant; K_D, equilibrium dissociation constant. Data are mean ± s.d. from three independent experiments.

PtdIns	Protein	Steady-state K_D (μM)	k_a ($M^{-1}s^{-1}$)	k_d (s^{-1})
PtdIns(4,5)P_2	TNFAIP8	4.06 ± 0.93	(1.13 ± 0.12) × 10^3	(8.94 ± 0.13) × 10^{-3}
	Entrance Mutant	11.6 ± 3.0	(1.05 ± 0.39) × 10^3	(8.24 ± 1.77) × 10^{-3}
	4Q Mutant	25.7 ± 13.1	(6.25 ± 3.11) × 10^2	(2.89 ± 1.47) × 10^{-3}
	L158W Mutant	30.2 ± 16.3	(3.37 ± 6.00) × 10^2	(2.20 ± 2.22) × 10^{-3}
	Trypsin inhibitor	>100	nb	nb
	PLCd-PH	2.47 ± 1.33	(1.42 ± 1.50) × 10^4	(8.45 ± 1.10) × 10^{-3}
PtdIns(3,4,5)P_3	TNFAIP8	3.80 ± 0.20	(1.36 ± 0.46) × 10^3	(7.26 ± 0.44) × 10^{-3}
	Entrance Mutant	13.2 ± 2.9	(6.71 ± 2.11) × 10^2	(7.79 ± 2.15) × 10^{-3}
	4Q Mutant	16.6 ± 2.0	(6.55 ± 4.20) × 10^2	(7.86 ± 3.96) × 10^{-3}
	L158W Mutant	20.6 ± 1.8	(3.36 ± 0.72) × 10^2	(4.13 ± 3.00) × 10^{-3}
	Trypsin inhibitor	>100	nb	nb
	GRP1-PH	1.95 ± 1.49	(6.02 ± 7.12) × 10^4	(6.08 ± 1.14) × 10^{-3}

3.3.4 TNFAIP8-phosphoinositides interactions are important for the cellular function of TNFAIP8

To further characterize if disrupting these TNFAIP8-phosphoinositides interactions would affect cellular function and signaling, we constructed TNFAIP8 WT, 2Q, 4Q, Entrance, L44W, L65W, L99W and L158W mutant into pGL-LU-EGFP lentiviral vector and re-expressed them in HL-60 TKO cell line (Figure 3.12). It has been shown previously that the migration defect of dHL-60s was able to be rescued by re-introducing a wild-type human TNFAIP8 isoform b transgene (Figure 2.5). We found that the chemotaxis defect of dHL-60 cells could be partially rescued by expressing TNFAIP8 2Q, 4Q or Entrance mutant transgene, while the expression of L44W, L65W, L99W and L158W mutant failed to upregulate the transmigration towards fMLP (Figure 3.13A). Consistent with dHL-60 cells, the transmigration defect of murine DKO $CD4^+$ T cells could be rescued by re-expressing wild-type TIPE2, but not by TIPE2 Entrance mutant that had reduced ability to bind phosphoinositides (the TIPE2 Entrance mutant had its 28H, 75R, 91R and 183K amino acid residues replaced by Q) (Figure 3.13B).

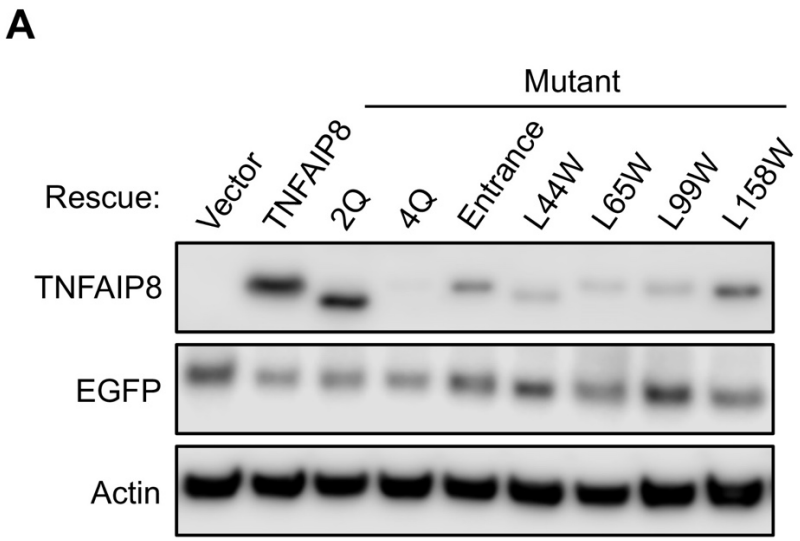

Figure 3.12 Transduction of lentiviral vectors expressing TNFAIP8 mutants into HL-60 cells

(A) The TNFAIP8 WT, 2Q, 4Q, Entrance, L44W, L65W, L99W and L158W mutant were constructed into pGL-LU-EGFP lentiviral vector and re-expressed in HL-60 TKO cell line. The lysates were analyzed by Western blot using TNFAIP8 polyclonal antibody and EGFP antibody. Actin served as a loading control.

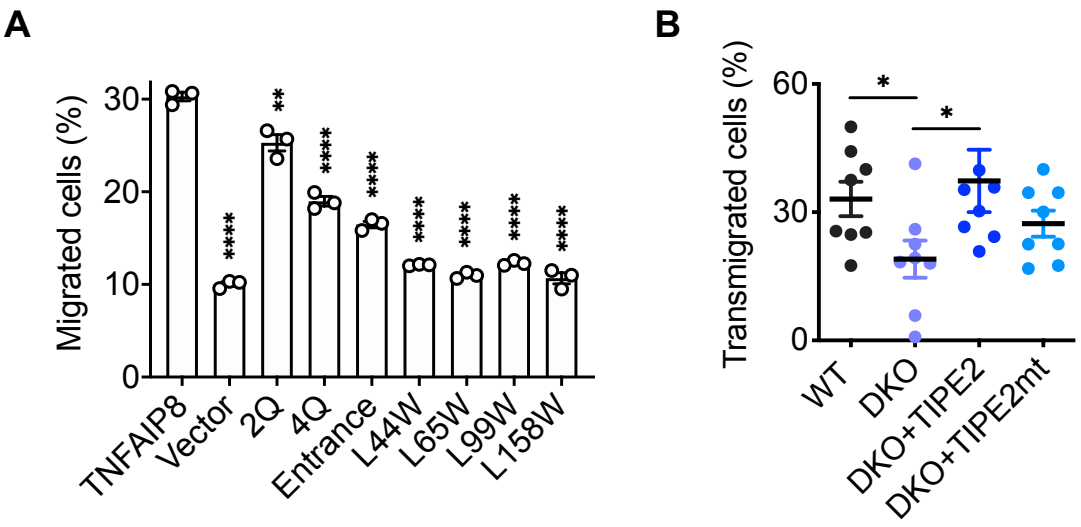

Figure 3.13 TNFAIP8 and TIPE2 mutants deficient in phosphoinositide interactions have diminished effects on promoting chemotaxis

(A) Transwell migration assay of dHL-60 TKO cells expressing TNFAIP8 mutants from lentiviral vectors (n = 3 biologically independent samples). Data are representative of three independent experiments from two clonal cell lines with similar results (mean ± s.e.m.). (B) Transmigration of DKO mouse $CD4^+$ T cells re-expressing TIPE2 or TIPE2 Entrance mutant (TIPE2mt) (n = 8 per group), as determined by the Transwell assay with CCL21. Data are pooled from three experiments (B). Values are mean ± s.e.m. of n biologically independent samples. *$P < 0.05$; **$P < 0.01$; ****$P < 0.0001$ (unpaired Student's t-test).

3.4 Discussion

In this part of study, we have optimized the purification procedures of TNFAIP8 and other proteins from *E. coli* for more quantitative investigations. The protein quality and long-term storage condition were validated through the size distribution of the hydrodynamics radius of molecules in solution by dynamic light scattering (DLS). We confirmed TNFAIP8 protein interacts with PtdIns(4,5)P_2 and PtdIns(3,4,5)P_3 present in lipid bilayers using the sedimentation-based binding assay and SPR analysis. The results further supported the hypothesis that the α0 helix of TNFAIP8 can function as a flexible lid of the hydrophobic cavity (Fayngerts et al., 2014; Schaaf et al., 2008), and the conformational change induced by PtdIns(3,4,5)P_3 binding may displace the lid and allow TNFAIP8 to extract PtdIns(4,5)P_2 from the lipid bilayer, solubilize it in the aqueous phase, and transfer it to the vesicles.

To acquire more mechanistic information, we studied the effects of TNFAIP8 on mediating the activities of phosphoinositide-binding proteins. We assessed the ability of TNFAIP8 to promote the phosphorylation of PtdIns(4,5)P_2 by PI3K, a key event at the front lamellipodium. We found that TNFAIP8 protein indeed increased the PI3K-catalyzed conversion to PtdIns(3,4,5)P_3 in a dose-dependent manner *in vitro*. Besides the enhancement of PtdIns(4,5)P_2-dependent signaling, TNFAIP8 also impacted cofilin-induced F-actin remodeling and actin dynamics. These results establish the functional significance of TNFAIP8 interaction with phosphoinositides, and indicate that TNFAIP8 can function through phosphoinositide second messengers at the leading edge of migratory cells.

Finally, mutagenesis analyses were performed to explore the structure and functional significances of the α0 helix and TIPE homology (TH) domain. To test the importance of the hydrophobic pocket in lipid binding capacity, we first compared the protein topographies of the crystal structures of TIPE family. We then replaced leucines 44, 65, 99, 158, which position towards the center of this cavity, with the much bulkier tryptophan to yield the TNFAIP8 L to W mutants. Same approach has been used to test the importance of the hydrophobic pockets in orphan nuclear hormone receptors proposed to bind phosphoinositides (Sablin, Krylova, Fletterick, & Ingraham, 2003). Of the four Hydrophobic Pocket mutants generated, L158W mutant was able to express at high level and be successfully purified. This indicates that the hydrophobic cavity formed by TH domain is important for the structural integrity or stability of TNFAIP8 protein. TNFAIP8 L158W mutant showed markedly diminished ability of phosphoinositides binding, which is consistent with the structural proposition that the fatty acid chains of phosphoinositides are positioned inside the TH domain pocket formed by the α1- α6 helixes, while the negatively charged phosphate head is accommodated by electrostatic interactions with the positively charged amino acids located at the entrance of the cavity as well as the more flexible α0 helix. Consistently, TNFAIP8 4Q and Entrance mutant both exhibited decreased phosphoinositide binding. Supporting these analyses, when re-expressed in TKO dHL-60 cells, these mutants failed to rescue the migratory defect of TNFAIP8 deficiency. These studies may help advise *in silico* drug screening and the development of pharmaceutical inhibitors targeting TNFAIP8 for its phosphoinositide interaction capacity.

CHAPTER 4

TNFAIP8 AND TIPE2 DIRECT MURINE LYMPHOCYTE MIGRATION

Work of this chapter is from:

Sun, H.*, Lin, M.*, Zamani, A., Goldsmith, J.R., Boggs, A.E., Li, M., Lee, C.N., Chen, X., Li, X., Li, T., Dorrity, B.L., Li, N., Lou, Y., Shi, S., Wang, W., Chen, Y.H. (2020). The TIPE Molecular Pilot That Directs Lymphocyte Migration in Health and Inflammation. *Scientific Reports*, *10*(1), pp.1-13.

*These authors contributed equally to this work

4.1 Introduction

Leukocyte migration in response to chemoattractants is essential for immune homeostasis and inflammation (Bloes et al., 2015; Kunkel & Butcher, 2002). *TIPE* gene single nucleotide polymorphisms (SNPs) are associated with the development of several inflammatory diseases including inflammatory bowel disease (IBD) with pyoderma gangrenosum (Weizman et al., 2014), multiple sclerosis (Hussman et al., 2016) and plantar fasciitis (S. K. Kim et al., 2018), as revealed from recent genome-wide association studies (GWAS). Similarly, TIPE2 regulates both innate and adaptive immunity, and is a risk factor for IBD, and one of the key driver genes that can cause IBD as revealed from the "functional genomics predictive network model" of IBD (Peters et al., 2017). TIPE2-deficient myeloid cells are hyper-responsive to Toll-like receptor activation and have enhanced phagocytic and bactericidal activities, and TIPE2-deficient mice are hypersensitive to intravenously induced septic shock (H. Sun et al., 2008, 2012; Z. Wang et al., 2012). In this study, we investigated whether TIPE2 and TNFAIP8 play redundant roles in controlling lymphocyte migration, using experimental autoimmune encephalomyelitis (EAE) as a mouse model for neural inflammation.

4.2 Materials and Methods

4.2.1 Complete blood counts (CBC) and isolation of blood neutrophils (BNs)

Blood was drawn from retro-orbital plexus of the eyes. CBC analysis was performed on an automated Hemavet FS950 instrument. BNs were isolated using Histopaque-1119 and Histopaque-1077 (Sigma-Aldrich) according to the manufacturer's instructions. The purity of BN populations was greater than 70% as determined by flow cytometry after staining with anti-Ly6G-APC (eBioscience), and the viability was greater than 90% as determined by trypan blue staining.

4.2.2 Isolation and enumeration of intestinal IELs

After transcardial perfusion of mice with PBS, Peyer's patches were removed, and the small intestines were collected and weighed. Intestinal epithelial cells and intraepithelial lymphocytes were stripped by shaking colonic tissue in PBS that contains 5% FBS, 2 mM EDTA, and 1 mM DTT, for 30 min at 37°C. After filtering through 70 μm cell strainers (BD Biosciences), cells were counted and the total number of cells per gram of intestinal tissue calculated. Cells were then incubated with Fc blockers for 15 min at RT, stained with fluorescent anti-CD45 and anti-CD3 antibodies, as well as with Zombie Aqua Fixable Viability kit (Biolegend), and analyzed by flow cytometry. The total numbers of $CD3^+$ and $CD45^+$ cells per gram of the small intestine in each mouse were normalized to those of the WT group for each experiment.

4.2.3 Ibidi μ-slide migration assay

Resting splenic $CD4^+$ T cells and blood neutrophils were tested in the Ibidi μ-slide migration assay to determine the migration directionality and speed, according to manufacturer's instructions (Ibidi). Briefly, resting WT, *Tnfaip8*$^{-/-}$, *Tipe2*$^{-/-}$, and DKO splenic $CD4^+$ T cells or neutrophils as prepared in the Transmigration Assay above were suspended in migration buffer (RPMI medium supplemented with 5% FBS and 1% HEPES), and loaded into Collagen IV-coated Ibidi μ-slides. After resting for 30-45 min at 37°C, CCL21 (for T cells) or CXCL1 (for neutrophils) was added to one of the reservoirs to a concentration of 200 ng/ml. For measuring the directionality and speed of random migration, cells were prepared as described above but with no chemoattractant added to the chamber. Cells were recorded every 45 sec for at least 2 h using a Leica DMI4000 microscope with Yokogawa CSU-X1 spinning disk confocal attachment at 10× magnification. Images were analyzed by Volocity software (Perkin Elmer) using the automated tracking protocol. Objects less than 16 μm^3 and static were excluded. Tracks less than 50 μm were also excluded. Cell velocity and vector angle between each track's starting and end points were obtained from Volocity using these settings. Velocity was defined as a cell's centroid movement in μm/min along the total path. Cell directionality (aka Directional Meandering Index, DMI) was defined as the cosine of the migration angle or the sine of the bearing angle. A value of 1 indicates migration directly towards the chemoattractant, while a value of -1 indicates migration away from the chemoattractant. The tracks were sorted by migration length, and tracks were selected from the middle of the videos (track time was ~60 min).

4.2.4 PtdIns(3,4,5)P_3 measurement in live CD4$^+$ T cells using biosensors

The PtdIns(3,4,5)P_3 in live cells was visualized using EGFP-tagged AKT-PH domain, which specifically binds to this phosphoinositide. Briefly, splenic CD4$^+$ T cells were stimulated with anti-CD3 and anti-CD28 for 40 h, and then transfected with GFP-C1-AKT-PH vector (Addgene) using mouse T cell Nucleofector Kit and Amaxa Nucleofector II (program X-001, Lonza). Cells were cultured for 24 h after the transfection in the presence of 10 ng/ml IL-2. The live CD4$^+$ T cells were purified using the Dead Cell Removal Kit (Miltenyi Biotec), cultured in fibronectin-coated slide chambers for 45 min, and then stimulated with 600 ng/ml CCL21 applied as a point source from a pipette, in the presence of 5 μM latrunculin A, at 37°C. The cells were recorded every 10 sec for at least 480 sec using a DeltaVision OMX-SR super-resolution microscope at 60× magnification. The images were analyzed using Volocity and ImageJ softwares. The relative Ptdins(3,4,5)P_3 level in each cell was calculated as follows: fluorescence intensity of 50% of the cell perimeter that faced the source of the chemokine / fluorescence intensity of 50% of the cell area that faced the source of the chemokine.

4.2.5 Immunofluorescence confocal microscopy of fixed CD4$^+$ T cells

Resting splenic CD4$^+$ T cells as prepared in the Transmigration Assay above were subjected to point-source stimulation with CCL21 at 1 μg/ml for 0, 1, and 10 min at 37°C. Cells were immediately fixed with 3% paraformaldehyde in PBS for 15 min at 37°C, permeabilized in PBS containing 0.1 % Triton X-100 and 3% BSA for 10 min at RT, and

blocked with PBS containing 5% normal goat serum and 3% BSA for 1 h at RT. The cells were stained overnight at 4°C with anti-TIPE2, anti-TNFAIP8 (Proteintech), or anti-Rac1-GTP (NewEast Biosciences) in 3% BSA, and then for 1 h at RT with secondary anti-rabbit IgG Fab-AlexaFluor 555, or anti-mouse IgM Fab-Alexa Fluor 488 (Thermo Fisher Scientific) in 3% BSA. Slides were dried and covered with ProLong Gold with DAPI (Invitrogen). Images were acquired on a Zeiss LSM 510 NLO/META and Zeiss LSM 710 confocal microscope and analyzed using LSM Image Browser, Zen lite (Zeiss), and ImageJ software. Up to 120 cells of each type and condition were analyzed. Morphological cell polarization was determined by phase contrast or differential interference microscopy. Unpolarized T cells were of round shape whereas the polarized cells had flat leading edges at the front (lamellipodia) and contracted uropodia at the rear. The Rac1-GTP polarization index was calculated using ImageJ by manually selecting each cell and then determining the coordinates for the center of the object (X_{object}, Y_{object}), and comparing that to the center of Rac1 fluorescent signal (X_{signal}, Y_{signal}), using the following formula that calculated the cellular polarization in terms of cartesian displacement of the center of the object from the center of the signal: $1 - \left|\frac{X_{signal}}{X_{object}} * \frac{Y_{signal}}{Y_{object}}\right|$.

4.2.6 Imaging Flow Cytometry

The ImageStream (Amnis) two camera system with 405, 488 and 658 nm lasers was used for imaging flow cytometry. The system was calibrated using SpeedBead (Amnis) prior to use and samples were acquired at optimized laser strength (50-100 mW) with an area classifier (number of pixels in μm^2) set at 25. Images (TNFAIP8 or TIPE2 in

channel 11, nucleus in channel 7, F-actin in channel 2, CD4 in channel 3, and bright field in either channel 1 or 9) were acquired for each cell at 60× magnification and ~20,000 cells were analyzed for each sample, and 2,000 cells were acquired for each compensation control. The integrated software INSPIRE (version 6.0.154, Amnis) was used for data collection. Analysis was performed on the compensated image files using algorithms in IDEAS (version 4.1.146, Amnis) image analysis software. The bright field area versus aspect ratio features were plotted and used to gate on single cells. The gradient root mean square (GRMS) was used to gate on cells that were in focus. The bright field aspect ratio score was plotted against a normalized frequency of cells to generate histograms. Polarized cells were defined as those that had low aspect ratio scores (<0.5) whereas unpolarized cells were those that had high aspect ratio scores (>0.8).

4.2.7 Experimental autoimmune encephalomyelitis (EAE)

The induction and clinical scoring of EAE in mice were performed as we described previously (Hilliard et al., 2002). Spinal cords of mice were harvested at the end of each experiment, fixed, paraffin-embedded, and sectioned. The sections were stained with hematoxylin and eosin, and analyzed using a wide field light microscope.

4.2.8 Bone marrow chimeric experiments

Bone marrow chimeric mice were generated as we described (Hilliard et al., 2002). Briefly, WT or DKO mice were sub-lethally irradiated, and injected intravenously with

bone marrow cells from DKO or WT mice (10^7 cells/mouse). For the mixed bone marrow chimeric experiment, bone morrow cells from CD45.1 WT and CD45.2 DKO mice were mixed at 1:1 ratio and injected into sub-lethally irradiated CD45.1 WT recipient mice. Seven weeks after bone marrow cell transfer, EAE was induced with myelin oligodendrocyte glycoprotein (MOG) 35-55 peptide, and scored on a scale of 0-5 as we described (Hilliard et al., 2002).

4.2.9 Adoptive transfer of EAE

Donor mice were immunized with MOG peptide and splenocytes were collected 7 days later. After stimulation with 20 μg/ml MOG peptide for three days in culture and removal of dead cells, the splenocytes were subjected to negative selection using EasySep Mouse $CD4^+$ T Cell Isolation Kit (STEMCELL, Cambridge, MA). The purified $CD4^+$ cells were injected to *Rag2*$^{-/-}$ recipient mice (2-3 x 10^6 cells/mouse) intravenously. Pertussis toxin (100 ng/mouse) was injected intraperitoneally on the day of the cell transfer and the day after. EAE was scored on a scale of 0-5 as we described (Hilliard et al., 2002).

4.2.10 Leukocyte tracking in mice

WT and *Tnfaip8*$^{-/-}$*Tipe2*$^{-/-}$ KO mice were immunized with MOG35-55 peptide as we described (Hilliard et al., 2002). Two weeks later, splenocytes were harvested and stimulated with MOG35-55 peptide (20 μg/ml) for 3 days. Live WT and KO cells were then labeled with fluorochromes CMTMR and CMFDA, respectively, mixed at 1:1 ratio,

and injected via tail vein (1 million cells/mouse) into B6 mice that had been immunized for EAE ten days earlier with MOG. Mice were sacrificed on the day of EAE onset, and their blood, spleens, and spinal cords collected. The percentages of transferred WT and KO cells among total leukocytes isolated from each sample were determined by flow cytometry.

4.3 Results

4.3.1 Complete loss of the directionality of leukocytes deficient in TNFAIP8 and TIPE2

To determine the potential roles of TIPE2 and TNFAIP8 in T lymphocyte migration, we isolated splenic $CD4^+$ T cells from wild-type (WT), *Tipe2*$^{-/-}$, *Tnfaip8*$^{-/-}$, and *Tipe2*$^{-/-}$*Tnfaip8*$^{-/-}$ (double knockout, or DKO) C57BL/6 mice, and studied them in both μ-slide (for two-dimensional migration) and Transwell chamber (for transmigration) assays. We found that TIPE2 and TNFAIP8 deficiency completely abolished the directionality of T cells during chemokine-induced migration (chemotaxis) (Figure 4.1). Specifically, in the μ-slide assay, time-lapse video microscopy that tracked the trajectory of individual migrating cells following treatment with chemokine CCL21 revealed that the WT T cells had a directionality of 0.79±0.08 (with 1.00 being the highest value of directionality); this was reduced to 0.02±0.12 for the DKO T cells (Figure 4.1a, b). WT T cells traveled with an average velocity of ~12 μm/minute, which was only slightly reduced for DKO T cells (Figure 4.1c). Notably, WT and DKO T cells not treated with chemokines migrated randomly with much-reduced speed (6.89 μm/minute for WT and 6.60 μm/minute for DKO group) and directionality (Figure 4.2a, b), indicating that chemokines could increase migration speed of both WT and KO T cells through chemokinesis. Importantly, deficiency in either TIPE2 or TNFAIP8 alone did not significantly affect either directionality or velocity. These results indicate that TIPE2 and TNFAIP8 play redundant roles in

controlling T cell directionality, and loss of one can be adequately compensated by the other.

Similarly, in the transwell assay, DKO T cells exhibited a severe defect in transmigration, although TIPE2 deficiency alone, but not that of TNFAIP8, also significantly reduced T cell transmigration (Figure 4.1d). The transmigration of both WT and DKO T cells could be reduced by inhibitors for either PI3-kinases (PI3Ks) or Rac, but the difference between WT and DKO T cells disappeared only in the presence of the Rac inhibitor (Figure 4.1e), suggesting that Rac is important for TIPE regulation of T cell migration. By flow cytometry, we found that the majority of migrating cells in this assay were central memory T cells ($CD4^{+}CD44^{high}CD62L^{-}$).

Notably, neither TIPE2 nor TNFAIP8 deficiency jeopardized random migration, as transmigration of single or double KO T cells in the absence of chemokines were either normal or slightly increased as compared to WT T cells (Figure 4.2c). Furthermore, chemokine CCL21 appeared to increase random transmigration of both WT and KO T cells (presumably through chemokinesis), since the chemokine-induced transmigration (Figure 4.1d) was calculated by subtracting random migration (Figure 4.2c) from total migration.

The effect of TIPE2 and TNFAIP8 on T cell migration was not limited to CCL21. CXCL12-induced migration of $CD4^{+}$ T cells was also significantly reduced in DKO group (Figure 4.2d). Additionally, the critical roles of TIPE2 and TNFAIP8 in establishing cell directionality were not restricted only to T cells. We previously reported that TIPE2 deficiency in murine neutrophils partially affected their chemotaxis (Fayngerts et al., 2017). Here we extended that observation to TNFAIP8 and found that neutrophils deficient

in both TIPE2 and TNFAIP8 completely lost their directionality (from 0.62±0.08 in the WT to 0.04±0.04 in the DKO group), while preserving relatively high migrating speed in response to chemokine CXCL1 (Figure 4.2e, f). Thus, TIPE proteins selectively control the direction of migration with minimal effects on the migration speed of leukocytes.

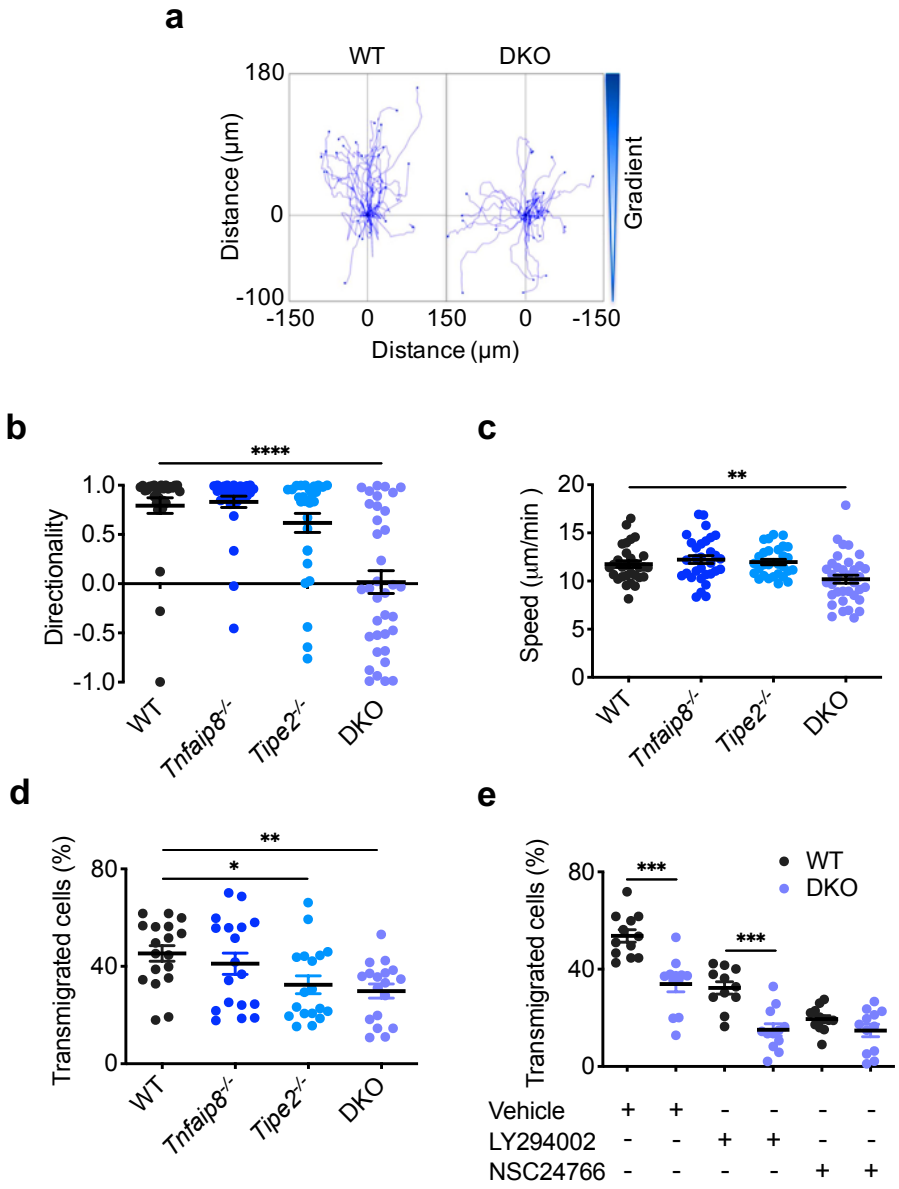

Figure 4.1 Complete loss of directionality, but not speed, of TIPE-deficient T cells

a-c, Migration tracks (a), directionality (b), and speed (c) of $CD4^+$ T cells from WT, *Tnfaip8*$^{-/-}$, *Tipe2*$^{-/-}$, and *Tnfaip8*$^{-/-}$*Tipe2*$^{-/-}$ (DKO) mice (4 mice per group), in response to CCL21, as determined in the µ-slide migration assay. n=25 cells per group (a); n=30 cells for WT, 31 for *Tnfaip8*$^{-/-}$, 29 for *Tipe2*$^{-/-}$ and 36 for DKO group (b, c). d,

e, Transmigration of $CD4^+$ T cells from mice of the indicated genotypes (4 mice per group) (d, n=18 samples per group), or cells treated with the PI3K inhibitor LY290004 or Rac inhibitor NSC23766 (e, n=12 per group), as determined in the transwell transmigration assay with CCL21. Data are representative of at least three independent experiments (a-c), or are pooled from four (d) or three experiments (e). Values are mean ± s.e.m. of *n* biologically independent samples (b-e). **P* < 0.05; ***P* < 0.01; ****P* < 0.001; *****P* < 0.0001 (Mann-Whitney *U* test (b) or Student's *t*-test (c-e)).

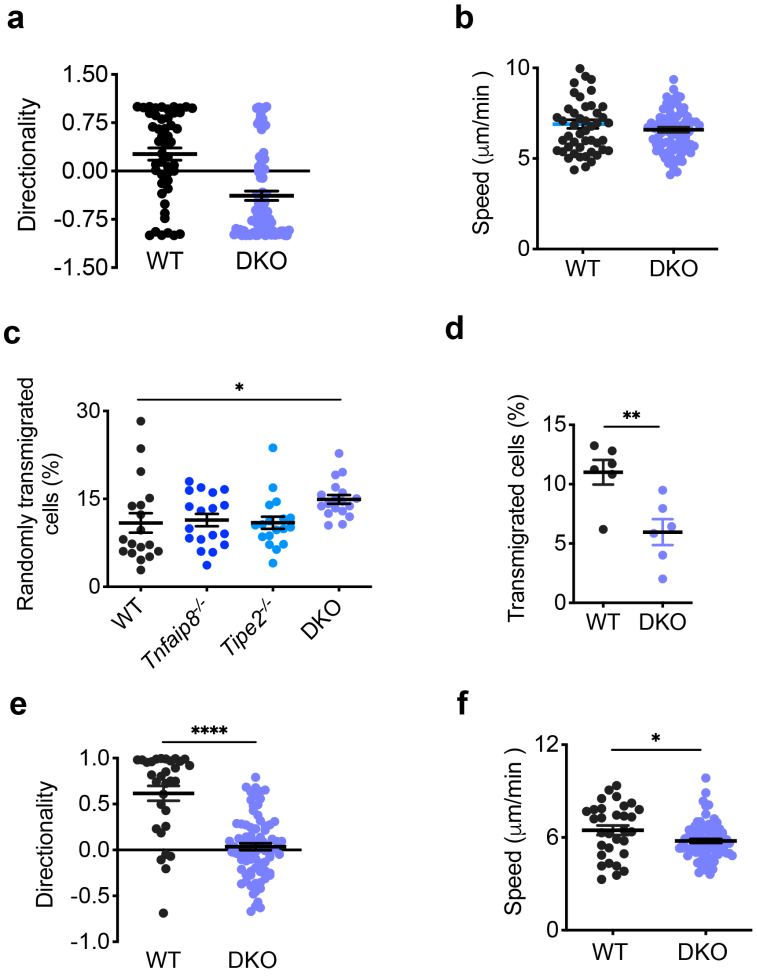

Figure 4.2 Effects of TIPE deficiency on T cell and neutrophil migration

a, b, Directionality (a) and speed (b) of $CD4^+$ T cells from WT and DKO mice (5 mice per group), in the absence of added chemokines, as determined in the μ-slide migration assay. n=49 cells for WT, and 84 for DKO group. c, Percentages of transmigrated $CD4^+$ T cells of the indicated genotypes in the absence of added chemokines as determined in the transmigration assay described in Fig. 1d (n=18 samples per group). d, Percentages of transmigrated $CD4^+$ T cells of WT and DKO groups (n=6 samples per group) in the presence of CXCL12. e, f, Directionality (e) and speed (f) of neutrophils from WT and

DKO mice (4 mice per group), in response to CXCL1, as determined in the μ-slide migration assay. n=31 cells for WT, and 79 for DKO group. Values are mean ± s.e.m., and are pooled from two (d) or four (c), or are representative of three (e, f) or two (a, b) independent experiments. $*P < 0.05$; $**P < 0.01$; $****P < 0.0001$ (Student's *t*-test (a, b, c, d, e, f))

4.3.2 TNFAIP8 and TIPE2 pilot lymphocytes through PI3Ks and Rac

To explore how TNFAIP8 and TIPE2 control cell directionality, we studied PI3Ks and Rac signals, as well as morphological polarization of T cells. PI3Ks signaling was measured in live T cells using a PtdIns(3,4,5)P_3-specific biosensor, i.e., the enhanced green fluorescent protein (eGFP)-tagged AKT-PH domain. By time-lapse video microscopy, we compared PtdIns(3,4,5)P_3 generation in WT and DKO T cells in response to point-source CCL21 stimulation over a period of 110 seconds (Figure 4.3a). CCL21-induced PtdIns(3,4,5)P_3 production occurred immediately after chemokine stimulation, at the side of the cell that faced the chemokine source, reaching its peak level ~60 seconds later. By contrast, no significant increases in PtdIns(3,4,5)P_3 were observed in DKO T cells. Consistent with these observations, chemokine-induced morphological polarization was significantly reduced in DKO T cells as compared to WT T cells (Figure 4.3b). TIPE2 has been reported to be a global inhibitor of Rac (Fayngerts et al., 2017; Z. Wang et al., 2012). In support of this view, Rac-GTP polarization occurred constitutively in DKO T cells, which was not further increased by chemokine treatment (Figure 4.3c, d). By contrast, WT T cells responded to the chemokine treatment by polarizing their Rac-GTP. These results indicate that TIPE proteins are essential for generating the phosphoinositide and Rac signals required for steering cells toward chemoattractants.

TIPE2 and TNFAIP8 were present in most parts of the cytosol and plasma membrane in unpolarized T cells. By contrast, in polarized T cells, both TIPE2 and TNFAIP8 moved to the leading edges of the cells, overlapping with F-actin (Figure 4.4a, b). During the CCL21-induced chemotaxis, leading edges of WT T cells were generated

mostly by pseudopod splitting, consistent with reports from others for granulocytes and *Dictyostelium discoideum* cells (Insall, 2010). In contrast, DKO T cells generated their leading edges by de novo pseudopod formation as frequently as pseudopod splitting (Figure 4.4c), indicating that the latter cells might have lost the ability to follow chemokine gradient.

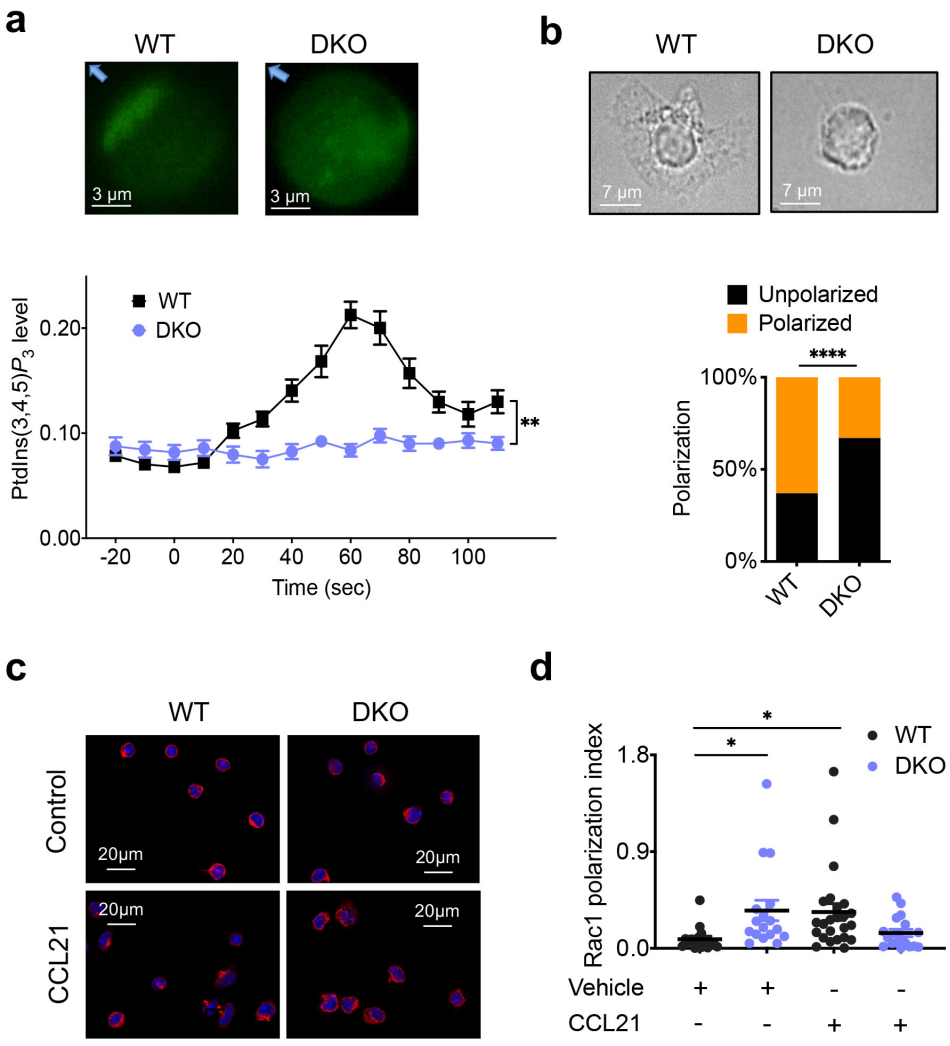

Figure 4.3 Essential roles of TIPE proteins in chemokine-induced PtdIns(3,4,5)P_3 generation, and morphological and Rac1-GTP polarization

a, PtdIns(3,4,5)P_3 levels detected by AKT-PH-GFP biosensor in live WT and DKO $CD4^+$ T cells, in response to point source stimulation of CCL21, as visualized by super-resolution fluorescence video microscopy. Upper panels show a WT and a DKO T cells 60 sec after CCL21 stimulation, with arrows pointing to the source of CCL21. The lower panel shows the changes in PtdIns(3,4,5)P_3 levels relative to Time 0 when CCL21 was

applied; values are mean ± s.e.m., with n=20 cells for each group. b, Morphological polarization of WT and DKO $CD4^+$ T cells, in response to point source stimulation of CCL21, as visualized by phase contrast microscopy. Upper panels show a polarized WT and an unpolarized DKO T cells 10 min after CCL21 stimulation. The lower panel shows the percentages of polarized and unpolarized cells 10 min after CCL21 stimulation; n=308 cells for WT and 304 cells for DKO group. c, d, Rac1-GTP polarization in WT and DKO $CD4^+$ T cells, in response to point source stimulation of CCL21, as visualized by immunofluorescence microscopy. Panel-c shows WT and DKO T cells 60 sec after incubation with CCL21 or medium alone (*Control*). Panel-d shows the calculated polarization index of each group treated as in Panel-c; n=16-24 cells for WT and 17-18 for DKO group. Values are mean ± s.e.m. The experiments were repeated independently at least three times (a-d) with similar results. $*P < 0.05$; $**P < 0.01$; $****P < 0.0001$ (Mann-Whitney *U* test (a) or Fisher's exact test (b) or Student's *t*-test (d)).

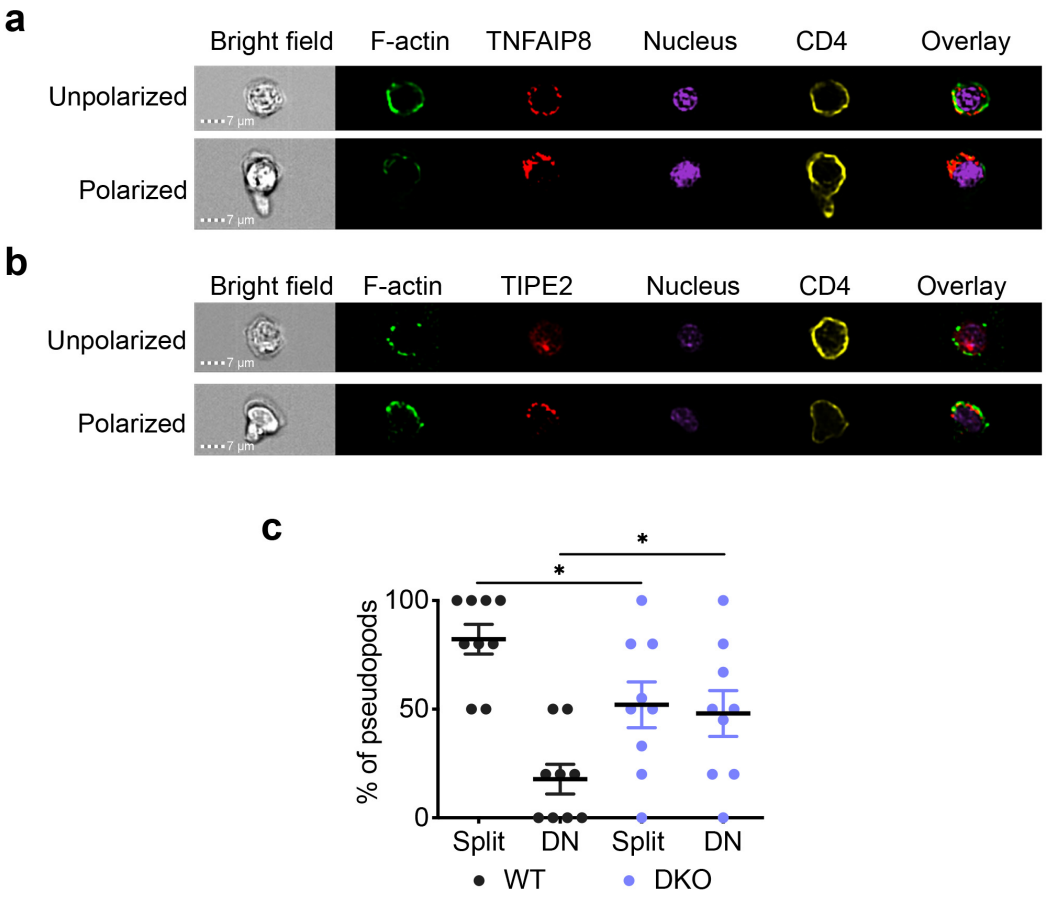

Figure 4.4 TIPE protein polarization, and pseudopod formation in CD4$^+$ T cells

a, b, Visualization of TNFAIP8 (a) and TIPE2 (b) together with F-actin and CD4 in polarized and unpolarized WT CD4$^+$ T cells 10 min after CCL21 stimulation by confocal imaging flow cytometry. c, Percentages of pseudopods formed de novo (DN) or by splitting the existing pseudopods (with a splitting angle < 90°) of WT and DKO T cells 0 to 120 sec after point source stimulation with CCL21, calculated by live cell video microscopy; n=9 samples for each group. Values are mean ± s.e.m. (c). The experiments were repeated at least three times with similar results (a-c). *P < 0.05 (Student's t-test (c)).

4.3.3 Abnormal positioning of leukocytes in mice deficient in TNFAIP8 and TIPE2 under steady state

Lymphocytes are deployed strategically throughout the body via two distinct modes of migration: directed and random migrations (Stachowiak, Wang, Huang, & Irvine, 2006; Xiong, Huang, Iglesias, & Devreotes, 2010). The degree to which each mode of migration contributes to the deployment of lymphocytes in each tissue is not well understood. Chemokines enhance not only directed migration but also random migration (Figure 4.1) (Stachowiak et al., 2006; Szatmary & Nossal, 2017). The selective defect in directed, but not random, migration of leukocytes deficient in TIPE2 and TNFAIP8 allowed us to examine the contribution of directed migration to tissue-specific deployment of leukocytes in mice. Deficiency in TIPE2 and TNFAIP8 significantly increased the total numbers of white blood cells (WBC) in the blood, which included both lymphocytes and neutrophils (Figure 4.5a). Deficiency in TIPE2 alone, but not in TNFAIP8, also significantly increased blood leukocyte numbers. The total $CD4^+CD8^-$ and $CD8^+CD4^-$ T cells in the thymus were also significantly increased in DKO mice (by ~2 fold) (Figure 4.5b). By contrast, the total $CD4^+CD8^-$ and $CD8^+CD4^-$ T cells in the spleen were significantly decreased in DKO mice (Figure 4.5c), suggesting a defect in T cell migration from thymus to spleen. The numbers of other leukocyte subsets except that of $CD11b^+Ly6G^+$ cells in the spleen were not significantly affected by TIPE2 and TNFAIP8 deficiency. The weights of, and total numbers of cells in, lymphoid organs, which included thymus, spleen, and mesenteric lymph node, were not significantly affected by TIPE2 and TNFAIP8 deficiency (Figure 4.6). This is consistent with our previous report that C57BL/6 mice deficient in either

TIPE2 or TNFAIP8 alone do not have significant changes in their total lymphocyte numbers in lymphoid organs under the steady state (before 10 weeks of age) (H. Sun et al., 2015; Z. Wang et al., 2012). These results indicate that, under steady state, directed migration is critical for T cell deployment to lymphoid organs, and that random migration (which can be significantly enhanced by chemokines) also plays an important role in leukocyte deployment to lymphoid organs.

Under steady-state, ~50% of T lymphocytes in the body are deployed to the mucosal epithelium (Guy-Grand et al., 2013). How intraepithelial lymphocytes (IELs) move into the mucosal epithelium is not well understood. Remarkably, the total numbers of $CD45^+$ and $CD3^+$ IELs in the intestinal epithelium decreased by ~50% in DKO mice (Figure 4.5d). This indicates that about half of the IELs move to the intestinal epithelium through TIPE-dependent migration.

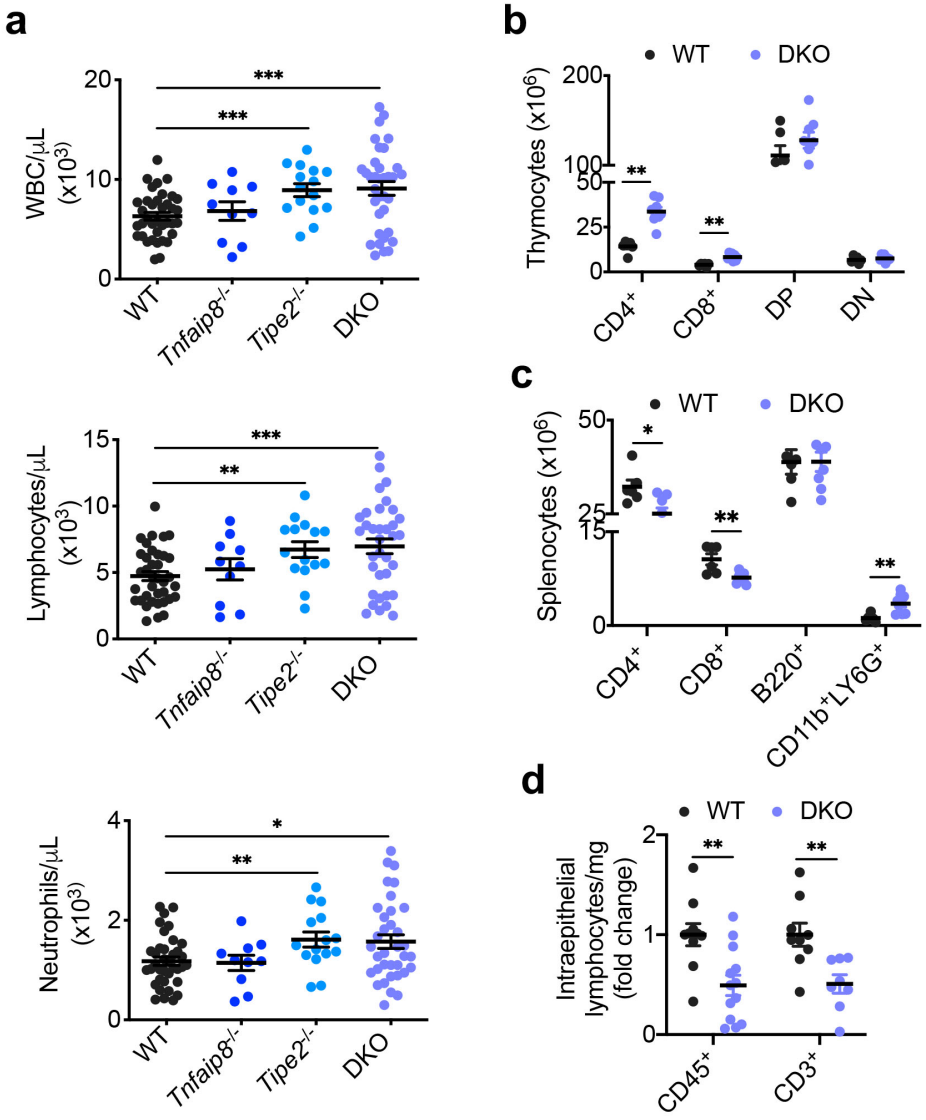

Figure 4.5 Abnormal positioning of leukocytes in tissues of TIPE-deficient mice under the steady state

a, The total white blood cell, lymphocyte, and neutrophil counts of the blood of normal 6-8-week-old WT (n=37), *Tnfaip8*$^{-/-}$ (n=10), *Tipe2*$^{-/-}$ (n=15), and DKO (n=35) mice. b, The numbers of the indicated cell subsets of thymus of WT (n=6) and DKO (n=8) mice as determined by flow cytometry. CD4^{+} and CD8^{+} denote the respective single positive

cells; DP denotes double positive cells; DN denotes double negative cells. c, The numbers of the indicated cell subsets of spleen of WT (n=6) and DKO (n=8) mice as determined by flow cytometry. d, Relative numbers of the indicated intraepithelial cells per mg of small intestine of WT (n=10 mice for $CD45^+$ and 9 for $CD3^+$ cells) and DKO (n=13 for $CD45^+$ and 8 for $CD3^+$ cells) mice as determined by flow cytometry. Data are normalized to the mean of the respective WT group. The values are mean ± s.e.m. (a-d), and are pooled from two (b-c) or three (a, d) independent experiments. $*P < 0.05$; $**P < 0.01$; $***P < 0.001$ (Student's *t*-test (a-d)).

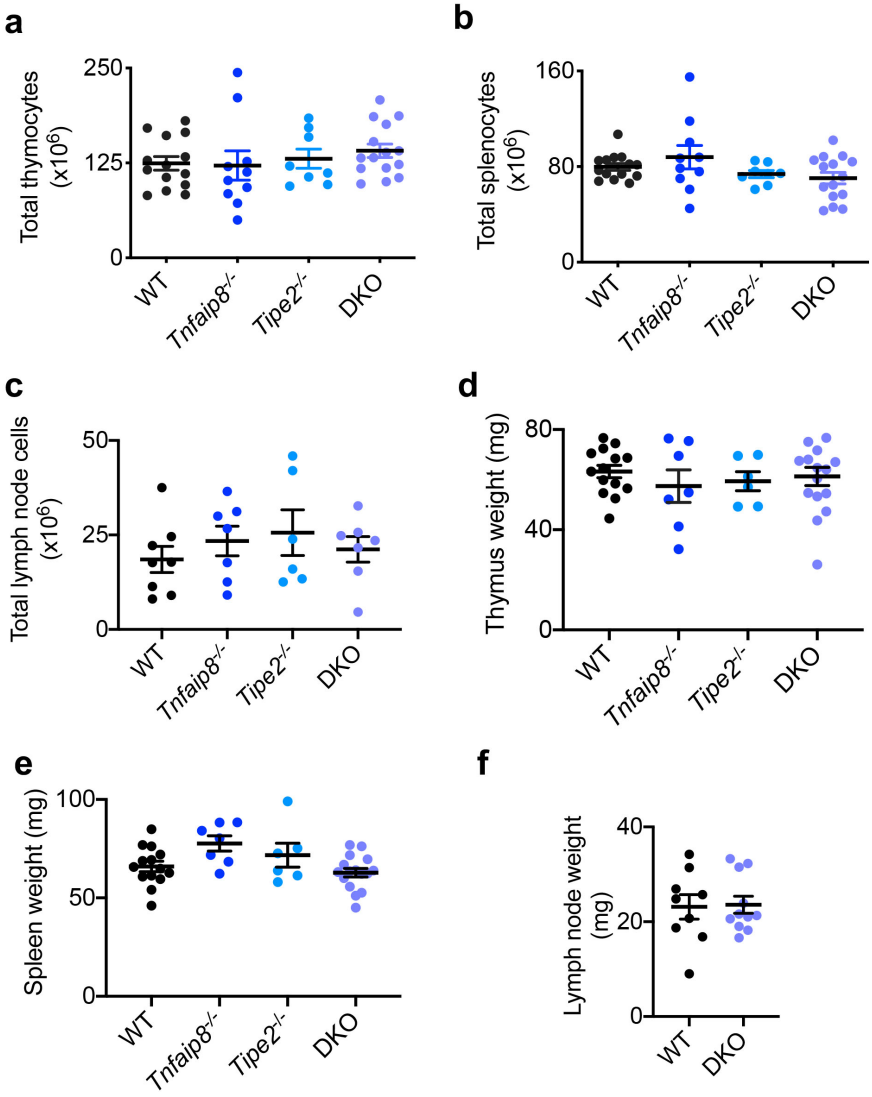

Figure 4.6 Weights and total cell numbers of thymus, spleen and mesentery lymph node

a, b, Total numbers of thymocytes (a) and splenocytes (b) of each 8-week-old WT (n=14), *Tnfaip8*$^{-/-}$ (n=10), *Tipe2*$^{-/-}$ (n=8), and DKO (n=15) mouse. c. Total numbers of mesentery lymph node cells of WT (n=8), *Tnfaip8*$^{-/-}$ (n=7), *Tipe2*$^{-/-}$ (n=6), and DKO (n=8) mice. d-f, Weights of thymus (d), spleen (e), and mesentery lymph node (f) of the

mice used in a-c. The values are mean ± s.e.m., and are pooled from three independent experiments (Student's *t*-test)(a-f).

4.3.4 Resistance of mice deficient in TNFAIP8 and TIPE2 to autoimmune encephalomyelitis

Under inflammatory conditions, lymphocytes can exit the blood circulation and enter non-lymphoid tissues. This is crucial for the development of inflammatory diseases such as multiple sclerosis (MS) (Calabresi et al., 2014; Derfuss et al., 2013). To determine the roles of TIPE2 and TNFAIP8 in experimental autoimmune encephalomyelitis (EAE), an animal model for MS, we immunized WT, *Tipe2*$^{-/-}$, *Tnfaip8*$^{-/-}$, and *Tipe2*$^{-/-}$*Tnfaip8*$^{-/-}$ DKO mice with myelin oligodendrocyte glycoprotein (MOG) peptide 35-55, and monitored daily for clinical signs of EAE (Figure 4.7a). We found that the onset and mean EAE scores were significantly reduced in all knockout groups with the DKO group being the most affected. This indicates that TIPE2 and TNFAIP8 play redundant roles in EAE, and loss of one is significantly compensated by the other. The fatality was reduced from 60% in the WT group to 0% in all KO groups. Consistent with these clinical findings, histological examination of spinal cord sections revealed significant differences in the degree of leukocyte infiltration between WT and KO groups (Figure 4.7b, c). In the WT group, multiple inflammatory foci were observed, with extensive leukocyte infiltration into the white matter. By contrast, leukocyte infiltration in KO mouse spinal cords was much less pronounced.

To define the roles of TIPE2 and TNFAIP8 expressed by hematopoietic cells, we studied EAE in irradiated WT and DKO female C57BL/6 mice that had received bone marrow from either WT or DKO mice 7 weeks earlier (Figure 4.7d). In the chimeric mice, ~90% of leukocytes were derived from donor bone marrow as determined by flow

cytometry. Notably, following immunization with MOG peptide, mice that received DKO bone marrow developed significantly less EAE than those reconstituted with WT cells. Therefore, loss of TIPE2 and TNFAIP8 in hematopoietic cells alone is sufficient to significantly hinder the development of EAE. Because not all hematopoietic cells in recipient mice can be eliminated by irradiation, whether and to what degree TIPE proteins expressed by non-hematopoietic cells contribute to EAE cannot be conclusively established in this model.

MOG-induced EAE is a T cell-initiated disease. To determine whether TIPE deficiency in T cell alone is sufficient to affect EAE, we adoptively transferred activated anti-MOG T cells from WT and DKO mice into Rag2-deficient B6 mice (that had endogenous myeloid but not lymphoid cells). We found that EAE was significantly diminished in mice received DKO T cells (Figure 4.8a). To measure anti-MOG responses of T cells, mice were sacrificed 10 days after immunization, and their splenocytes cultured in the presence of the MOG peptide. DKO cell cultures produced increased interleukin (IL)-2 and IL-17A as compared to WT cultures (Figure 4.7e, f). Because the frequency of MOG-specific T cells in different groups could be different, we also compared responses of purified $CD4^+$ T cells from naïve mice to anti-CD3 and anti-CD28 stimulation *in vitro*. Similar to its effect on anti-MOG responses, TIPE2 and TNFAIP8 double deficiency increased T cell responses to anti-CD3 and anti-CD28 stimulation (unpublished data). These results indicate that reduced EAE in TIPE-deficient mice is not due to reduced T cell responses to MOG.

4.3.5 Abnormal positioning of leukocytes in the central nervous system of mice deficient in TNFAIP8 and TIPE2 during autoimmune encephalomyelitis

Reduced EAE in TIPE-deficient mice could be due to reduced migration of KO T cells into the central nervous system (CNS), to which access of leukocytes is tightly controlled by the blood-brain barriers (Engelhardt & Ransohoff, 2012; Minagar & Alexander, 2003). In the mixed bone marrow chimeric mice that had both CD45.1 WT and CD45.2 DKO T cells, markedly reduced numbers of DKO T cells were found in the CNS as compared to WT T cells, following the onset of EAE (Figure 4.8b). Similarly, upon co-transfer into mice with EAE, CMTMR-labeled DKO cells showed a marked defect in infiltrating CNS, as compared to CMFDA-labeled WT cells in the same mice (Figure 4.8c). This was accompanied by a significant increase of the transferred DKO cells in the blood and spleen of the mice. These results indicate that T cells deficient in TNFAIP8 and TIPE2 have a severe defect in infiltrating the CNS during neural inflammation.

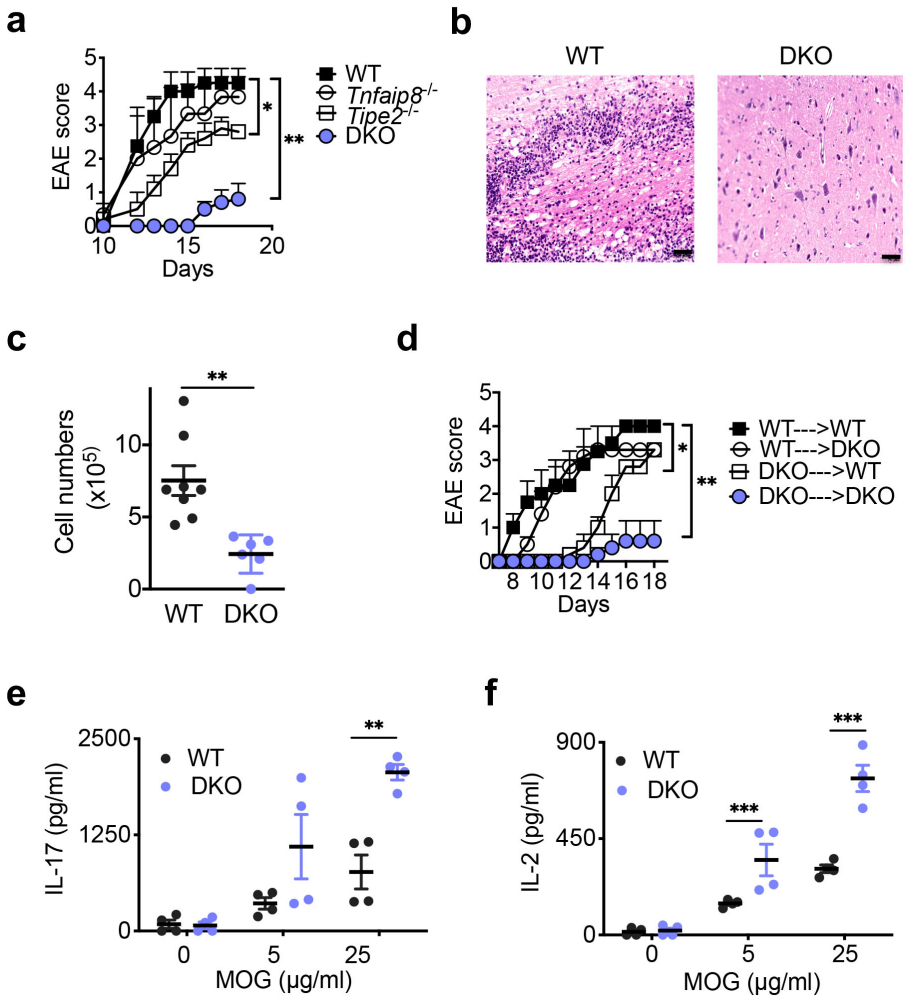

Figure 4.7 The effects of TIPE deficiency on EAE, leukocyte infiltration of the nervous tissue, and T cell response to MOG

a, Clinical EAE scores of WT, *Tnfaip8*$^{-/-}$, *Tipe2*$^{-/-}$, and DKO mice (n=5 for each group) immunized with MOG35-55 peptide. b, Spinal cord sections stained with hematoxylin and eosin of WT and DKO mice. Scale bar = 50 μm. c, The numbers of leukocytes isolated from each spinal cord of WT (n=8) and DKO (n=6) mice 20 days after immunization with MOG. d, EAE scores of irradiated WT and DKO mice (n=5 for each group) that had received WT or DKO bone marrow cells before being immunized with

MOG. e, f, The concentrations of IL-17A (e) and IL-2 (f) in the splenocyte cultures of WT and DKO EAE mice (n=4 per group), cultured with or without the MOG peptide for 24 h, as measured by ELISA. Data are representative of two (d) or three (a, b) independent experiments, or are pooled from two experiments (c, e, f). Values are mean ± s.e.m. $*P < 0.05$; $**P < 0.01$; $***P < 0.001$ (Mann-Whitney *U* test (a, d) or Student's *t*-test (c, e, f)).

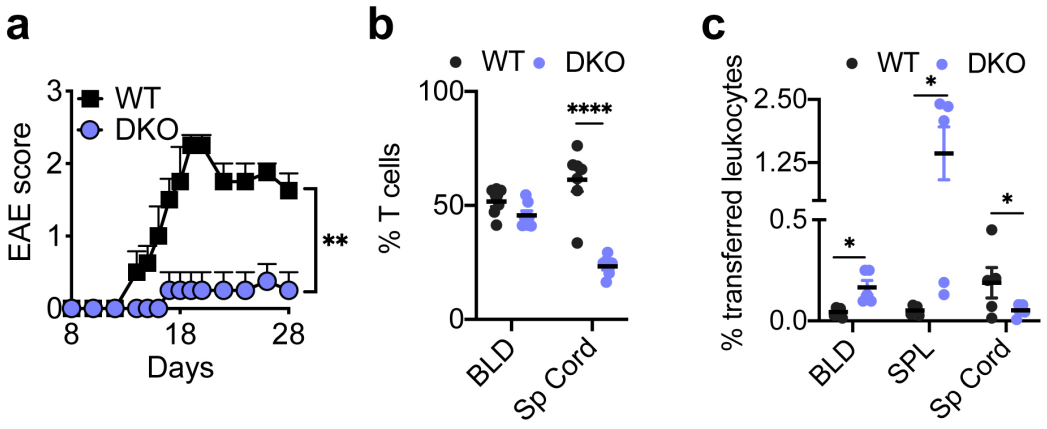

Figure 4.8 Abnormal positioning of leukocytes in the nervous tissue of TIPE-deficient mice during encephalomyelitis

a, EAE scores of *Rag2*$^{-/-}$ mice (n=4 mice per group) that were injected with MOG-specific WT or DKO CD4^{+} T cells. b, The percentages of WT CD45.1^{+} and DKO CD45.2^{+} T cells among total CD3^{+} T cells in the blood (*BLD*) and spinal cord (*Sp Cord)* of EAE mice (n=7 mice per group) that were injected with WT and DKO bone marrow cells at 1:1 ratio. Samples were collected one day after EAE onset. c, The percentages of transferred CMTMR-labeled WT and CMFDA-labeled DKO cells among total leukocytes in the blood (*BLD*), spleen (*SPL*), and spinal cord (*Sp Cord)* of EAE mice (n=5 mice per group) that were injected with the respective MOG-specific WT and DKO CD4^{+} T cells at 1:1 ratio. Samples were collected on the day of the EAE onset. The values are mean ± s.e.m. (a-c), and are pooled from two independent experiments (b, c) or are representative of four independent experiments (a). *$P < 0.05$; **$P < 0.01$; ****$P < 0.0001$ (Mann-Whitney *U* test (a, b) or Student's *t*-test (c)).

4.4 Discussion

Results in this study prompted us to propose that TIPE proteins are the long-sought-after molecular pilot of leukocytes (Figure 5.2). Following chemokine receptor activation, TIPE proteins serve as the pilot of cell migration by steering cells along the chemokine gradient through at least two distinct mechanisms (Figure 5.2). First, at the membrane-cytosol interface, PI3Ks alone may not be effective in catalyzing reactions of membrane-anchored phosphoinositides (Schaaf et al., 2008). Because of its unique membrane-cytosol interfacial localization and its water solubility, TIPE-anchored PIP2 serves as a "primed' or "presented" substrate for PI3Ks. Therefore, at the cell front, TIPEs promote leading edge formation by enhancing/exciting phosphoinositide signaling, leading to enhanced recruitment and activation of the downstream signaling molecules. Second, in the cytosol or away from the leading edge, the water soluble TIPEs serve as an inhibitor of Rac, preventing it from moving to the membrane as we reported (Z. Wang et al., 2012). This inhibitory mechanism is important for maintaining the polarized state of the cell, i.e., by preventing additional leading edge formation. Thus, by regulating both PI3Ks and Rac, TIPE proteins confer the directionality of migration. In summary, we discovered that TIPE family of proteins controls lymphocyte migration and deployment in healthy and diseased animals. These results may not only advance our understanding of the biology of lymphocyte trafficking but also help develop new TIPE-based strategies to treat lymphocyte-related diseases. For example, agents that block TIPE function could be effective for treating inflammatory diseases such as MS. However, the same agents could also reduce the host's ability to mobilize immune cells to fight against infectious microbes.

Therefore, future studies are needed to evaluate the therapeutic and adverse effects of TIPE-blocking agents for the treatment of inflammatory diseases.

CHAPTER 5

DISCUSSION AND FUTURE DIRECTIONS

5.1 Global inhibitor and local enhancer theory

Several lines of evidence in this study establish that TNFAIP8 plays an important role in cell migration by acting as a "dual-role regulator" in response to external stimuli (Figure 5.1 and Figure 5.2). Our results support that TNFAIP8 can control the spatial and temporal distribution of GPCRs downstream signaling, and mediate the activities of phosphoinositide-binding proteins. It can enhance the generation of PtdIns(3,4,5)P_3 at the front membranes, therefore reinforcing a positive feedback loop that amplifies the PI3K signaling at the leading edge. Besides the PI3K-dependent pathway, TNFAIP8 interaction with PtdIns(4,5)P_2 may also result in release and diffuse of the plasma membrane (PM)-bound pool of unphosphorylated and inactive cofilin to the nearby F-actin compartment (to actively exert its severing function). In addition, TNFAIP8 can serve as a cytosolic inhibitor of Rac/Cdc42 and function through the PAK-LIMK-cofilin pathway, thus controlling trailing edge formation and suppressing secondary leading edge generation (Bravo-Cordero et al., 2013; Ghosh et al., 2004). This way TNFAIP8 may be built into a machinery of both short-range positive feedback and long-range inhibition, which helps to amplify and translate the shallow chemical gradients into axes of cell polarity.

These findings are consistent with the computationally predicted existence of essential regulators that operate as local enhancers and global inhibitors, relaying chemokine-induced signal transduction for cytoskeletal dynamics (Huang, Tang, Shi, Iglesias, & Devreotes, 2013; Iglesias & Devreotes, 2012; Kamakura et al., 2013; Tang et al., 2014; Thapa & Anderson, 2012). In this LEGI-BEN (local-excitation, global-inhibition-biased excitable network) model, the enhancers operate locally at the leading

edge, whereas the inhibitors function globally (Bhowmik, Rappel, & Levine, 2016; Xiong et al., 2010). It has been suspected that migrating cells may possess an internal compass that controls the directionality of migration (Franca-Koh & Devreotes, 2004; Rickert et al., 2000; Swaney et al., 2010). Recent studies revealed that only moderate effects on chemotaxis were observed in the PI(3)K$\gamma^{-/-}$ cells, suggesting that when phosphoinositide levels were reduced, signaling through another parallel pathway may compensate for this defect (Ferguson et al., 2006; Nishio et al., 2006). Consistent with the proposed compass model for directional sensing (Franca-Koh, Kamimura, & Devreotes, 2007), receptor signaling through GPCRs may orient the cell's compass and activate the PtdIns(3,4,5)P_3 pathway and parallelly the TIPE regulated pathway for controlling chemotaxis (Figure 5.2).

Rho family of small GTPases are well known to be regulated by GEFs, GAPs and RhoGDIs. RhoGDIs can inhibit Rac by extracting prenylated Rac-GDP from plasma membrane and by decreasing the rate of nucleotide dissociation. RhoGDIs have also been reported to be able to prevent the degradation of Rho GTPases. Our study reported here indicates that TIPE family might represent a unique class of negative regulator of Rho GTPases, distinct from the aforementioned molecules. Since TIPE2 preferentially associates with dominant negative Cdc42-17N but not the constitutively active Cdc42-61L mutant, it is possible that TIPEs may bind and stabilize an inhibitory complex, which is dissociated by GPCR signaling upon chemokine stimulation. TIPEs may thus maintain the quiescent cellular state by sequestering PtdIns(4,5)P_2, Rho GTPases and/or heterotrimeric G proteins in the cytosolic pool. TIPEs might also use similar mechanisms of RhoGDIs to inhibit Rho GTPases and prevent their membrane translocation as well as function.

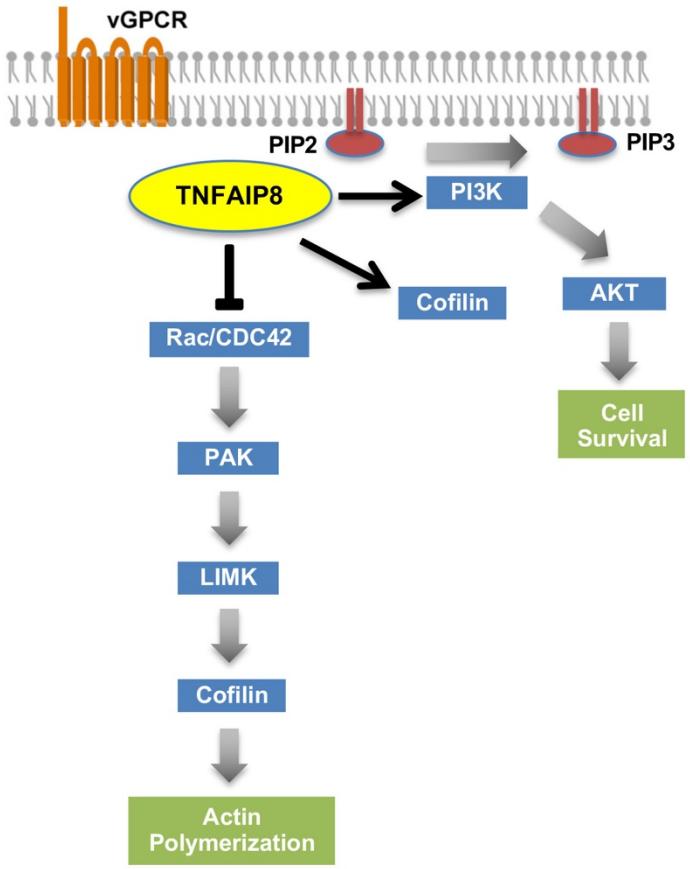

Figure 5.1 A schematic model of TNFAIP8 actions

TNFAIP8 can enhance the generation of PtdIns(3,4,5)P_3 at the front membranes, therefore reinforcing a positive feedback loop that amplifies PI3K signaling at the leading edge. TNFAIP8 interaction with PtdIns(4,5)P_2 may also result in release and diffuse of the plasma membrane (PM)-bound pool of unphosphorylated and inactive cofilin to the nearby F-actin compartment. In addition, TNFAIP8 can serve as a cytosolic inhibitor of Rac/Cdc42 and function through the PAK-LIMK-cofilin pathway, thus controlling trailing edge formation and suppressing secondary leading edge generation.

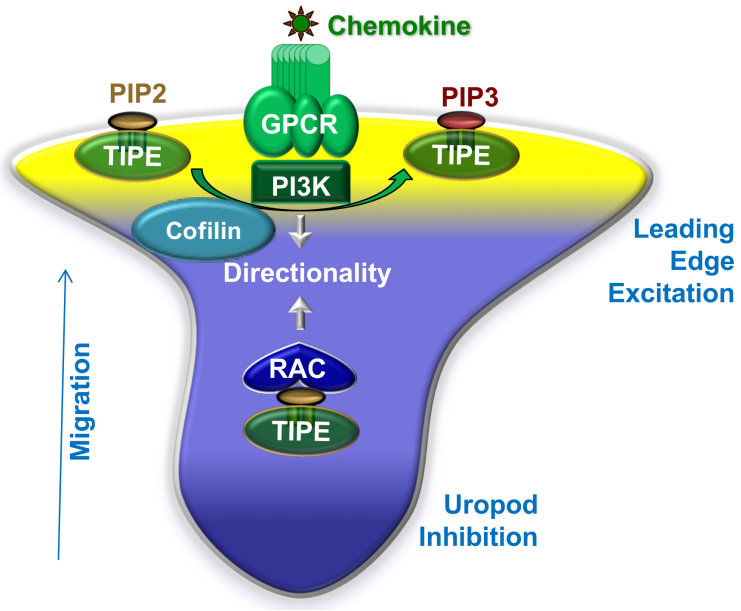

Figure 5.2 TIPE proteins can confer the directionality of migration by regulating both PI3Ks and Rho GTPases

TIPEs can regulate polarization in a spatial-specific manner and direct cell migration. Following GPCR activation, TIPE proteins serve as the pilot of cell migration by steering cells along the chemokine gradient through two distinct mechanisms. First, because of their unique membrane-cytosol interfacial localization and water solubility, TIPEs-anchored PIP2 serves as a "primed" substrate for PI3Ks. Therefore, at the cell front TIPEs promote leading edge formation by enhancing phosphoinositide signaling, leading to recruitment and activation of the downstream cascades. Second, in the cytosol or away from the leading edge, the water soluble TIPEs serve as an inhibitor of Rho GTPases such as Rac, preventing it from membrane translocation/activation. This inhibitory mechanism is important for preventing multiple leading edge formation and thus maintaining the polarization of the cell.

5.2 Conservative functions of TIPE family proteins

The TIPE TH domain is highly homologous among TIPE family members, and conserved through evolution in vertebrates. TIPE2 has been reported to be able to regulate both carcinogenesis and inflammation (Gus-Brautbar et al., 2012), and is crucial for the polarization of myeloid cells (Fayngerts et al., 2017; H. Sun et al., 2008). We have also recently found that TNFAIP8 and TIPE2 play redundant roles in controlling murine lymphocyte migration. TNFAIP8 or TIPE2-deficient $CD4^+$ T cells exhibited reduced migration towards CCL21 gradients, while double knockout (DKO) T cells showed most significant defects in chemotaxis. Therefore, loss of both TIPE2 and TNFAIP8, but not either alone in lymphocytes is required to eliminate directional migration. This Dual Molecular Redundancy (DMR) ensures that the directional migration is maintained in case one TIPE family protein fails (resulting from gene mutation or downregulation). This enhances the overall robustness of the biological system, similar to what the DMR does in electric engineering (Stanisavljevic, Schmid, & Leblebici, 2009).

The functions of TIPEs may also be differentially regulated by other sequences present in the proteins, such as the N-terminal regions. For example, the unique N-terminus of TIPE3, which is not shared by other family members, has been reported to act in a dominant-negative manner (Fayngerts et al., 2014). This raises the question as to whether the many transcript variants and protein isoforms of TNFAIP8 in both mice and human may be transcriptionally regulated to exert diverse cell-type specific functions.

5.3 TNFAIP8 and GPCR interaction

The TH domain is conserved through evolution and is found in invertebrates such as fruit fly, unicellular eukaryotes such as Entamoeba, as well as vertebrates. G protein interacting protein 1 (Gip1) has recently been found to regulate GPCR signaling of chemotaxis in eukaryote Dictyostelium discoideum by binding and sequestering heterotrimeric G proteins in the cytosolic pool. Interestingly, the crystal structure of the C-terminal region of Gip1 shows cylinder-like folding with a central hydrophobic cavity, in homology to TIPE TH domain (Kamimura, Miyanaga, & Ueda, 2016; Miyagawa et al., 2018). Dictyostelium deficient in Gip1 exhibits severe defects in following the gradient of the chemoattractant cyclic adenosine monophosphate (cAMP), indicating that Gip1 is also essential in regulating the directional migration of Dictyostelium discoideum (Kamimura et al., 2016). These findings suggest that the TIPE TH domain may play an important conservative role in eukaryotic chemotaxis. These also implicate that TNFAIP8 and GPCR complexes may interact in HL-60 cells to regulate chemotaxis.

TNFAIP8 has been reported to directly interact with Gαi and couple with Gαi-coupled dopamine-D2short (D2S) receptor to reduce cell death and induce cellular transformation (Laliberté et al., 2010). Through yeast two-hybrid screening and confirmation by co-IP and pull-down assays, TNFAIP8, TIPE1, and TIPE2 have been showed to preferentially interact with Gαi proteins, but not other Gα proteins that not associated with chemokine receptors. Deletion of the last 15 amino acids of TNFAIP8 C-terminus was sufficient to disrupt this interaction (Laliberté et al., 2010). Thus, it is likely that TIPE proteins can sense chemoattractant gradient through GPCRs. We have observed

that TIPE2 preferentially localized to the plasma membranes in dHL-60s in response to CXCL8 treatment (Figure 2.7D). It would be interesting to test the interactions between TNFAIP8 and Gαi proteins by co-IP in HL-60 cells. We could also inhibit Gαi activity by the selective Gαi inhibitor pertussis toxin and examine if this affects TNFAIP8 membrane translocation after stimulation. These studies will clarify if Gαi is responsible for recruiting TNFAIP8 protein to the site of chemoattractant activation.

5.4 TNFAIP8 in inflammation and cancer

Existing evidences support the notion that TNFAIP8 is an oncogene in human cancers. More than half of human cancers exhibit aberrantly dysregulated phosphoinositide signaling, yet how these lipid signals are controlled remain not fully understood. While somatic mutations of PI3K, PTEN and Ras account for many cases of the aberrant phosphoinositide signaling, other mechanisms for its dysregulation are also being discovered. We found that TNFAIP8 interacts with PtdIns(4,5)P_2 and PtdIns(3,4,5)P_3, and is likely to be hijacked by tumor cells to facilitate malignant transformation. Some studies suggest that TNFAIP8 may be an inhibitor of caspases-induced apoptosis. Reports have shown that overexpression of TNFAIP8 in some cancer cell lines inhibited TNFα-induced apoptosis by suppressing caspase-3 and caspase-8 activities, while TNFAIP8 knockdown enhanced cell death (Kumar et al., 2000; C. Zhang et al., 2006). More work will be needed to elucidate the roles of TNFAIP8 in regulating proliferation and cell death signaling in tumorigenesis.

TNFAIP8 is originally identified as one of the most differentially expressed genes in primary and matched metastatic head and neck squamous cell carcinoma (HNSCC) from the same patient (Kumar et al., 2000; Patel et al., 1997), which raises the question of transcriptional control mechanisms of TNFAIP8 gene. TNFAIP8 expression has been reported to be induced by TNFα and high glucose stimulation, as well as activation of NF-κB in various cell types (Horrevoets et al., 1999; H.-G. Zhang et al., 2004). The orphan nuclear receptor chicken ovalbumin upstream promoter transcription factor I (COUP-TFI) has been identified as a transcriptional repressor of TNFAIP8 gene (Ling-juan Zhang, Liu, Gafken, Kioussi, & Leid, 2009), which is involved in the induction of TNFAIP8 promoter by TNFα. However, the detailed molecular mechanisms between COUP-TFI and TNFα signaling remain elusive. These findings support the notion that TNFAIP8 links a molecular bridge from inflammation to cancer by combining TNFα/NF-κB to phosphoinositide signaling pathway (Figure 5.3).

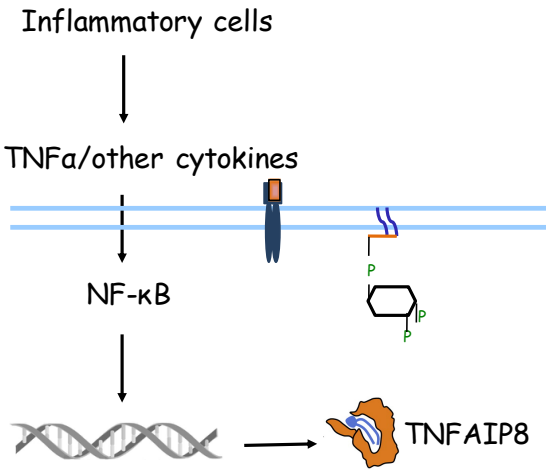

Figure 5.3 TNFAIP8 links a molecular bridge from inflammation to cancer by combining TNFα/NF-κB to phosphoinositide signaling pathway

TNFAIP8 expression can be induced by TNFα and activation of NF-κB, possibly through COUP-TFI (which is identified as a transcriptional repressor of TNFAIP8 gene).

5.5 Concluding remarks

In this study, we have conducted CRISPR/cas9-mediated TNFAIP8 gene knockout in human HL-60 cell line (Figure 2.1 and Figure 2.2). In addition to decreased proliferation and cell survival (Figure 2.3), defective migration and adhesion upon cytokine and fMLP stimulation were observed in these differentiated neutrophil-like cells (Figure 2.5 and Figure 2.6). We have confirmed that TNFAIP8 was in the cytosol in various cell types under resting condition, and TIPE2 translocated to plasma membranes after cytokine stimulation in dHL-60s (Figure 2.7). Moreover, TNFAIP8 could affect cellular phosphoinositide levels, and we showed increased total PtdIns(3,4,5)P_3 and PtdIns(4)P but reduced PtdIns(4,5)P_2 levels in TNFAIP8-deficient dHL-60 cells under resting condition (Figure 2.8). Additionally, we confirmed increased total PtdIns(3,4,5)P_3 levels in TNFAIP8 and TIPE2-deficient murine splenocytes, thymocytes and $CD4^+$ T cells in quiescent states (Figure 2.9). Through pharmaceutical inhibitors, co-IP/GST pull-down and flow cytometric studies, we have established that TNFAIP8 can regulate cell migration through Rho GTPases-dependent signaling and cofilin-mediated actin remodeling (Figure 2.10 and Figure 2.12), which is essential for leading edge formation (Figure 2.11).

To acquire mechanistic information, we have optimized the purification of TIPE proteins from *E. coli* (Figure 3.1 and Figure 3.2) and showed TNFAIP8 protein interacts with PtdIns(4,5)P_2 and PtdIns(3,4,5)P_3 present in lipid bilayers using the sedimentation-based binding assay (Figure 3.3A) and SPR assay (Figure 3.3B, Figure 3.11 and Table 4). Furthermore, we found TNFAIP8 can function as a phosphoinositide transfer protein *in vitro* (Figure 3.4). We also demonstrated that TNFAIP8 protein increased the PI3K-

catalyzed conversion of PtdIns(4,5)P_2 to PtdIns(3,4,5)P_3 in a dose-dependent manner through an enzymatic assay (Figure 3.5). In addition, we found TIPEs may also be able to steer cells by remodeling actin cytoskeleton through cofilin (Figure 3.6 and Figure 3.7). Crystal structure reveals that the fatty acid chains of phosphoinositides are likely involved in the hydrophobic pocket formed by the α1-α6 helixes of the TIPE TH domain, while the negatively charged phosphate head group is likely accommodated by electrostatic interactions with the positively charged amino acids located at the entrance of the cavity as well as the more flexible α0 helix. To provide additional insight to these hypotheses, mutagenesis analyses were performed to explore the structure and functional significance of the TIPE homology (TH) domain (Figure 3.8 and Figure 3.9). The effects of the TNFAIP8 mutants predicted from mutagenesis analyses have been assessed for phosphoinositide binding by lipid-protein overlay (Figure 3.10) and SPR assay (Figure 3.11 and Table 4) *in vitro*. Finally, the validated interaction-deficient mutants have been re-expressed in TNFAIP8 knockout murine T cells and HL-60 cells for cellular function characterization (Figure 3.12 and Figure 3.13).

We have also investigated murine leukocytes deficient in both TNFAIP8 and TIPE2, and observed complete loss of the directionality (Figure 4.1 and Figure 4.2). We found TNFAIP8 and TIPE2 pilot murine lymphocytes through PI3Ks and Rac (Figure 4.3 and Figure 4.4). Furthermore, We observed abnormal positioning of leukocytes in mice deficient in TNFAIP8 and TIPE2 under steady state (Figure 4.5 and Figure 4.6). Additionally, using experimental autoimmune encephalomyelitis (EAE) as a mouse model, we found TNFAIP8 and TIPE2-deficient mice were resistance to autoimmune

encephalomyelitis, and exhibited abnormal positioning of leukocytes in the central nervous system during autoimmune encephalomyelitis (Figure 4.7 and Figure 4.8). These findings indicate that TNFAIP8 and TIPE2 play redundant roles in controlling murine lymphocyte infiltration.

In summary, we discovered that TNFAIP8 is important to control cell migration, and may represent a molecular bridge from inflammation to caner by combining TNFα/NF-κB and phosphoinositide signaling. TNFAIP8 may represent a novel negative regulator of Rho GTPases, similar to the unique class of Rho GDP-dissociation inhibitors (RhoGDIs). Once sensing the chemokine stimulation, possibly through GPCRs, it may polarize along the chemoattractant gradient. Additionally, it can steer cells by enhancing phosphoinositide signaling through PI3K and remodeling actin cytoskeleton dynamics through cofilin. Thus, TNFAIP8 may contribute to short-range positive feedback as well as long-range inhibition, which helps to amplify the shallow chemokine gradients into cellular polarity. This study could not only advance our understanding of the biology of inflammation and tumorigenesis, but also help *in silico* drug screening and develop new TIPE-based strategies to combat malignant human diseases.

PUBLICATIONS

The following papers have been published in support of this dissertation.

The TIPE Molecular Pilot That Directs Lymphocyte Migration in Health and Inflammation

Sun, H.*, **Lin, M.***, Zamani, A., Goldsmith, J.R., Boggs, A.E., Li, M., Lee, C.N., Chen, X., Li, X., Li, T., Dorrity, B.L., Li, N., Lou, Y., Shi, S., Wang, W., Chen, Y.H. (2020). The TIPE Molecular Pilot That Directs Lymphocyte Migration in Health and Inflammation. *Scientific Reports*, *10*(1), pp.1-13.

*These authors contributed equally to this work

Abstract

Lymphocytes are some of the most motile cells of vertebrates, constantly navigating through various organ systems. Their specific positioning in the body is delicately controlled by site-specific directional cues such as chemokines. While it has long been suspected that an intrinsic molecular pilot, akin to a ship's pilot, guides lymphocyte navigation, the nature of this pilot is unknown. Here we show that the TIPE (TNF-α-induced protein 8-like) family of proteins pilot lymphocytes by steering them toward chemokines. TIPE proteins are carriers of lipid second messengers. They mediate chemokine-induced local generation of phosphoinositide second messengers, but inhibit global activation of the small GTPase Rac. TIPE-deficient T lymphocytes are completely pilot-less: they are unable to migrate toward chemokines despite their normal ability to move randomly. As a consequence, TIPE-deficient mice have a marked defect in positioning their T lymphocytes to various tissues, both at the steady-state and during inflammation. Thus, TIPE proteins pilot lymphocytes during migration and may be targeted for the treatment of lymphocyte-related disorders.

Direction of leukocyte polarization and migration by the phosphoinositide-transfer protein TIPE2

Fayngerts, S.A., Wang, Z., Zamani, A., Sun, H., Boggs, A.E., Porturas, T.P., Xie, W., **Lin, M.**, Cathopoulis, T., Goldsmith, J.R. and Vourekas, A., 2017. Direction of leukocyte polarization and migration by the phosphoinositide-transfer protein TIPE2. *Nature immunology*, *18*(12), p.1353.

Abstract

The polarization of leukocytes toward chemoattractants is essential for the directed migration (chemotaxis) of leukocytes. How leukocytes acquire polarity after encountering chemical gradients is not well understood. We found here that leukocyte polarity was generated by TIPE2 (TNFAIP8L2), a transfer protein for phosphoinositide second messengers. TIPE2 functioned as a local enhancer of phosphoinositide-dependent signaling and cytoskeleton remodeling, which promoted leading-edge formation. Conversely, TIPE2 acted as an inhibitor of the GTPase Rac, which promoted trailing-edge polarization. Consequently, TIPE2-deficient leukocytes were defective in polarization and chemotaxis, and TIPE2-deficient mice were resistant to leukocyte-mediated neural inflammation. Thus, the leukocyte polarizer is a dual-role phosphoinositide-transfer protein and represents a potential therapeutic target for the treatment of inflammatory diseases.

REFERENCES

Ahn, S.-H., Deshmukh, H., Johnson, N., Cowell, L. G., Rude, T. H., Scott, W. K., … Fowler Jr, V. G. (2010). Two genes on A/J chromosome 18 are associated with susceptibility to Staphylococcus aureus infection by combined microarray and QTL analyses. *PLoS Pathogens*, *6*(9), e1001088–e1001088. https://doi.org/10.1371/journal.ppat.1001088

Alexander, S., Koehl, G. E., Hirschberg, M., Geissler, E. K., & Friedl, P. (2008). Dynamic imaging of cancer growth and invasion: a modified skin-fold chamber model. *Histochemistry and Cell Biology*, *130*(6), 1147–1154. https://doi.org/10.1007/s00418-008-0529-1

Alexander, S., Weigelin, B., Winkler, F., & Friedl, P. (2013). Preclinical intravital microscopy of the tumour-stroma interface: invasion, metastasis, and therapy response. *Current Opinion in Cell Biology*, *25*(5), 659–671. https://doi.org/https://doi.org/10.1016/j.ceb.2013.07.001

Beseničar, M., Maček, P., Lakey, J. H., & Anderluh, G. (2006). Surface plasmon resonance in protein–membrane interactions. *Chemistry and Physics of Lipids*, *141*(1), 169–178. https://doi.org/https://doi.org/10.1016/j.chemphyslip.2006.02.010

Bhowmik, A., Rappel, W.-J., & Levine, H. (2016). Excitable waves and direction-sensing inDictyostelium discoideum: steps towards a chemotaxis model. *Physical Biology*, *13*(1), 16002. https://doi.org/10.1088/1478-3975/13/1/016002

Binkowski, A., Tseng, J., Liang, J., Dundas, J., Turpaz, Y., & Ouyang, Z. (2006). CASTp: computed atlas of surface topography of proteins with structural and topographical mapping of functionally annotated residues. *Nucleic Acids Research*, *34*(suppl_2), W116–W118. https://doi.org/10.1093/nar/gkl282

Binkowski, T. A., Naghibzadeh, S., & Liang, J. (2003). CASTp: Computed Atlas of Surface Topography of proteins. *Nucleic Acids Research*, *31*(13), 3352–3355. Retrieved from https://www.ncbi.nlm.nih.gov/pubmed/12824325

BLIGH, E. G., & DYER, W. J. (1959). A rapid method of total lipid extraction and purification. *Canadian Journal of Biochemistry and Physiology*, *37*(8), 911–917. https://doi.org/10.1139/o59-099

Bloes, D. A., Kretschmer, D., & Peschel, A. (2015). Enemy attraction: bacterial agonists for leukocyte chemotaxis receptors. *Nature Reviews Microbiology*, *13*(2), 95–104. https://doi.org/10.1038/nrmicro3390

Bravo-Cordero, J. J., Magalhaes, M. A. O., Eddy, R. J., Hodgson, L., & Condeelis, J. (2013). Functions of cofilin in cell locomotion and invasion. *Nature Reviews Molecular Cell Biology*, *14*, 405. Retrieved from https://doi.org/10.1038/nrm3609

Calabresi, P. A., Radue, E.-W., Goodin, D., Jeffery, D., Rammohan, K. W., Reder, A. T., … Lublin, F. D. (2014). Safety and efficacy of fingolimod in patients with relapsing-remitting

multiple sclerosis (FREEDOMS II): a double-blind, randomised, placebo-controlled, phase 3 trial. *The Lancet Neurology*, *13*(6), 545–556. https://doi.org/https://doi.org/10.1016/S1474-4422(14)70049-3

Carrigan, S. O., Weppler, A. L., Issekutz, A. C., & Stadnyk, A. W. (2005). Neutrophil differentiated HL-60 cells model Mac-1 (CD11b/CD18)-independent neutrophil transepithelial migration. *Immunology*, *115*(1), 108–117. https://doi.org/10.1111/j.1365-2567.2005.02131.x

Chen, C., Tian, W., Lei, X., Liang, J., & Zhao, J. (2018). CASTp 3.0: computed atlas of surface topography of proteins. *Nucleic Acids Research*, *46*(W1), W363–W367. https://doi.org/10.1093/nar/gky473

Chen, L., Yang, X., Yang, X., Fan, K., Xiao, P., Zhang, J., & Wang, X. (2016). Association between the expression levels of tumor necrosis factor-α-induced protein 8 and the prognosis of patients with gastric adenocarcinoma. *Experimental and Therapeutic Medicine*, *12*(1), 238–244. https://doi.org/10.3892/etm.2016.3327

Cho, S. W., Kim, S., Kim, J. M., & Kim, J.-S. (2013). Targeted genome engineering in human cells with the Cas9 RNA-guided endonuclease. *Nature Biotechnology*, *31*(3), 230–232. https://doi.org/10.1038/nbt.2507

Clark, J., Anderson, K. E., Juvin, V., Smith, T. S., Karpe, F., Wakelam, M. J. O., … Hawkins, P. T. (2011). Quantification of PtdInsP3 molecular species in cells and tissues by mass spectrometry. *Nature Methods*, *8*(3), 267–272. https://doi.org/10.1038/nmeth.1564

Collins, S. J. (1987). The HL-60 promyelocytic leukemia cell line: proliferation, differentiation, and cellular oncogene expression. *Blood*, *70*(5), 1233 LP – 1244. Retrieved from http://www.bloodjournal.org/content/70/5/1233.abstract

Cong, L., Ran, F. A., Cox, D., Lin, S., Barretto, R., Habib, N., … Zhang, F. (2013). Multiplex Genome Engineering Using CRISPR/Cas Systems. *Science*, *339*(6121), 819 LP – 823. https://doi.org/10.1126/science.1231143

Corey, S., Eguinoa, A., Puyana-Theall, K., Bolen, J. B., Cantley, L., Mollinedo, F., … Stephens, L. R. (1993). Granulocyte macrophage-colony stimulating factor stimulates both association and activation of phosphoinositide 3OH-kinase and src-related tyrosine kinase(s) in human myeloid derived cells. *The EMBO Journal*, *12*(7), 2681–2690. https://doi.org/10.1002/j.1460-2075.1993.tb05929.x

Crespo, C. L., Vernieri, C., Keller, P. J., Garrè, M., Bender, J. R., Wittbrodt, J., & Pardi, R. (2014). The PAR complex controls the spatiotemporal dynamics of F-actin and the MTOC in directionally migrating leukocytes. *Journal of Cell Science*, *127*(20), 4381 LP – 4395. https://doi.org/10.1242/jcs.146217

Cui, J., Hao, C., Zhang, W., Shao, J., Zhang, N., Zhang, G., & Liu, S. (2015). Identical expression profiling of human and murine TIPE3 protein reveals links to its functions. *The Journal of Histochemistry and Cytochemistry : Official Journal of the Histochemistry Society*, *63*(3), 206–216. https://doi.org/10.1369/0022155414564871

Cui, J., Zhang, G., Hao, C., Wang, Y., Lou, Y., Zhang, W., … Liu, S. (2011). The expression of

TIPE1 in murine tissues and human cell lines. *Molecular Immunology*, *48*(12), 1548–1555. https://doi.org/https://doi.org/10.1016/j.molimm.2011.04.023

Derfuss, T., Kuhle, J., Lindberg, R., & Kappos, L. (2013). Natalizumab Therapy for Multiple Sclerosis. *Semin Neurol*, *33*(01), 26–36. https://doi.org/10.1055/s-0033-1343793

Dong, Q.-Z., Zhao, Y., Liu, Y., Wang, Y., Zhang, P.-X., Jiang, G.-Y., … Wang, E.-H. (2010). Overexpression of SCC-S2 correlates with lymph node metastasis and poor prognosis in patients with non-small-cell lung cancer. *Cancer Science*, *101*(6), 1562–1569. https://doi.org/10.1111/j.1349-7006.2010.01557.x

Dowler, S., Kular, G., & Alessi, D. R. (2002). Protein Lipid Overlay Assay. *Science's STKE*, *2002*(129), pl6 LP-pl6. https://doi.org/10.1126/stke.2002.129.pl6

Duan, D., Zhu, Y.-Q., Guan, L.-L., & Wang, J. (2014). Upregulation of SCC-S2 in immune cells and tumor tissues of papillary thyroid carcinoma. *Tumour Biology : The Journal of the International Society for Oncodevelopmental Biology and Medicine*, *35*(5), 4331–4337. https://doi.org/10.1007/s13277-013-1568-3

Engelhardt, B., & Ransohoff, R. M. (2012). Capture, crawl, cross: the T cell code to breach the blood–brain barriers. *Trends in Immunology*, *33*(12), 579–589. https://doi.org/https://doi.org/10.1016/j.it.2012.07.004

Etienne-Manneville, S. (2004). Cdc42 - the centre of polarity. *Journal of Cell Science*, *117*(8), 1291 LP – 1300. https://doi.org/10.1242/jcs.01115

Fayngerts, S. A., Wang, Z., Zamani, A., Sun, H., Boggs, A. E., Porturas, T. P., … Chen, Y. H. (2017). Direction of leukocyte polarization and migration by the phosphoinositide-transfer protein TIPE2. *Nature Immunology*, *18*, 1353. Retrieved from https://doi.org/10.1038/ni.3866

Fayngerts, S. A., Wu, J., Oxley, C. L., Liu, X., Vourekas, A., Cathopoulis, T., … Chen, Y. H. (2014). TIPE3 Is the Transfer Protein of Lipid Second Messengers that Promote Cancer. *Cancer Cell*, *26*(4), 465–478. https://doi.org/https://doi.org/10.1016/j.ccr.2014.07.025

Ferguson, G. J., Milne, L., Kulkarni, S., Sasaki, T., Walker, S., Andrews, S., … Stephens, L. (2006). PI(3)Kγ has an important context-dependent role in neutrophil chemokinesis. *Nature Cell Biology*, *9*, 86. Retrieved from https://doi.org/10.1038/ncb1517

FOLCH, J., LEES, M., & SLOANE STANLEY, G. H. (1957). A simple method for the isolation and purification of total lipides from animal tissues. *The Journal of Biological Chemistry*, *226*(1), 497–509. Retrieved from http://europepmc.org/abstract/MED/13428781

Franca-Koh, J., & Devreotes, P. N. (2004). Moving Forward: Mechanisms of Chemoattractant Gradient Sensing. *Physiology*, *19*(5), 300–308. https://doi.org/10.1152/physiol.00017.2004

Franca-Koh, J., Kamimura, Y., & Devreotes, P. N. (2007). Leading-edge research: PtdIns(3,4,5)P3 and directed migration. *Nature Cell Biology*, *9*, 15. Retrieved from https://doi.org/10.1038/ncb0107-15

Gallagher, R., Collins, S., Trujillo, J., McCredie, K., Ahearn, M., Tsai, S., … Gallo, R. (1979).

Characterization of the continuous, differentiating myeloid cell line (HL-60) from a patient with acute promyelocytic leukemia. *Blood*, *54*(3), 713 LP – 733. Retrieved from http://www.bloodjournal.org/content/54/3/713.abstract

Garneau, J. E., Dupuis, M.-È., Villion, M., Romero, D. A., Barrangou, R., Boyaval, P., … Moineau, S. (2010). The CRISPR/Cas bacterial immune system cleaves bacteriophage and plasmid DNA. *Nature*, *468*(7320), 67–71. https://doi.org/10.1038/nature09523

Ghosh, M., Song, X., Mouneimne, G., Sidani, M., Lawrence, D. S., & Condeelis, J. S. (2004). Cofilin Promotes Actin Polymerization and Defines the Direction of Cell Motility. *Science*, *304*(5671), 743 LP – 746. https://doi.org/10.1126/science.1094561

Ginsberg, M. H., Du, X., & Plow, E. F. (1992). Inside-out integrin signalling. *Current Opinion in Cell Biology*, *4*(5), 766–771. https://doi.org/https://doi.org/10.1016/0955-0674(92)90099-X

Goldsmith, J. R., Fayngerts, S., & Chen, Y. H. (2017). Regulation of inflammation and tumorigenesis by the TIPE family of phospholipid transfer proteins. *Cellular & Molecular Immunology*, *14*(6), 482–487. https://doi.org/10.1038/cmi.2017.4

Gregor, C. E., Foeng, J., Comerford, I., & McColl, S. R. (2017). *Chapter Four - Chemokine-Driven CD4+ T Cell Homing: New Concepts and Recent Advances* (F. W. B. T.-A. in I. Alt, Ed.). https://doi.org/https://doi.org/10.1016/bs.ai.2017.03.001

Guillou, H., Lécureuil, C., Anderson, K. E., Suire, S., Ferguson, G. J., Ellson, C. D., … Stephens, L. R. (2007). Use of the GRP1 PH domain as a tool to measure the relative levels of PtdIns(3,4,5)P3 through a protein-lipid overlay approach. *Journal of Lipid Research* , *48*(3), 726–732. https://doi.org/10.1194/jlr.D600038-JLR200

Gupta, G. P., & Massagué, J. (2006). Cancer Metastasis: Building a Framework. *Cell*, *127*(4), 679–695. https://doi.org/10.1016/j.cell.2006.11.001

Gus-Brautbar, Y., Johnson, D., Zhang, L., Sun, H., Wang, P., Zhang, S., … Chen, Y. H. (2012). The Anti-inflammatory TIPE2 Is an Inhibitor of the Oncogenic Ras. *Molecular Cell*, *45*(5), 610–618. https://doi.org/https://doi.org/10.1016/j.molcel.2012.01.006

Guy-Grand, D., Vassalli, P., Eberl, G., Pereira, P., Burlen-Defranoux, O., Lemaitre, F., … Bandeira, A. (2013). Origin, trafficking, and intraepithelial fate of gut-tropic T cells. *Journal of Experimental Medicine*, *210*(9), 1839–1854. https://doi.org/10.1084/jem.20122588

Hansen, M. D. H., & Nelson, W. J. (2001). Serum-activated assembly and membrane translocation of an endogenous Rac1:effector complex. *Current Biology*, *11*(5), 356–360. https://doi.org/https://doi.org/10.1016/S0960-9822(01)00091-4

Hao, C., Zhang, N., Geng, M., Ren, Q., Li, Y., Wang, Y., … Liu, S. (2016). Clinical Significance of TIPE2 Protein Upregulation in Non-Hodgkin's Lymphoma. *Journal of Histochemistry & Cytochemistry*, *64*(9), 556–564. https://doi.org/10.1369/0022155416662262

Harburger, D. S., & Calderwood, D. A. (2009). Integrin signalling at a glance. *Journal of Cell Science*, *122*(2), 159 LP – 163. https://doi.org/10.1242/jcs.018093

Henkels, K. M., Frondorf, K., Gonzalez-Mejia, M. E., Doseff, A. L., & Gomez-Cambronero, J. (2011). IL-8-induced neutrophil chemotaxis is mediated by Janus kinase 3 (JAK3). *FEBS Letters*, *585*(1), 159–166. https://doi.org/https://doi.org/10.1016/j.febslet.2010.11.031

Hilliard, B. A., Mason, N., Xu, L., Sun, J., Lamhamedi-Cherradi, S.-E., Liou, H.-C., … Chen, Y. H. (2002). Critical roles of c-Rel in autoimmune inflammation and helper T cell differentiation. *The Journal of Clinical Investigation*, *110*(6), 843–850. https://doi.org/10.1172/JCI15254

Hitomi, J., Christofferson, D. E., Ng, A., Yao, J., Degterev, A., Xavier, R. J., & Yuan, J. (2008). Identification of a Molecular Signaling Network that Regulates a Cellular Necrotic Cell Death Pathway. *Cell*, *135*(7), 1311–1323. https://doi.org/10.1016/j.cell.2008.10.044

Homola, J., Yee, S. S., & Gauglitz, G. (1999). Surface plasmon resonance sensors: review. *Sensors and Actuators B: Chemical*, *54*(1), 3–15. https://doi.org/https://doi.org/10.1016/S0925-4005(98)00321-9

Horrevoets, A. J. G., Fontijn, R. D., van Zonneveld, A. J., de Vries, C. J. M., ten Cate, J. W., & Pannekoek, H. (1999). Vascular Endothelial Genes That Are Responsive to Tumor Necrosis Factor- In Vitro Are Expressed in Atherosclerotic Lesions, Including Inhibitor of Apoptosis Protein-1, Stannin, and Two Novel Genes. *Blood*, *93*(10), 3418–3431. https://doi.org/10.1182/blood.V93.10.3418.410k23_3418_3431

Hsu, P. D., Scott, D. A., Weinstein, J. A., Ran, F. A., Konermann, S., Agarwala, V., … Zhang, F. (2013). DNA targeting specificity of RNA-guided Cas9 nucleases. *Nature Biotechnology*, *31*(9), 827–832. https://doi.org/10.1038/nbt.2647

Hu, R., Qiu, X., Hong, S., Meng, L., Hong, X., Qiu, J., … Liu, Z. (2016). Clinical significance of TIPE expression in gastric carcinoma. *OncoTargets and Therapy*, Vol. 9, pp. 4473–4481. https://doi.org/10.2147/OTT.S100593

Huang, C.-H., Tang, M., Shi, C., Iglesias, P. A., & Devreotes, P. N. (2013). An excitable signal integrator couples to an idling cytoskeletal oscillator to drive cell migration. *Nature Cell Biology*, *15*, 1307. Retrieved from https://doi.org/10.1038/ncb2859

Hussman, J. P., Beecham, A. H., Schmidt, M., Martin, E. R., McCauley, J. L., Vance, J. M., … Pericak-Vance, M. A. (2016). GWAS analysis implicates NF-κB-mediated induction of inflammatory T cells in multiple sclerosis. *Genes and Immunity*, *17*(5), 305–312. https://doi.org/10.1038/gene.2016.23

Iglesias, P. A., & Devreotes, P. N. (2012). Biased excitable networks: how cells direct motion in response to gradients. *Current Opinion in Cell Biology*, *24*(2), 245–253. https://doi.org/https://doi.org/10.1016/j.ceb.2011.11.009

Insall, R. H. (2010). Understanding eukaryotic chemotaxis: a pseudopod-centred view. *Nature Reviews Molecular Cell Biology*, *11*(6), 453–458. https://doi.org/10.1038/nrm2905

Jin, T., Xu, X., & Hereld, D. (2008). Chemotaxis, chemokine receptors and human disease. *Cytokine*, *44*(1), 1–8. https://doi.org/https://doi.org/10.1016/j.cyto.2008.06.017

Jinek, M., Chylinski, K., Fonfara, I., Hauer, M., Doudna, J. A., & Charpentier, E. (2012). A

Programmable Dual-RNA–Guided DNA Endonuclease in Adaptive Bacterial Immunity. *Science*, *337*(6096), 816 LP – 821. https://doi.org/10.1126/science.1225829

JoVE, Cambridge, M. (2016). The Transwell Migration Assay. *JoVE Science Education Database*, 2–3. https://doi.org/doi: 10.3791/5644

Justus, C. R., Leffler, N., Ruiz-Echevarria, M., & Yang, L. V. (2014). In vitro cell migration and invasion assays. *Journal of Visualized Experiments : JoVE*, (88), 51046. https://doi.org/10.3791/51046

Kamakura, S., Nomura, M., Hayase, J., Iwakiri, Y., Nishikimi, A., Takayanagi, R., … Sumimoto, H. (2013). The Cell Polarity Protein mInsc Regulates Neutrophil Chemotaxis via a Noncanonical G Protein Signaling Pathway. *Developmental Cell*, *26*(3), 292–302. https://doi.org/10.1016/j.devcel.2013.06.008

Kamimura, Y., Miyanaga, Y., & Ueda, M. (2016). Heterotrimeric G-protein shuttling via Gip1 extends the dynamic range of eukaryotic chemotaxis. *Proceedings of the National Academy of Sciences*, *113*(16), 4356 LP – 4361. https://doi.org/10.1073/pnas.1516767113

Kavran, J. M., Klein, D. E., Lee, A., Falasca, M., Isakoff, S. J., Skolnik, E. Y., & Lemmon, M. A. (1998). Specificity and Promiscuity in Phosphoinositide Binding by Pleckstrin Homology Domains. *Journal of Biological Chemistry* , *273*(46), 30497–30508. https://doi.org/10.1074/jbc.273.46.30497

Kim, H., & Kim, J.-S. (2014). A guide to genome engineering with programmable nucleases. *Nature Reviews Genetics*, *15*(5), 321–334. https://doi.org/10.1038/nrg3686

Kim, J.-S., Park, J., Kim, M.-S., Ha, J.-Y., Jang, Y.-W., Shin, D. H., & Son, J. H. (2017). The Tnfaip8-PE complex is a novel upstream effector in the anti-autophagic action of insulin. *Scientific Reports*, *7*(1), 6248. https://doi.org/10.1038/s41598-017-06576-3

Kim, S. K., Ioannidis, J. P. A., Ahmed, M. A., Avins, A. L., Kleimeyer, J. P., Fredericson, M., & Dragoo, J. L. (2018). Two Genetic Variants Associated with Plantar Fascial Disorders. *Int J Sports Med*, *39*(04), 314–321. https://doi.org/10.1055/s-0044-100280

Klinker, J. F., Wenzel-Seifert, K., & Seifert, R. (1996). G-Protein-coupled receptors in HL-60 human leukemia cells. *General Pharmacology: The Vascular System*, *27*(1), 33–54. https://doi.org/https://doi.org/10.1016/0306-3623(95)00107-7

Krause, K. H., Schlegel, W., Wollheim, C. B., Andersson, T., Waldvogel, F. A., & Lew, P. D. (1985). Chemotactic peptide activation of human neutrophils and HL-60 cells. Pertussis toxin reveals correlation between inositol trisphosphate generation, calcium ion transients, and cellular activation. *The Journal of Clinical Investigation*, *76*(4), 1348–1354. https://doi.org/10.1172/JCI112109

Kumar, D., Gokhale, P., Broustas, C., Chakravarty, D., Ahmad, I., & Kasid, U. (2004). Expression of SCC-S2, an antiapoptotic molecule, correlates with enhanced proliferation and tumorigenicity of MDA-MB 435 cells. *Oncogene*, *23*(2), 612–616. https://doi.org/10.1038/sj.onc.1207123

Kumar, D., Whiteside, T. L., & Kasid, U. (2000). Identification of a Novel Tumor Necrosis

Factor-α-inducible Gene, SCC-S2, Containing the Consensus Sequence of a Death Effector Domain of Fas-associated Death Domain-like Interleukin- 1β-converting Enzyme-inhibitory Protein . *Journal of Biological Chemistry* , *275*(4), 2973–2978. https://doi.org/10.1074/jbc.275.4.2973

Kunkel, E. J., & Butcher, E. C. (2002). Chemokines and the Tissue-Specific Migration of Lymphocytes. *Immunity*, *16*(1), 1–4. https://doi.org/https://doi.org/10.1016/S1074-7613(01)00261-8

Laliberté, B., Wilson, A. M., Nafisi, H., Mao, H., Zhou, Y. Y., Daigle, M., & Albert, P. R. (2010). TNFAIP8: A new effector for Galpha(i) coupling to reduce cell death and induce cell transformation. *Journal of Cellular Physiology*, *225*(3), 865–874. https://doi.org/10.1002/jcp.22297

Lauffenburger, D. A., & Horwitz, A. F. (1996). Cell Migration: A Physically Integrated Molecular Process. *Cell*, *84*(3), 359–369. https://doi.org/https://doi.org/10.1016/S0092-8674(00)81280-5

Lee, A., & Lemmon, M. A. (2001). 48 - Analysis of Phosphoinositide Binding by Pleckstrin Homology Domain from Dynamin. In W. E. Balch, C. J. Der, & A. B. T.-M. in E. Hall (Eds.), *Regulators and Effectors of Small GTPases* (Vol. 329, pp. 457–468). https://doi.org/https://doi.org/10.1016/S0076-6879(01)29107-1

Lee, D., Kim, M.-S., Park, J., Jhon, G.-J., Son, H. J., & Shin, H. D. (2014). A Preliminary X-ray Study of Murine Tnfaip8/Oxi-α. *International Journal of Molecular Sciences* , Vol. 15. https://doi.org/10.3390/ijms15034523

Li, Y., Jing, C., Chen, Y., Wang, J., Zhou, M., Liu, X., … Guo, X. (2015). Expression of tumor necrosis factor α-induced protein 8 is upregulated in human gastric cancer and regulates cell proliferation, invasion and migration. *Molecular Medicine Reports*, *12*(2), 2636–2642. https://doi.org/10.3892/mmr.2015.3690

Liu, W., Chen, Y., Xie, H., Guo, Y., Ren, D., Li, Y., … Yi, F. (2018). TIPE1 suppresses invasion and migration through down-regulating Wnt/β-catenin pathway in gastric cancer. *Journal of Cellular and Molecular Medicine*, *22*(2), 1103–1117. https://doi.org/10.1111/jcmm.13362

Lou, Y., Sun, H., Morrissey, S., Porturas, T., Liu, S., Hua, X., & Chen, Y. H. (2014). Critical Roles of TIPE2 Protein in Murine Experimental Colitis. *The Journal of Immunology*, *193*(3), 1064 LP – 1070. https://doi.org/10.4049/jimmunol.1400415

Lowe, J. M., Nguyen, T.-A., Grimm, S. A., Gabor, K. A., Peddada, S. D., Li, L., … Fessler, M. B. (2016). The novel p53 target TNFAIP8 variant 2 is increased in cancer and offsets p53-dependent tumor suppression. *Cell Death And Differentiation*, *24*, 181. Retrieved from https://doi.org/10.1038/cdd.2016.130

Mali, P., Yang, L., Esvelt, K. M., Aach, J., Guell, M., DiCarlo, J. E., … Church, G. M. (2013). RNA-guided human genome engineering via Cas9. *Science (New York, N.Y.)*, *339*(6121), 823–826. https://doi.org/10.1126/science.1232033

Merlot, S., & Firtel, R. A. (2003). Leading the way: directional sensing through phosphatidylinositol 3-kinase and other signaling pathways. *Journal of Cell Science*,

116(17), 3471 LP – 3478. https://doi.org/10.1242/jcs.00703

Mertens, A. E. E., Rygiel, T. P., Olivo, C., van der Kammen, R., & Collard, J. G. (2005). The Rac activator Tiam1 controls tight junction biogenesis in keratinocytes through binding to and activation of the Par polarity complex . *Journal of Cell Biology*, *170*(7), 1029–1037. https://doi.org/10.1083/jcb.200502129

Millius, A., & Weiner, O. D. (2009). *Chemotaxis in Neutrophil-Like HL-60 Cells BT - Chemotaxis: Methods and Protocols* (T. Jin & D. Hereld, Eds.). https://doi.org/10.1007/978-1-60761-198-1_11

Minagar, A., & Alexander, J. S. (2003). Blood-brain barrier disruption in multiple sclerosis. *Multiple Sclerosis Journal*, *9*(6), 540–549. https://doi.org/10.1191/1352458503ms965oa

Miyagawa, T., Koteishi, H., Kamimura, Y., Miyanaga, Y., Takeshita, K., Nakagawa, A., & Ueda, M. (2018). Structural basis of Gip1 for cytosolic sequestration of G protein in wide-range chemotaxis. *Nature Communications*, *9*(1), 4635. https://doi.org/10.1038/s41467-018-07035-x

Mouneimne, G., DesMarais, V., Sidani, M., Scemes, E., Wang, W., Song, X., … Condeelis, J. (2006). Spatial and Temporal Control of Cofilin Activity Is Required for Directional Sensing during Chemotaxis. *Current Biology*, *16*(22), 2193–2205. https://doi.org/https://doi.org/10.1016/j.cub.2006.09.016

Nishimura, T., Yamaguchi, T., Kato, K., Yoshizawa, M., Nabeshima, Y., Ohno, S., … Kaibuchi, K. (2005). PAR-6–PAR-3 mediates Cdc42-induced Rac activation through the Rac GEFs STEF/Tiam1. *Nature Cell Biology*, *7*(3), 270–277. https://doi.org/10.1038/ncb1227

Nishio, M., Watanabe, K., Sasaki, J., Taya, C., Takasuga, S., Iizuka, R., … Sasaki, T. (2006). Control of cell polarity and motility by the PtdIns(3,4,5)P3 phosphatase SHIP1. *Nature Cell Biology*, *9*, 36. Retrieved from https://doi.org/10.1038/ncb1515

Nobes, C. D., & Hall, A. (1999). Rho GTPases Control Polarity, Protrusion, and Adhesion during Cell Movement. *The Journal of Cell Biology*, *144*(6), 1235 LP – 1244. https://doi.org/10.1083/jcb.144.6.1235

Patel, S., Wang, F.-H., Whiteside, T. L., & Kasid, U. (1997). Identification of seven differentially displayed transcripts in human primary and matched metastatic head and neck squamous cell carcinoma cell lines: Implications in metastasis and/or radiation response. *Oral Oncology*, *33*(3), 197–203. https://doi.org/https://doi.org/10.1016/S0964-1955(96)00065-6

Paul, C. D., Mistriotis, P., & Konstantopoulos, K. (2017). Cancer cell motility: lessons from migration in confined spaces. *Nature Reviews Cancer*, *17*(2), 131–140. https://doi.org/10.1038/nrc.2016.123

Peters, L. A., Perrigoue, J., Mortha, A., Iuga, A., Song, W., Neiman, E. M., … Schadt, E. E. (2017). A functional genomics predictive network model identifies regulators of inflammatory bowel disease. *Nature Genetics*, *49*(10), 1437–1449. https://doi.org/10.1038/ng.3947

Prunier, C., Prudent, R., Kapur, R., Sadoul, K., & Lafanechère, L. (2017). LIM kinases: cofilin

and beyond. *Oncotarget*, *8*(25), 41749–41763. https://doi.org/10.18632/oncotarget.16978

Ran, F. A., Hsu, P. D., Wright, J., Agarwala, V., Scott, D. A., & Zhang, F. (2013). Genome engineering using the CRISPR-Cas9 system. *Nature Protocols*, *8*(11), 2281–2308. https://doi.org/10.1038/nprot.2013.143

Rickert, P., Weiner, O. D., Wang, F., Bourne, H. R., & Servant, G. (2000). Leukocytes navigate by compass: roles of PI3Kgamma and its lipid products. *Trends in Cell Biology*, *10*(11), 466–473. https://doi.org/10.1016/s0962-8924(00)01841-9

Ridley, A. J. (2001). Rho GTPases and cell migration. *Journal of Cell Science*, *114*(15), 2713 LP – 2722. Retrieved from http://jcs.biologists.org/content/114/15/2713.abstract

Ridley, A. J., Schwartz, M. A., Burridge, K., Firtel, R. A., Ginsberg, M. H., Borisy, G., … Horwitz, A. R. (2003). Cell Migration: Integrating Signals from Front to Back. *Science*, *302*(5651), 1704 LP – 1709. https://doi.org/10.1126/science.1092053

Rusten, T. E., & Stenmark, H. (2006). Analyzing phosphoinositides and their interacting proteins. *Nature Methods*, *3*(4), 251–258. https://doi.org/10.1038/nmeth867

Sablin, E. P., Krylova, I. N., Fletterick, R. J., & Ingraham, H. A. (2003). Structural Basis for Ligand-Independent Activation of the Orphan Nuclear Receptor LRH-1. *Molecular Cell*, *11*(6), 1575–1585. https://doi.org/10.1016/S1097-2765(03)00236-3

Sai, J., Walker, G., Wikswo, J., & Richmond, A. (2006). The IL Sequence in the LLKIL Motif in CXCR2 Is Required for Full Ligand-induced Activation of Erk, Akt, and Chemotaxis in HL60 Cells. *Journal of Biological Chemistry* , *281*(47), 35931–35941. https://doi.org/10.1074/jbc.M605883200

Sánchez-Madrid, F., & Angel del Pozo, M. (1999). Leukocyte polarization in cell migration and immune interactions. *The EMBO Journal*, *18*(3), 501 LP – 511. https://doi.org/10.1093/emboj/18.3.501

Sanjana, N. E., Shalem, O., & Zhang, F. (2014). Improved vectors and genome-wide libraries for CRISPR screening. *Nature Methods*, *11*(8), 783–784. https://doi.org/10.1038/nmeth.3047

Schaaf, G., Ortlund, E. A., Tyeryar, K. R., Mousley, C. J., Ile, K. E., Garrett, T. A., … Bankaitis, V. A. (2008). Functional Anatomy of Phospholipid Binding and Regulation of Phosphoinositide Homeostasis by Proteins of the Sec14 Superfamily. *Molecular Cell*, *29*(2), 191–206. https://doi.org/https://doi.org/10.1016/j.molcel.2007.11.026

Schmidt, A., & Hall, A. (2002). Guanine nucleotide exchange factors for Rho GTPases: turning on the switch. *Genes & Development*, *16*(13), 1587–1609. https://doi.org/10.1101/gad.1003302

Shalem, O., Sanjana, N. E., Hartenian, E., Shi, X., Scott, D. A., Mikkelsen, T. S., … Zhang, F. (2014). Genome-Scale CRISPR-Cas9 Knockout Screening in Human Cells. *Science*, *343*(6166), 84 LP – 87. https://doi.org/10.1126/science.1247005

Song, X., Chen, X., Yamaguchi, H., Mouneimne, G., Condeelis, J. S., & Eddy, R. J. (2006). Initiation of cofilin activity in response to EGF is uncoupled from cofilin phosphorylation

and dephosphorylation in carcinoma cells. *Journal of Cell Science*, *119*(14), 2871 LP – 2881. https://doi.org/10.1242/jcs.03017

Springer, T. A., & Dustin, M. L. (2012). Integrin inside-out signaling and the immunological synapse. *Current Opinion in Cell Biology*, *24*(1), 107–115. https://doi.org/https://doi.org/10.1016/j.ceb.2011.10.004

Stachowiak, A. N., Wang, Y., Huang, Y.-C., & Irvine, D. J. (2006). Homeostatic Lymphoid Chemokines Synergize with Adhesion Ligands to Trigger T and B Lymphocyte Chemokinesis. *The Journal of Immunology*, *177*(4), 2340 LP – 2348. https://doi.org/10.4049/jimmunol.177.4.2340

Stanisavljevic, M., Schmid, A., & Leblebici, Y. (2009). Optimization of Nanoelectronic Systems Reliability Under Massive Defect Density Using Distributed R-fold Modular Redundancy (DRMR). *2009 24th IEEE International Symposium on Defect and Fault Tolerance in VLSI Systems*, 340–348. https://doi.org/10.1109/DFT.2009.54

Steeg, P. S. (2016). Targeting metastasis. *Nature Reviews Cancer*, *16*(4), 201–218. https://doi.org/10.1038/nrc.2016.25

Sun, H., Gong, S., Carmody, R. J., Hilliard, A., Li, L., Sun, J., … Chen, Y. H. (2008). TIPE2, a Negative Regulator of Innate and Adaptive Immunity that Maintains Immune Homeostasis. *Cell*, *133*(3), 415–426. https://doi.org/https://doi.org/10.1016/j.cell.2008.03.026

Sun, H., Lou, Y., Porturas, T., Morrissey, S., Luo, G., Qi, J., … Chen, Y. H. (2015). Exacerbated Experimental Colitis in TNFAIP8-Deficient Mice. *The Journal of Immunology*, *194*(12), 5736 LP – 5742. https://doi.org/10.4049/jimmunol.1401986

Sun, H., Zhuang, G., Chai, L., Wang, Z., Johnson, D., Ma, Y., & Chen, Y. H. (2012). TIPE2 Controls Innate Immunity to RNA by Targeting the Phosphatidylinositol 3-Kinase–Rac Pathway. *The Journal of Immunology*, *189*(6), 2768 LP – 2773. https://doi.org/10.4049/jimmunol.1103477

Sun, Z., Liu, X., Song, J. H., Cheng, Y., Liu, Y., Jia, Y., … Wang, Z. (2016). TNFAIP8 overexpression: a potential predictor of lymphatic metastatic recurrence in pN0 esophageal squamous cell carcinoma after Ivor Lewis esophagectomy. *Tumor Biology*, *37*(8), 10923–10934. https://doi.org/10.1007/s13277-016-4978-1

Swaney, K. F., Huang, C.-H., & Devreotes, P. N. (2010). Eukaryotic Chemotaxis: A Network of Signaling Pathways Controls Motility, Directional Sensing, and Polarity. *Annual Review of Biophysics*, *39*(1), 265–289. https://doi.org/10.1146/annurev.biophys.093008.131228

Szatmary, A. C., & Nossal, R. (2017). Determining whether observed eukaryotic cell migration indicates chemotactic responsiveness or random chemokinetic motion. *Journal of Theoretical Biology*, *425*, 103–112. https://doi.org/https://doi.org/10.1016/j.jtbi.2017.05.014

Takagi, J., Petre, B. M., Walz, T., & Springer, T. A. (2002). Global Conformational Rearrangements in Integrin Extracellular Domains in Outside-In and Inside-Out Signaling. *Cell*, *110*(5), 599–611. https://doi.org/https://doi.org/10.1016/S0092-8674(02)00935-2

Talmadge, J. E., & Fidler, I. J. (2010). AACR Centennial Series: The Biology of Cancer

Metastasis: Historical Perspective. *Cancer Research*, *70*(14), 5649 LP – 5669. https://doi.org/10.1158/0008-5472.CAN-10-1040

Tang, M., Wang, M., Shi, C., Iglesias, P. A., Devreotes, P. N., & Huang, C.-H. (2014). Evolutionarily conserved coupling of adaptive and excitable networks mediates eukaryotic chemotaxis. *Nature Communications*, *5*, 5175. Retrieved from https://doi.org/10.1038/ncomms6175

Thapa, N., & Anderson, R. A. (2012). PIP2 signaling, an integrator of cell polarity and vesicle trafficking in directionally migrating cells. *Cell Adhesion & Migration*, *6*(5), 409–412. https://doi.org/10.4161/cam.21192

Thapa, N., Tan, X., Choi, S., Lambert, P. F., Rapraeger, A. C., & Anderson, R. A. (2016). The Hidden Conundrum of Phosphoinositide Signaling in Cancer. *Trends in Cancer*, *2*(7), 378–390. https://doi.org/10.1016/j.trecan.2016.05.009

Tortorella, D., & London, E. (1994). Method for Efficient Pelleting of Small Unilamellar Model Membrane Vesicles. *Analytical Biochemistry*, *217*(2), 176–180. https://doi.org/https://doi.org/10.1006/abio.1994.1106

Tsujita, K., & Itoh, T. (2015). Phosphoinositides in the regulation of actin cortex and cell migration. *Biochimica et Biophysica Acta (BBA) - Molecular and Cell Biology of Lipids*, *1851*(6), 824–831. https://doi.org/https://doi.org/10.1016/j.bbalip.2014.10.011

van Rheenen, J., Condeelis, J., & Glogauer, M. (2009). A common cofilin activity cycle in invasive tumor cells and inflammatory cells. *Journal of Cell Science*, *122*(3), 305 LP – 311. https://doi.org/10.1242/jcs.031146

Vivanco, I., & Sawyers, C. L. (2002). The phosphatidylinositol 3-Kinase–AKT pathway in human cancer. *Nature Reviews Cancer*, *2*(7), 489–501. https://doi.org/10.1038/nrc839

Wang, T., Wei, J. J., Sabatini, D. M., & Lander, E. S. (2014). Genetic screens in human cells using the CRISPR-Cas9 system. *Science (New York, N.Y.)*, *343*(6166), 80–84. https://doi.org/10.1126/science.1246981

Wang, W., Eddy, R., & Condeelis, J. (2007). The cofilin pathway in breast cancer invasion and metastasis. *Nature Reviews Cancer*, *7*(6), 429–440. https://doi.org/10.1038/nrc2148

Wang, W., Goswami, S., Sahai, E., Wyckoff, J. B., Segall, J. E., & Condeelis, J. S. (2005). Tumor cells caught in the act of invading: their strategy for enhanced cell motility. *Trends in Cell Biology*, *15*(3), 138–145. https://doi.org/10.1016/j.tcb.2005.01.003

Wang, Z., Fayngerts, S., Wang, P., Sun, H., Johnson, D. S., Ruan, Q., … Chen, Y. H. (2012). TIPE2 protein serves as a negative regulator of phagocytosis and oxidative burst during infection. *Proceedings of the National Academy of Sciences of the United States of America*, *109*(38), 15413–15418. https://doi.org/10.1073/pnas.1204525109

Weizman, A., Huang, B., Berel, D., Targan, S. R., Dubinsky, M., Fleshner, P., … McGovern, D. P. B. (2014). Clinical, Serologic, and Genetic Factors Associated with Pyoderma Gangrenosum and Erythema Nodosum in Inflammatory Bowel Disease Patients. *Inflammatory Bowel Diseases*, *20*(3), 525–533.

https://doi.org/10.1097/01.MIB.0000442011.60285.68

Wirtz, D., Konstantopoulos, K., & Searson, P. C. (2011). The physics of cancer: the role of physical interactions and mechanical forces in metastasis. *Nature Reviews Cancer*, *11*(7), 512–522. https://doi.org/10.1038/nrc3080

Wu, X., Ma, Y., Cheng, J., Li, X., Zheng, H., Jiang, L., & Zhou, R. (2017). TIPE1 function as a prognosis predictor and negative regulator of lung cancer. *Oncotarget*, Vol. 8, pp. 78496–78506. https://doi.org/10.18632/oncotarget.19655

Xiong, Y., Huang, C.-H., Iglesias, P. A., & Devreotes, P. N. (2010). Cells navigate with a local-excitation, global-inhibition-biased excitable network. *Proceedings of the National Academy of Sciences*, *107*(40), 17079 LP – 17086. https://doi.org/10.1073/pnas.1011271107

Yang, M., Zhao, Q., Wang, X., Liu, T., Yao, G., Lou, C., & Zhang, Y. (2014). TNFAIP8 overexpression is associated with lymph node metastasis and poor prognosis in intestinal-type gastric adenocarcinoma. *Histopathology*, *65*(4), 517–526. https://doi.org/10.1111/his.12413

Zahn, S., Zwirner, Jör., Spengler, H.-P., & Götze, O. (1997). Chemoattractant receptors for interleukin-8 and C5a: expression on peripheral blood leukocytes and differential regulation on HL-60 and AML-193 cells by vitamin D3 and all-trans rètinoic acid. *European Journal of Immunology*, *27*(4), 935–940. https://doi.org/10.1002/eji.1830270420

Zhang, C., Chakravarty, D., Sakabe, I., Mewani, R. R., Boudreau, H. E., Kumar, D., … Kasid, U. N. (2006). Role of SCC-S2 in Experimental Metastasis and Modulation of VEGFR-2, MMP-1, and MMP-9 Expression. *Molecular Therapy*, *13*(5), 947–955. https://doi.org/10.1016/j.ymthe.2005.11.020

Zhang, C., Kallakury, B. V, Ross, J. S., Mewani, R. R., Sheehan, C. E., Sakabe, I., … Kasid, U. N. (2013). The significance of TNFAIP8 in prostate cancer response to radiation and docetaxel and disease recurrence. *International Journal of Cancer*, *133*(1), 31–42. https://doi.org/10.1002/ijc.27996

Zhang, H.-G., Hyde, K., Page, G. P., Brand, J. P. L., Zhou, J., Yu, S., … Mountz, J. D. (2004). Novel tumor necrosis factor α–regulated genes in rheumatoid arthritis. *Arthritis & Rheumatism*, *50*(2), 420–431. https://doi.org/10.1002/art.20037

Zhang, Li, Mao, Y. S., Janmey, P. A., & Yin, H. L. (2012). *Phosphatidylinositol 4, 5 Bisphosphate and the Actin Cytoskeleton BT - Phosphoinositides II: The Diverse Biological Functions* (T. Balla, M. Wymann, & J. D. York, Eds.). https://doi.org/10.1007/978-94-007-3015-1_6

Zhang, Ling-juan, Liu, X., Gafken, P. R., Kioussi, C., & Leid, M. (2009). A chicken ovalbumin upstream promoter transcription factor I (COUP-TFI) complex represses expression of the gene encoding tumor necrosis factor alpha-induced protein 8 (TNFAIP8). *The Journal of Biological Chemistry*, *284*(10), 6156–6168. https://doi.org/10.1074/jbc.M807713200

Zhang, X., Wang, J., Fan, C., Li, H., Sun, H., Gong, S., … Shi, Y. (2008). Crystal structure of TIPE2 provides insights into immune homeostasis. *Nature Structural &Amp; Molecular Biology*, *16*, 89. Retrieved from https://doi.org/10.1038/nsmb.1522

Zhang, Y., Wang, M.-Y., He, J., Wang, J.-C., Yang, Y.-J., Jin, L., … Zhou, X.-Y. (2012). Tumor Necrosis Factor-α Induced Protein 8 Polymorphism and Risk of Non-Hodgkin's Lymphoma in a Chinese Population: A Case-Control Study. *PLOS ONE*, *7*(5), e37846. Retrieved from https://doi.org/10.1371/journal.pone.0037846

Zhang, Z., Liang, X., Gao, L., Ma, H., Liu, X., Pan, Y., … Ma, C. (2015). TIPE1 induces apoptosis by negatively regulating Rac1 activation in hepatocellular carcinoma cells. *Oncogene*, *34*(20), 2566–2574. https://doi.org/10.1038/onc.2014.208